Formability analysis of AA6061 aluminum alloy sheets in Single Point Incremental Forming

Assefa Leramo Anore

A Thesis Submitted to:

The department of Mechanical Design and Manufacturing Engineering

School of Mechanical, Chemical and Materials Engineering

Presented in Partial Fulfillment of the Requirement for the Degree of Master's in Manufacturing Engineering

Office of Graduate Studies

Adama Science and Technology University

Adama, Ethiopia

January, 2021

Formability analysis of AA6061 aluminum alloy sheets in Single Point Incremental Forming

Assefa Leramo Anore

Advisor: Devendra Kumar Sinha (PhD)
Co-advisor: Perumalla Janaki Ramulu (PhD)

A Thesis Submitted to:
The department of Mechanical Design and Manufacturing Engineering

School of Mechanical, Chemical and Materials Engineering

Presented in Partial Fulfillment of the Requirement for the Degree of Master's in Manufacturing Engineering

Office of Graduate Studies

Adama Science and Technology University

Adama, Ethiopia
January, 2021

Thesis Approval sheet

We, the undersigned, members of the Board of Examiners of the final open defense by Assefa Leramo Anore have read and evaluated his thesis entitled "***Formability analysis of AA6061 aluminum alloy sheets in Single Point Incremental Forming*** " and examined the candidate. This is, therefore, to certify that the thesis has been accepted in partial fulfillment of the requirement of the Degree of Master's of Science in Manufacturing Engineering.

______________________	______________________	______________________
Name of the Student	Signature	Date
______________________	______________________	______________________
Supervisor /Advisor	Signature	Date
______________________	______________________	______________________
Co-Supervisor /Co-Advisor	Signature	Date
______________________	______________________	______________________
External examiner	Signature	Date
______________________	______________________	______________________
Internal Examiner	Signature	Date
______________________	______________________	______________________
Chairperson	Signature	Date
______________________	______________________	______________________
Program chair	Signature	Date
______________________	______________________	______________________
School Dean	Signature	Date
______________________	______________________	______________________
Post Graduate Dean	Signature	Date

DECLARATION

I hereby declare that this MSc Thesis is my original work and has not been presented for a degree in any other university, and all sources of material used for this thesis have been duly acknowledged.

Name: ____

Signature:____

This MSc Thesis has been submitted for examination with my approval as thesis advisor.

Name: ____

Signature:____

Date of submission: 25, January 2021

ACKNOWLEDGEMENT

Above all, I thank Almighty God for always being with me in all my endeavours and giving me endurance to complete my study.

Special acknowledgment and warmest appreciation is for my respected and diligent adviser, Dr. Devendra Kumar Sinha, for his invaluable comments, criticism and professional advice from the inception to completion of the thesis, without which this thesis would have remained an insurmountable task.

Also my sincere gratitude and appreciation goes to my Co-advisor Dr. Perumalla Janaki Ramulu for being there always to help unlimitedly without his contribution realizing my study is extensively laborious, thus due appreciation goes to him.

I would like to thank and appreciate Mechanical Design and Manufacturing Engineering staff and respected lecturers namely: Dr. Moera Gutu, Dr. Habtamu Beri, Dr. Venkatesh for their guidance and motivation during study.

I would like to thank and give appreciation to Sr Martha, for her unlimited support, morale and technical advice in continuation of the study and preparation of this document. Also I would like to express my sincere thanks to Abate Shake who has supported me on allowing his office and internet throughout the study, and for his unreserved appreciations and encouragement.

Finally, and most importantly, my gratitude and love goes out to my family. Special thanks to my wife, my love, Mengiste, who has always believed in me and has never let me give up. To my parents, Leramo and Erchafe, for their unlimited sacrifices and everything they have done for me to become what I am today. To my brothers and sisters, Zeleke, Abebe, Sr.Martha, Delibame and Amarech, who have always been unbelievably supportive and encouraging. It is through the support and love of family and friends that I am who I am and know where I want to be.

Lastly, I dedicate this thesis to my wife and children (Meron and Abenezer)!!!

Abstract

Recently, Single Point Incremental Forming has caught the devotion of automotive, aerospace and medical industries as a marginal to conventional stamping process as an economical process capable of manufacturing sheet metal prototypes bereft of expensive dies. The first objective of the study was to determine the nature of maximum wall angles and thinning expected during the single point incremental forming process on AA6061 aluminum alloy with different thickness. The second objective was to study the effect of different process parameters on the maximum wall angle and average thinning. Thorough experiments were accompanied based on the Response Surface Method approach for input process parameters namely; step depth (0.2mm, 0.5mm and 0.8mm), tool diameter (5mm, 10mm and 15mm), feed rate (1000mm/min, 1500mm/min and 2000mm/min) and material thickness (0.8mm, 1.0mm and 1.2mm). The responses of formability were maximum wall angles and thinning measured for different process parameters and their interactions (step depth, tool diameter, feed rate and material thickness). Based on the numerical simulation and experimental results, several conclusions were made on the effects of process parameters on the maximum wall angle and thinning. Analysis of variance (ANOVA) was used to identify the significant control factors and their interactions. From the experimental findings, an attempt was made to find the optimal combination of the process parameters on the basis of a proposed predictive mathematical model. The maximum wall angle value achieved was 77.81˚, with a 5mm tool diameter, feed rate of 1000 mm/min, step depth of 0.2 mm and a material thickness of 0.8mm and the maximum thinning was 0.8563mm, with a 5mm tool diameter, feed rate of 1000 mm/min, step depth of 0.8 mm and a material thickness of 1.2mm. Finally, the study proposed guidelines for forming thick sheets and improving formability and production rate of SPIF process.

Keywords: Incremental forming; Single Point Incremental Forming; Formability; Optimization; Parameter

Table of Contents

LIST OF TABLES

List of Figures and Illustrations

List of Acronyms, Abbreviations and Symbols

A%	the elongation percentage
ADSIF	Accumulative Double-Sided Incremental Forming
AISF	Asymmetric Incremental Sheet Forming
ASTM	American Standard for Testing Materials
BUT	Bending Under Tension
C3D8	full integration
C3D8I	full integration with incompatible deformation modes
C3D8R	reduced integration
CAD	Computer Aided Design
CAE	Computer-Aided Engineering
CAM	Computer Aided Manufacturing
CMM	Coordinate Measuring Machine
CNC	Computer Numerical Control
DOF	Degrees Of Freedom
DSIF	Double-Sided Incremental Forming
FEA	Finite Element Analysis
FEM	Finite Element Method
FFLD	Fracture Forming Limit Diagram
FFLL	Fracture Forming Limit Line
FLC	Forming Limit Curves
FLD	Forming Limit Diagram
FSPIF	Feature-assisted Single-Point Incremental Forming
GTN	Gurson-Tvergaard-Needleman
IEMI	Institute of Engineering, Medical and Industrial
ISF	Incremental Sheet Forming

ISMF	Incremental Sheet Metal Forming
K	Strength coefficient
MK	Marciniak–Kuczynski
n	strain hardening coefficient's
ORB	Oblique Roller Ball
R	normal anisotropy index
RD	Refinement/Derefinement
RESS	Reduced Enhanced Solid-Shell
r_n	Lankford coefficient
RSM	Response Surface Method
S4R	shell element with reduced integration
SPIF	Single-Point Incremental Forming
SQP	Sequential Quadratic Programming
STL	StereoLithography
TPIF	Two Point Incremental Forming
TTS	Through-Thickness-Shear
UTM	Universal Testing Machine
UTS	Ultimate Tensile Strength
VRB	Vertical Roller Ball
WJ	Water Jet forming
YS	Yield Strength

CHAPTER ONE

INTRODUCTION

1.1 Background

Sheet metal forming is a widely used and powerful manufacturing process nowadays. Finished products have good quality, were geometrically accurate and parts were prepared to be used. Additionally, it was used for large consignments which repay the tools cost, producing large extents of components during a short time interval. However, the opportunity to use conventional stamping processes to build low production of batches or personalized prototypes was naturally very affluent.

In Research and Development processes, prototype manufacturing was a significant step in product development. Subsequently, it was imperative to shorten the product's life-cycle and costs in its initial development. As a result, the Incremental Sheet Forming (ISF) technology looks as a new possibility to decline the cost problem in small volume production. It introduced the use of metallic sheet for small batches production in an economic way without the need of expensive or dedicated tools. In fact, the study and development of this process have been growing over the last two decades.

Incremental Sheet Forming (ISF)

The description of "incremental forming" asylums numerous techniques with common features. This initial section will focus on the generality of the process as well as on its definition. The following clarification would describe the resemblances between different alternatives of Incremental Sheet Forming (ISF). The conventional spinning and shear spinning were forming processes closely related to ISF, but there were some fundamental dissimilarities. In general, with the spinning perception the workpiece was clamped to a gyrating mandrel while the spinning tool movement deforms it by means of several increments Emmens *et al.*(2010). This process was appropriate for axisymmetric products only. In the conventional spinning the component was formed through a series of extensive strokes with a forming tool. Shear spinning was similar, however the basic discrepancy was the fact that the tool was in permanent contact with the workpiece Jeswiet *et al.* (2005). Other consideration which distinguishes both variants of spinning was the final sheet thickness. In conventional spinning the final thickness was kept constant while in shear spinning the thickness was considerably abridged due to stretching mechanisms Wong *et al.*(2003); Emmens *et al.*(2010). The final produced component using the spinning method was always axisymmetric and the mould in the rotating mandrel determines the final shape.

Since the 20th century until nowadays, many patents and developments have been performed on the ISF topic. The interest has been growing due to its advantageous applications, focused on the flexibility offered by the process. Nevertheless, the preliminary idea of ISF with a single tool was firstly stated in the patent of Leszak, (1967). The real approximation to the well-known current ISF was reviewed by Mason in 1978 Emmens *et al.* (2010) for application on small batches of customized parts. The concept proposes the use of a single spherical/hemispherical tool with numerical control in three axes. The use of this method was possible with the advance of technology, more specifically with the appearance of numerical control machines. Later, the work of Mason was continued in Japan and it gave rise to new patents Emmens *et al.* (2010).

The ISF processes evolved more intensively since the 90's and new variants were developed and patented Emmens *et al*. (2010). In the literature, ISF processes are referenced as belonging to a group called Asymmetric Incremental Sheet Forming (AISF).

The AISF concept can include different configurations Jeswiet *et al.* (2005), as shown Fig. 1.1. Its variants allow producing complex sheet components by CNC drive system of a simple tool, with or without the combined use of simple dies. The main common aspect in these variants is the use of a hemispherical forming tool in constant contact with the workpiece. The sheet is also clamped at its edges using a blank holder (Fig. 1.1). During forming, the tool travels along the workpiece, following a specific trajectory determined by the user.

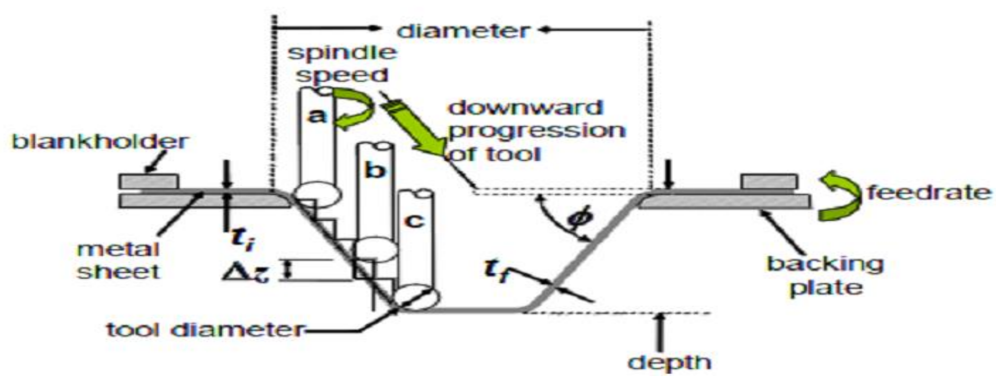

Figure 1. 1 Asymmetric incremental sheet forming variants Jeswiet *et al.* (2005).

Single Point Incremental Sheet Forming (SPIF)

Single point incremental forming (SPIF) is a novel pioneering and viable solution for the rapid prototyping and the manufacturing of small batch sheet parts. The process was carried out at room temperature (cold forming) and requires a CNC machining centre, a hemispherical headed tool and a simple support to fix the sheet being formed. The flexibility of the process was mainly related to the fact that SPIF does not require a dedicated die to operate as compared to other forming processes. Consequently, the lead-time and cost of tooling along with the die cost can be avoided. This technique allows a relatively fast and cheap production of small series of sheet metal parts Ham and Jeswiet, (2005). The process flinches from a flat sheet metal blank, clamped on a sufficiently rigid dress and mounted on the table of a CNC machine. It can be used for forming of symmetric and non-symmetric parts in a wide range of thicknesses from 100 microns up to several mm Vollertsen et al. (2007)

The incremental step-down size (Axial depth, Δz) is the amount of material deformed for each passage of the forming tool (alike to depth of cut in machining). The step size affects both the machining time and the surface quality of the part produced and its value is set in CAM software. Feed rate is the speed at which forming tool moves around the mill-bed (similar to cut rate in machining) and it directly affects the machining time for forming. It is measured in mm/minute. The spindle speed is the rotation speed at which the tool rotates. The spindle rotation speed varies the heat generated due to friction at the contact point between the material and the forming tool and its values are also set in the CNC milling machine along with the CAM software. The angle between the horizontal, under formed sheet metal and the deformed sheet metal is defined as the forming angle (Ø). This is the line of the deformed blank sheet metal as shown in Fig. 1.1. The forming angle can be used as a measure of material formability. The maximum angle (Ø max) is the greatest angle formed in a shape without any failures Ham and Jeswiet, (2006).

The SPIF concept represents a breakpoint with traditional forming processes. The classic press-stamping process generally deforms the sheet metal in only one stroke (even if multiple steps can occur). The sheet was forced by a punch against a mould, stretching the blank to the desired shape, while the edges were restrained by a blank holder, allowing however some sliding. In the SPIF process, on the other hand, the sheet was gradually deformed by a localized force. The final part was obtained by a toolpath strategy according to the desired final shape. Schematically, Fig. 1.2 illustrates the SPIF process setup.

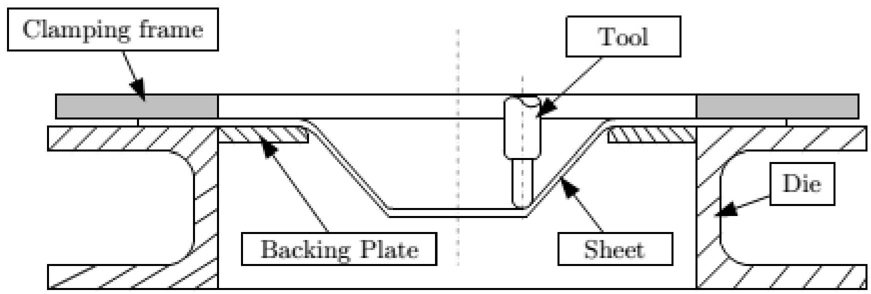

Figure 1. 2 Single Point Incremental Forming (SPIF) setup Sena *et al*., (2011).

The sheet was previously clamped along its edges using a clamping frame (blank holder). A backing plate was essential to provide an angle change at clamped region and decrease the springback effect during the forming progress. Springback phenomena could also be abridged using a compensatory algorithm Allwood *et al.* (2010). The tool was guided through a numerical control system, which describes the toolpath according to the desired final shape. The toolpath could be controlled by using a CAD/CAM software, where a variation in the final shape could be fast and inexpensive. The pre-programmed contour conglomerates the continuous contact of the tool along the sheet surface with successive small downward displacements. After each vertical increment, a new contour started in the next horizontal plane.

In general, the main practical setup of the SPIF method comprises in the following steps: first, the final product is modelled by a CAD (Computer Aided Design) software, which allows creating a neutral file selected by the user. Next, the neutral file was exported to a CAM (Computer Aided Manufacturing) package. The first step for CAM package was to check the CAD file to visualize potential errors and then the toolpath was created Jeswiet *et al*., (2005). Next, the sheet was rigidly fixed on the frame, and the forming tool was controlled with a three-axis CNC (Computer Numerical Control) software machine. Afterwards, during the process, the forming tool was in permanent contact with the sheet surface and moves vertically in each contour. Finally, the spherical/hemispherical tool repeats all these operations until the end of the toolpath, to obtain the final product.

Summarize SPIF process benefits according to Jeswiet *et al.* (2005) and Hirt *et al.*, (2006) are the component can be directly formed from the CAD software, the process can be used in rapid prototyping to produce small number of parts in sheet metal and in polymers, it does not require expensive tools, i.e., punch and die. However, a backing plate can be necessary to create an angle change near the clamped region, a conventional CNC milling machine can be adopted for this process, the component sizes are limited to the machine table size, the operation is quiet and relatively without noise, the nature of the process involves deformation mechanisms that increase the material formability, the changes on the component design can be rapidly accommodated changing the CAM file. The limitations are a large forming time compared with the conventional stamping process, process limited to small production batches or prototypes, it is mandatory the use of multistage forming for steep wall angles, increasing the manufacturing time, some springback can occur after unclamping the component, lower geometric accuracy, particularly near the convex radii and bending edges areas.

Aluminium and its alloys are used in aerospace, automotive, appliances, and food packaging due to their high strength to weight ratio and corrosion resistance. Aluminum–magnesium–silicon (Al–Mg–Si) alloys denoted as 6XXX series are medium strength heat treatable alloys. They have excellent formability and good corrosion resistance characteristics Murtha, (2010). There has been considerable industrial interest in these alloys because two-thirds of all extruded products are made of aluminum, and 90% of those are made of 6XXX series alloys. In this series, AA6061 is one of the most widely used alloys Buha et al. (2016). Due to these reasons, an AA 6061 alloy sheet is considered in this research for the formability study on SPIF.

Formability in SPIF can be defined in terms of the maximum draw angle and it is measured in terms of a tangent line from the unformed sheet surface to the deformed surface. Knowing $Ø_{max}$ can be the first step in determining whether the SPIF process is a good forming application for a given material and sheet thickness. The forming limit curve in incremental forming is quite different from the corresponding one in conventional forming as shown in Fig. 1.3. Much higher strains may be achieved in incremental forming than in traditional processes. Such circumstance can be justified taking into account the peculiarity of the process mechanics. Plastic deformation induced by the small size punch is strongly localized and confined to the close vicinity of the contact area, and then it incrementally progresses as the tool moves along the assigned path. As a consequence higher strains can be attained in the material before that fracture occurs. Furthermore the forming limit curve for incremental forming processes typically has the shape of a straight line with a negative slope in the first quadrant of the Forming Limit Diagram Ham and Jeswiet, (2007).

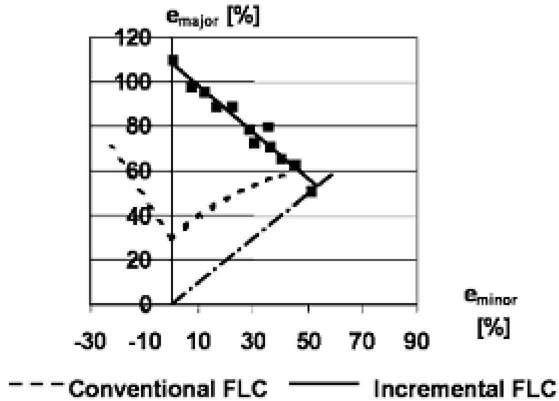

Figure 1. 3 AA 1050-0 Forming Limit Diagram Ham and Jeswiet, (2007)

1.2 Statement of the Problem

Newly evolving Incremental Sheet Metal Forming (ISMF) process, in the similar manner like previous forming technologies, comprises various affecting input parameters in-terms of step depth, tool diameter, feed rate, and material thickness, type of materials, type of tool, tool geometry etc., that accommodatingly excite the features of finished parts. In enactment of development of ISMF forming technique to an industrially reliable and economically feasible technology, it is highly vital to develop an appropriate empirical model. In the last two decades, extensive research has been carried out by investigators but still, there is a shortage of thorough understanding of the effects of the process parameters and their interactions in the SPIF process which is very vital in optimizing the process for better response qualities Behera *et al*. (2014). To alleviate these contradictions detailed investigation of process parameters and their respective interactions were in need.

The main problem in the formability analysis of such a process of a relatively large number of involving input parameters (step depth, tool diameter, feed rate, and material thickness) is limited ability of the developed empirical model to deal with the diversity of optimized process arrangements according to the different design necessities based on experimental and numerical investigations. Generally, formability analysis has considered a limited number of varying input parameters (step depth, tool diameter, feed rate, and material thickness) to investigate the formability of material under a limiting assumptions or special arrangement of the experiments. Additionally, preceding research concerning the effect of predictor parameters (step depth, tool diameter, feed rate, and material thickness) upon formability analysis of sheet material by ISF on AA6061 aluminum alloy, primarily have not taken into account the interactional effects of parameters (tool diameter and feed rate, sheet thickness and step depth, feed rate and sheet thickness, sheet thickness and tool diameter, feed rate and step depth, and tool diameter and step depth).

1.3 Objectives

1.3.1 General objective

The general objective of thesis is to:
Study material formability, maximum wall angles and analyze the performance of the SPIF process parameters impact on AA6061 aluminum alloy.

1.3.2 Specific objectives

The specific objectives of this thesis are to:

- Establish a set of experiments to determine the forming limits and the maximum forming angles for the aluminum alloy AA6061 materials in relation with SPIF forming parameters such as step size, tool diameter, feed rate, and material thickness
- Develop an empirical model to predict the formability based on maximum wall angle and thinning phenomenon
- Determine the formability of the deformed parts in terms of optimum depth, thickness reduction and maximum wall angles
- Estimate the influence of input process parameter and their interactions on wall thickness distribution and maximum wall angles of AA6061.

1.4 Significance of the Study

The achievements of this thesis directly benefits Institute of Engineering (Automotive and Aerospace), Medical and Industrial (IEMI) by introducing new strategies in forming sheet metal and/or other sheet material without using mould or die in producing desired parts. This thesis is the attempt of analyzing and optimizing incremental formability on aluminum alloys AA6061 which plays an important role for IEMI in experimenting on other material as well as improve the quality of final part. Moreover, this thesis allows continuing researching and developing incremental sheet forming for medical implant and automobile application in the future.

The direct beneficiaries this thesis are design engineers, researchers, automotive industries, aerospace industries, medical industries as biomedical applications e.g., medical implants and industrial appliances manufacturer e.g., Solar cooker

1.5 Scope and Limitations

The work done within this thesis could be divided in two main areas: Firstly, experiments and numerical analysis would be conducted based on general single point incremental forming experimental design and numerical analysis on the same material using simple shape, particularly Varying Wall Angle Conical Frustum (Truncated Cone), aiming the study of the process as well as to analyze the single point incremental forming result proposed in the desired parts. Secondly, mechanical testing had to be performed of the AA6061 aluminum alloy to study the material characteristics and to use the obtained information to plot the fracture forming limit line (FFL).

The limitation like loss of AA6061 grade material, loss of well-organized heat treatment center for tool treatment, lack of milling machine with five axis and the current COVID-19 situation delayed the accessing of AA6061 material.

1.6 Organization of Thesis

The present thesis is alienated into five chapters.

The first chapter provides a summarized review on the field of Incremental Sheet Forming (ISF) and its variants. The process concept is introduced and practical aspects are described for each variant. A detailed description is given on the SPIF process. The main research topics are here defined along with the research objectives.

The second chapter presents an updated literature review of the state of the art of SPIF process. It aims a review based on the experimental developments and an in-depth lecture in the numerical simulation analysis. The results presented are from recently published works.

The third chapter gives a comprehensive description of the experimental techniques, theoretical thinning, Numerical simulation and Design of Experiment utilized for material characterization and formability limits determination, an overview of the SPIF experimental set-up and finally a short description of the CAD/CAM design development.

The fourth chapter presents the results and discussion related factors as indicator of formability of AA6061 based on detailed analysis through straight groove test, Varying Wall Angle Conical

Frustum, effects of chemical composition, Maximum Wall Angle, Thinning effects and Optimization of the process parameters.

Lastly, general conclusions and future work are given in chapter five. It is expected that the present work contributes towards a better understanding of the formability, forming limits and thinning effects of SPIF manufacturing process.

CHAPTER TWO

LITERATURE REVIEW

Single point incremental forming (SPIF) is an emerging technique within sheet metal prototyping and small batch production, as previously outlined. Research interest has grown over the last few years, both experimentally and numerically. According to the current state of the art review, it can cover a range of relevant topics presented in distinct sections below. The present literature review deals with the state of the art on important process parameters, the experimental and numerical developments of SPIF process.

2.1 Important process parameter in the SPIF

A number of novelists have studied the final product in order to analyze the influence of several parameters involved in the SPIF process. In summary, the following forming parameters are important in SPIF: the geometry of the forming tool, the sheet material, the sheet thickness, the toolpath, the stepdown increment size, the forming speeds (rotation and relative motion) and lubrication Kim and Park, (2002); Kopac and Kampus, (2005); Cerro *et al.* (2006); Duflou *et al*. (2007b); Durante *et al.* (2009); Ambrogio *et al.* (2010b).

2.1.1 Forming tool

Characteristically in SPIF process the tool tip is spherical and guarantees a continuous contact point across the metal sheet surface. The pertinent variables to the forming tool are its shape, dimension, and material. This variable combination disturbs the surface quality, the time production, and the geometry limitation of the final component. In most applications, the spherical tip is solid and made out of steel. However, to reduce friction and increase tool lifetime can be used other options, such as, surface coating or a free rotating ball tool tip. The application of a polymeric material on the tool tip is used to avoid chemistry reactions or to improve surface quality. There is a wide range of tool diameters, from 4 mm, until a large spherical diameter as 100 mm. The spherical tool diameter values usually are between 4 mm to 15 mm Jeswiet *et al.* (2005). Therefore, the optimum tool depends of the product shape, the type of material and the depth at which then spherical tool will work. The diameter depends also on component dimension and the negative slope (concave shape) of the wall angle. In the wall angle of the component (α) there is a point from which the tool diameter contact is maximum (Fig. 2.1). This instant occurs when the contact point is tangent to the spherical surface. Fig. 2.1 illustrates the tangential wall limit with a spherical tool.

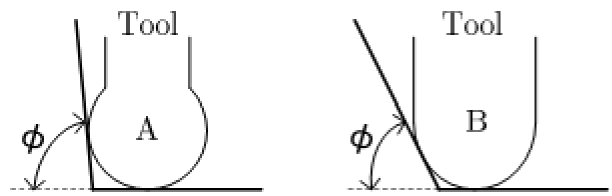

Figure 2. 1 Wall contact with the forming tool Jeswiet *et al.* (2005)

To attain a member with a vertical wall angle, it is necessary to select a forming tool with larger diameter than the sphere body support. The impartial is to avoid contact between the sheet wall and the sphere support, as presented in Fig. 2.1A. The body support of the hemispherical head is used to mount the tool on the CNC milling machine shaft. Fig.2.1B presents a tool configuration used to build a part with a small slope wall. Experiments have demonstrated that smaller diameter tools allow higher metal sheet formability than the use of tools with large diameter Kim and Park, (2002); Jeswiet *et al.*, (2005); Bhattacharya *et al*. (2011).

Ham and Jeswiet (2006) have premeditated the effect of the spherical diameter on the maximum wall slope angle. The research work confirmed a substantial increase on the maximum wall angle when tools with smaller diameters are used. The high formability with small diameter tools is a consequence of the force concentration and strains on a small area.

2.1.2 Material and sheet thickness

The material and the sheet thickness may limit the formability. The formability involved is the result of the sheet characteristics, its material and its geometry. Fratini *et al.* (2004) explored the effect of material proprieties on the formability. The tensile test was used for each selected material to determine its parameters. The material parameters were the following ones: Lankford coefficient (r_n), ultimate tensile strength (UTS), strength coefficient (K), strain hardening coefficient's (n), and the elongation percentage (A%). From their SPIF experiments, for each material and using statistical analysis, they determined the influence of the above-mentioned material proprieties. Their analysis concluded that the interaction between the strength coefficient (K) and strain hardening coefficients (n) had the utmost influence on formability. Generally, higher hardening coefficients will provide higher formability.

Ham and Jeswiet (2006) executed a research about the influence of the sheet thickness on the maximum wall angle and showed that increasing the thickness contributes to increase the wall angle. The maximum wall angle defines an indicator of formability. In this work, the interaction between the increasing thickness and the tool size decrease was analyzed. The research showed a significant improvement in the wall angle when the tool diameter decreases and the sheet thickness increases.

2.1.3 Forming speed

The tool rotation speed and the travel velocity over the sheet surface influence the sliding friction and the frictional heating at the tool/sheet interface. The process time and the final surface quality of the part are the final results which evaluate process performance. The tool relative motion over the sheet is directly proportional to the heat generated by friction. Increasing the speed improves the material formability due to the heating. However, there are negative effects, like higher speed rate, generates higher surface roughness, increases the tool wear and the lubricant film disappears faster. The high rotational velocity increases the probability to develop marks on the sheet surface Jeswiet *et al.* (2005); Ambrogio *et al.* (2010b); Hamilton and Jeswiet, (2010).

2.1.4 Toolpath and vertical increment

Numerous experimental studies have been performed to find an optimum toolpath which gives the best results in terms of surface quality. The toolpath and the vertical increment are defined together on the CAM package. These parameters have direct impact on the surface finish, dimensional accuracy, thickness variation, formability, and processing time. Ham and Jeswiet (2006) used the forming maximum angle to measure the material formability of AA3003. In their work, they have analyzed the influence of the vertical step in the maximum wall angle and it was concluded that there is no significant effect on the final wall angle. Hence, it was shown that the vertical increment has an insignificant influence on the formability.

Attanasio and coworkers Attanasio *et al.* (2006; Attanasio *et al.* (2008) accomplished two different toolpaths. In the first experiment the tool followed a series of consecutive contours using a constant vertical step (ΔZ), Fig. 2.2.a. With this strategy, the sheet is marked at the transition point between consecutive toolpath contours. The second toolpath type tested an experiment with constant "scallop height" (*h*), Fig. 2.2.b. The tool follows a series of consecutive contours with a variable vertical step (ΔZ) in order to keep a constant value of scallop height (*h*). This strategy avoids the marked transition points and improves the final surface quality.

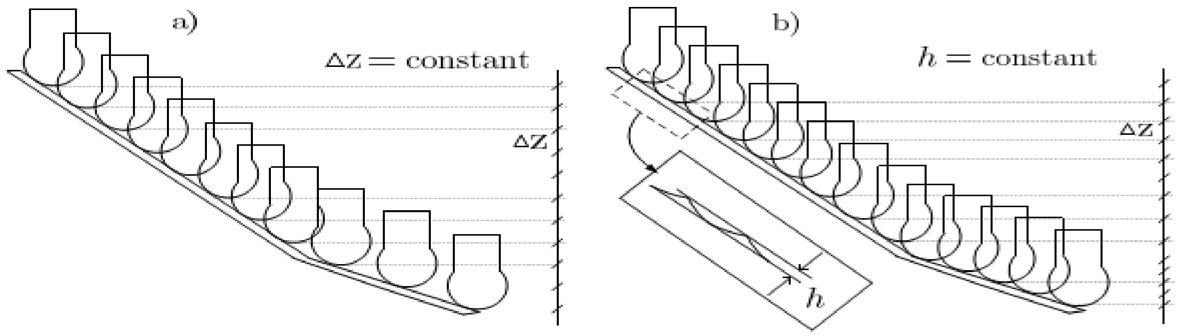

Figure 2. 2 Schematic representation of a) constant vertical incremental (ΔZ) and b) constant scallop height (*h*) Attanasio *et al.*(2006; Attanasio *et al.* (2008).

The vertical step size inclines to be related with the wall angle and roughness at the sheet surface. A small step size requires more process time to form the component but the surface quality improves. These experimental investigations demonstrated how relevant is the toolpath with a variable step depth (depending on the part geometry). In particular, a correct value of the maximum step depth (ΔZ) and the scallop height (*h*) must be chosen in order to obtain good results in terms of surface quality, geometric accuracy and thickness of a final component.

2.1.5 Machinery used in SPIF

Equipment planned for SPIF covers different topologies of machines used in the industry and in academic research. The execution of SPIF process presents essential aspects: it uses a simple spherical/hemispherical tip to build different shapes and the main process feature is the numerical control of the tool axis. The axis control depends of the degrees of freedom (DOF) available on the machine. There are different equipment's to produce a component using the SPIF method, such as adopting a CNC milling machine, a robotic arm or a purposely built machine.

The most common applications to perform SPIF experiments has been carried out using an adapted CNC milling machine. Their advantages are the easy upgrade to work as SPIF machine, easily found in industry, considerable stiffness and large productivity rate. On the other hand, it offers a limited number of DOF Jeswiet *et al.* (2005). For instance, this choice is the one of

Shim and Park (2001), Filice *et al*. (2002), Jeswiet et al. (2002), Fratini *et al*. (2004), Ceretti *et al*. (2004), Ambrogio *et al*. (2005; 2010a; b), Kopac and Kampus (2005), Araghi *et al*. (2009), Dejardin *et al*. (2010), just to mention some research groups.

Nowadays, purposely built machines for SPIF process are commercially available, such as the one developed by the Amino Corporation Amino *et al*. (2002). However, a number of academic research groups have developed their own machine to perform the SPIF process. As examples, the machine from Julian Allwood's group at University of Cambridge Allwood *et al*. (2005) and the innovative prototype machine called SPIF-A at University of Aveiro (Alves de Sousa *et al*. (2014). This last referred SPIF machine introduced a Stewart platform Yau, (2001) adaptation, allowing six independent degrees of freedom. Fig. 2.3 exhibits the innovative prototype machine developed at University of Aveiro based on Stewart platform purposely adopted for SPIF.

Figure 2. 3 Prototype machine for SPIF from University of Aveiro Yau, (2001).

2.2 Experimental research and developments

In the last years, the SPIF process was intensively investigated and experimental evolutions allowed achieving accuracies at industrial level. The following experimental development overview includes the process optimization and the understanding of its physical characteristics, which influence the forming process.

2.2.1 Influence of SPIF parameters on formability and thinning

Jeswiet et al., (2005a) designates that formability in incremental sheet metal forming is much higher than the one reported in deep drawing. Most of the studies related to formability in ISMF are experimental in nature. Accurate prediction of formability helps in assisting better design of part geometry and corresponding tool path. It has been well accepted that conventional forming limits are not suitable for incremental forming even when path dependency of strains are considered. The forming limit of a sheet metal in conventional forming is defined to be the state at which a localized thinning of sheet initiates when it is formed into a product shape in a stamping process. Formability of sheet metals in conventional forming is at present characterized by the Forming Limit Diagram (FLD) introduced in 1960s by Keeler and Backhofen (1964). The forming limit is conventionally described as plot of major principal strain vs. minor principal strain. It must cover as much as possible the strain domain which occurs in industrial sheet metal forming processes. The curves are established by experiments that provide pair of the values of limiting major and minor principal strains obtained for various loading patterns (equi-biaxial, biaxial, plane strain and uniaxial). A schematic representation comparing the forming limit curves of conventional forming (stamping/deep drawing) with that of single-point incremental forming is shown in Fig. 2.4a. It can be clearly seen that the forming limit curve for incremental forming is a straight line with a negative slope in the positive region of minor strain whereas the conventional one is present in both the regions of minor strain. Deformed grid obtained during incremental forming shown in Fig. 2.4b, c indicates that the deformation that occurs varies from plane strain to biaxial stretching.

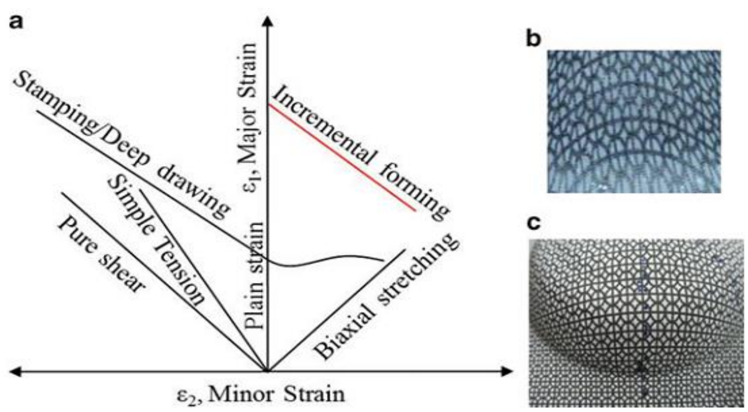

Figure 2. 4 Schematic representation of forming limit curve in SPIF against conventional forming Keeler and Backhofen, (1964).

Kim and Park (2002) have used the groove test mentioned above to study the effect of different process parameters on the formability of fully annealed Al-1050 sheets by conducting experiments, and their trends are presented in Fig. 2.5. It is also reported that the use of freely rotating ball tool enhances the formability as the friction along the tool work interface reduces.

Formability decreases with increase in tool diameter and incremental depth. In addition, they carried out finite element analysis using PAMSTAMP – explicit to understand the effect of process parameters on the deformation.

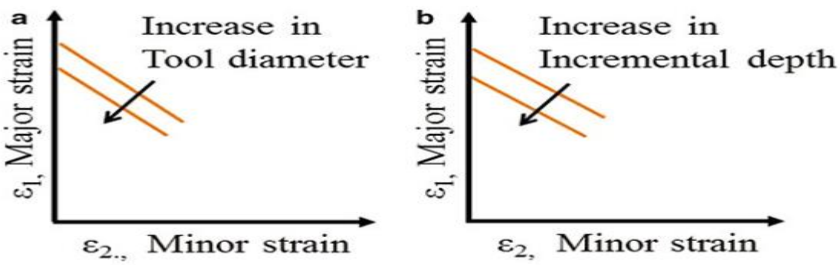

Figure 2. 5 Variation of formability with tool diameter and incremental depth during groove test Kim and Park, (2002).

Filice et al. (2002) proposed experimental tests aiming at achieving different straining conditions that occur in incremental forming to study the formability. They formed a truncated pyramid to obtain the conditions of plane strain deformation and proposed a geometry with two straight grooves perpendicular to each other (tool path shown in Fig. 2.6) to achieve almost pure biaxial stretching condition at the center of the geometry. In addition, they proposed to form truncated cone geometry with a spiral tool path explained earlier to achieve the conditions between plane strain and biaxial states. In all the cases, they formed the components using hemispherical ended tool till failure and generated the forming limit curves for incremental forming.

Later, Fratini et al. (2004) have carried out experimental study to understand the effect of material properties on the formability in SPIF for commonly used sheet materials namely, copper, brass, high-strength steel, deep drawing quality steel, AA1050-O, and AA6114-T4, in sheet metal industry. They measured strain-hardening constant (K), strain hardening exponent (n), normal anisotropy index (R), ultimate tensile strength, and percentage elongation (%PE) of all the materials by conducting tensile tests. Truncated cones and pyramids of varying wall angles were formed till failure, to study the influence of abovementioned process parameters on formability of incremental forming and perform statistical analysis. Based on the analysis, they concluded that strain-hardening exponent, strain-hardening constant, and normal anisotropy index have high, medium, and low influence respectively. Ultimate tensile strength has negligible influence, whereas percentage elongation has medium influence. Among the interactive terms, only interaction between strain hardening exponent with strain-hardening constant and percentage elongation are significant, whereas the others are insignificant. In addition, they reported the influence of same process parameters on conventional forming limit diagram also.

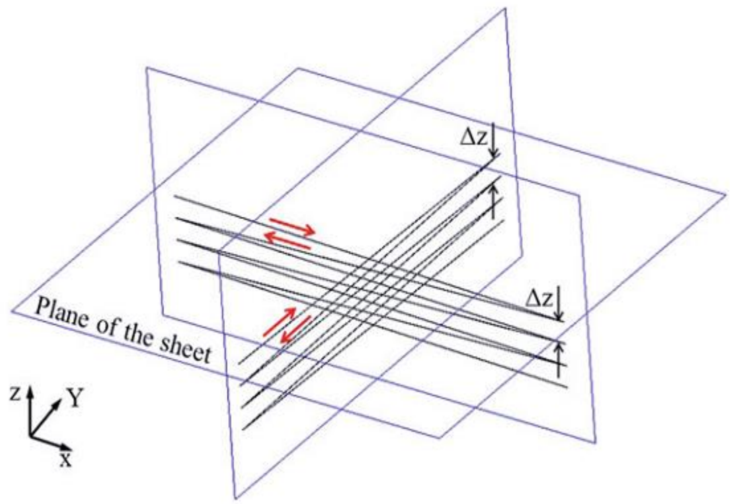

Figure 2. 6 Tool path to achieve biaxial stretching at the center of two perpendicular straight grooves Filice et al. (2002)

Ham and Jeswiet (2006) used two fractional factorial designs of experiments to study the effect of process variables on formability of AA3003. First set of design (wall angle, vertical step size/ incremental depth, base/component opening diameter, component depth, feed rate, and spindle speed) indicates that feed rate, spindle rotation speed, step size, and forming angle decide whether a part can be successfully formed or not. It was also reported that faster spindle rotation speed improves formability. Second set of experiments (vertical step size, sheet thickness, and tool diameter) reveals that vertical step size (they used 0.05, 0.127, and 0.25 mm) has little effect on the maximum forming angle. Material thickness, tool size, and the interaction between material thickness and tool size have a considerable influence on maximum forming angle. Later they Ham and Jeswiet, (2007) used Box-Behnken design of experiments to study the forming limits in SPIF. They considered five parameters, namely, material type (three different aluminum alloys), thickness, formed shape (cone, pyramid, and dome), tool size, and incremental step size, at three levels for the experimentation. Material type has significant effect; the one having lower ultimate tensile strength will have greater formability. Shape also has some influence on the formability as the type of deformation is dependent on geometry. Allwood et al. (2007) conducted experiments using Al 5251-H22 sheets to explain the reasons behind higher forming limits observed in incremental forming and shown that the lines joining corresponding points on the upper and lower surfaces of sheet formed by SPIF remain almost normal to the surface in meridional plane (Fig. 2.7), indicating that the deformation in this plane is predominantly pure bending and stretching. Whereas measurements indicated that there is a relative movement between corresponding points parallel to the tool movement direction, suggesting that shear occurs in this direction. Due to the presence of through- thickness shear, the tensile stresses responsible for fracture get reduced; hence, formability is higher in incremental forming.

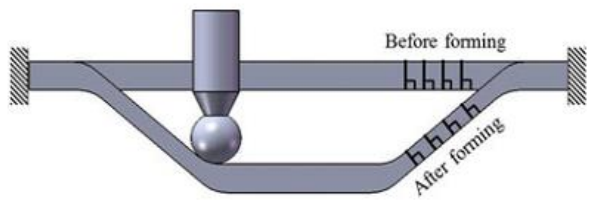

Figure 2. 7 Deformation behavior in meridional plane Allwood et al. (2007)

To lessen the number of experiments required to test the forming limits, Hussain and Gao (2007) considered an axisymmetric component with varying wall angles along the depth direction. The cross section of the component parallel to the incremental depth direction is chosen as circular profile, and the same is shown schematically in Fig. 2.8. Components are formed till the failure depth and quantified the formability as wall angle at that height. Later conical components with failure angle obtained using varying angle components mentioned above are formed, and it is concluded that formable wall angles obtained by forming conical cups are more accurate but time-consuming. This work is extended Hussain et al. (2007a) by forming components with different cross-sectional profiles, namely, elliptical, exponential, and parabolic, and found that the forming limits are different for different profiles (lowest for circular and highest for exponential). Based on the above observation, they concluded that the forming limits depend on history of forming in ISMF.

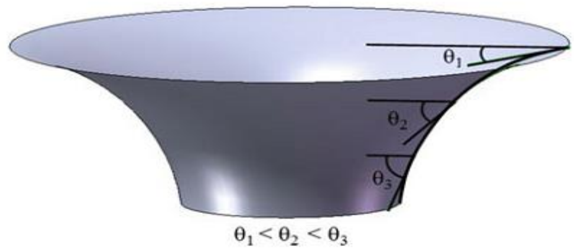

Figure 2. 8 Funnel geometry to evaluate formability Hussain and Gao, (2007)

Hamilton and Jeswiet (2010) studied and analyzed the effect of forming at high feed rate and tool rotational speed in SPIF. They concluded that tool rotational speed does not have significant effect during SPIF and forming at high feed (5,080–8,890 mm/min) produced similar thickness distribution as of low feed. Thus, higher feed rate (less forming time) can be used to reduce the forming time, making ISMF process suitable for industrial applications.

Bhattacharya et al. (2011) piloted experiments to study the effect of incremental sheet metal forming process variables on maximum formable angle. Box-Behnken method is used to design the experiments for formability study. From the experimental results it was concluded that during incremental forming, the formability decreases with increase in tool diameter. The formable angle first increases and then decreases with incremental depth. The variation in the formable angle is not significant in the range of incremental depths that are used in their work to produce good surface finish. To predict thickness during the SPIF, a simple model is proposed considering the overlap in deformation (Fig. 2.9a) and thus estimated the deformed sheet thickness more accurately. Ratio of mean stress value to the yield stress value for all the experiments conducted for formability study at the maximum formable angle is calculated by them using the force equilibrium analysis, and its value is found to be very close to unity at all conditions, hence, used the same as the failure criterion. Maximum formable angles predicted using a triaxiality criterion mentioned above for plane stretching conditions are in very good agreement with the experimental results (Fig. 2.9b). Duflou et al. (2007b, 2008a) have demonstrated that the use of local heating (using NdYAG laser) ahead of tool reduces the forming forces and enhances the formability of the material. They used TiAl6V4 sheets of 0.6 mm thickness. Cone with 56° wall angle and 30 mm depth is successfully formed with local heating, whereas the maximum angle that could be formed without heating using the same parameters is only 32°.

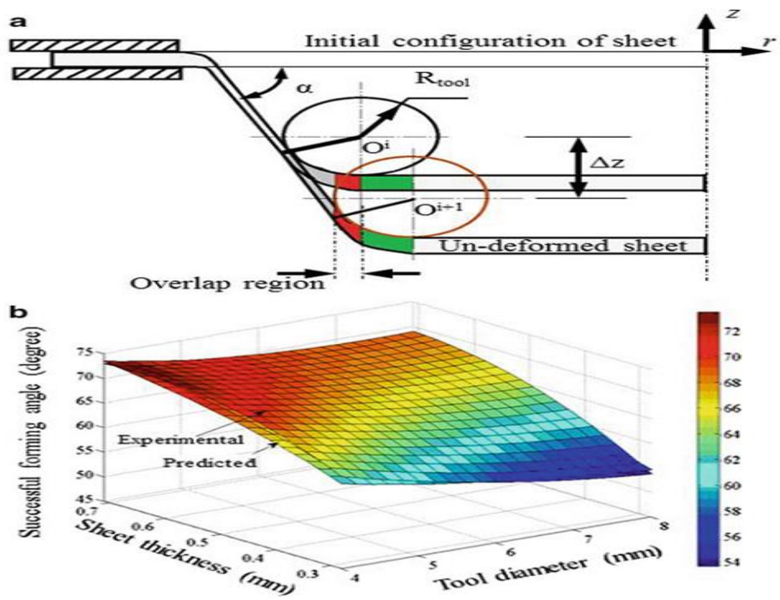

Figure 2. 9 (a) Schematic showing the consideration of overlap in thickness calculation. (b) Comparison of predictions of formable angle using triaxiality criterion with the experimental results Bhattacharya et al. (2011)

Park and Kim (2003) studied the formability of annealed aluminum sheet by forming different shapes using both positive and negative incremental forming. While forming a truncated pyramid with negative single point incremental forming, cracks occurred at the corners due to biaxial deformation, but no cracks appeared during positive forming (in positive forming a suitable jig support is used – Fig. 2.10). Strain measurements with the help of a grid indicated that in negative forming both plane strain and biaxial stretching are present whereas in positive forming only plain strain stretching is present.

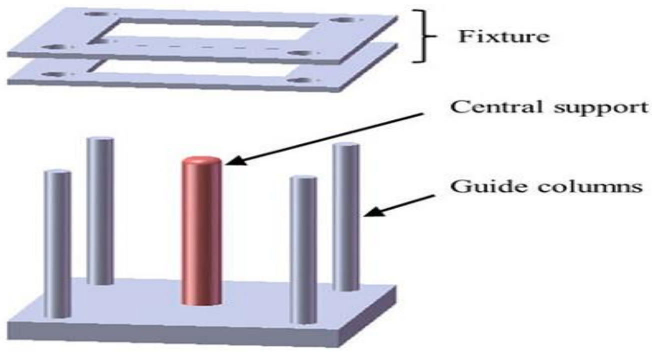

Figure 2. 10 Tool configuration used to form truncated pyramid in positive forming Park and Kim, (2003)

Once more, Jackson and Allwood (2009) have conducted experimental study to explain the deformation mechanism in SPIF (Fig. 2.11a) and TPIF (Fig. 2.11b, with full pattern support) to that of forming the same geometry using conventional pressing operation and to evaluate the validity of sine law and in turn to relate the thickness measurements to the deformation mechanics. For the abovementioned purpose, they used copper plate of 3 mm thickness, cut into two halves. Faces of each half are machined flat and 1.5 mm *1.5 mm grid pattern was marked. Later these plates were brazed together and used for forming conical components by SPIF, TPIF, and pressing. After forming the components are heated to separate the two halves. Then the formed geometry, thickness, and strains are measured. Local coordinate system shown in Fig. 2.11c is used for strain measurement, where m, θ, and t are meridional, tool movement, and thickness directions, respectively. After analyzing the measured thickness, geometry, and strains, they concluded that in both SPIF and TPIF, deformation is a combination of stretching as well as shear and the same increases with the successive tool laps in the meridional direction with the greatest strain component being shear in the tool movement direction and shear occurs perpendicular to the tool movement direction in both SPIF and TPIF but is more significant in SPIF. Deformation mechanism in SPIF and TPIF is significantly different from the idealized mechanism of shear spinning on which sine-law thickness is proposed.

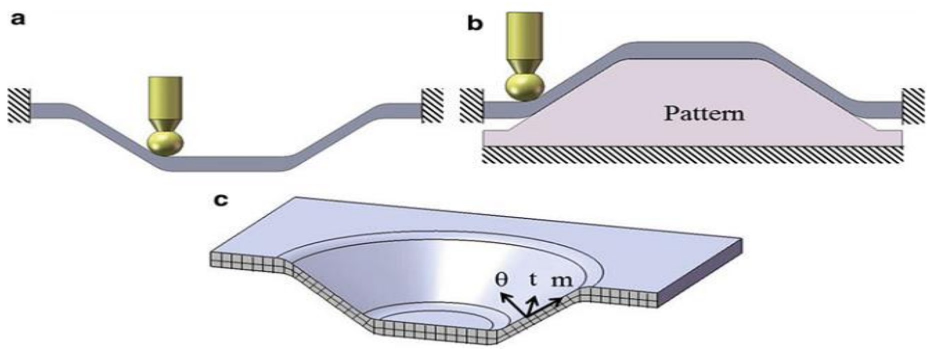

Figure 2. 11 Incremental forming configurations used for experimental study and grid for measuring Jackson and Allwood, (2009)

Single-pass SPIF can successfully form wall angles up to 70˚ for various aluminum as well as steel sheets of 1 mm initial thickness Jeswiet et al. (2005a) using suitable process parameters such as incremental depth, tool diameter, and forming speed. However, forming a wall angle close to 90˚ using SPIF is challenging. There have been a few attempts to increase the maximum formable angle by using multi-pass single-/two-point incremental forming Hirt et al. (2004); Skjoedt et al. (2008); Duflou et al. (2008b). Hirt et al. (2004) proposed and implemented a multi-pass forming strategy with partial support die (Fig. 2.12) to form components with steep walls which cannot be formed using single-pass incremental forming. The stages involved in their strategy are:

1) First, form the shallow angle component with final desired component height (Fig. 2.15b).
2) Next, the wall angle is increased in steps of 3-5˚ by moving the forming tool alternatively upwards and downwards as shown in Fig. 2.12c, d.

Exhausting the above strategy, first, they made a pyramidal component with 45˚ wall angle in the stage 1 and then formed up to 81˚ wall angle. Thickness measured by them revealed that the thickness at any location along the wall is more than the thickness predicted by sine law for 81˚. This can be attributed to the availability of more material as the component is formed to the final desired height in stage 1 and upward movement of tool in later stages. In addition, they performed finite element analysis along with damage criterion of Gurson-Tvergaard-Needleman to predict the damage evolution during incremental forming process and predicted that the damage increases with increase in tool diameter as well as incremental depth.

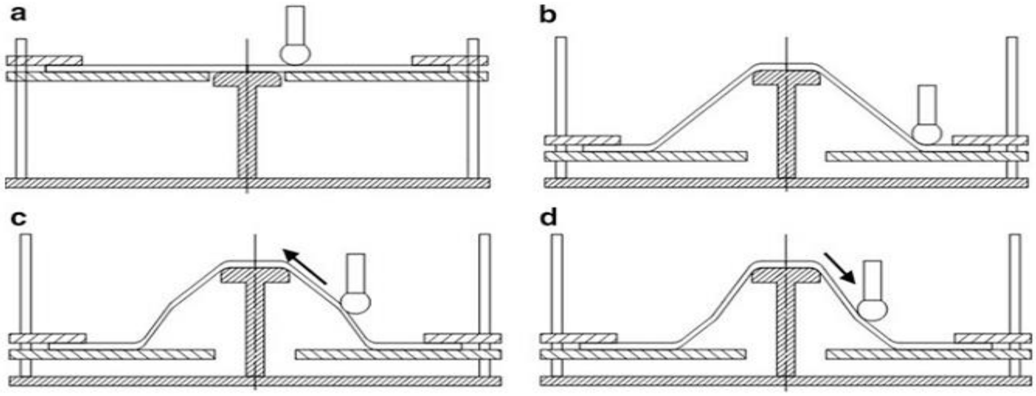

Figure 2. 12 Multistage forming strategy using TPIF to increase formable wall angle Hirt et al. (2004)

Kim and Yang (2000) compared two double-pass strategies for SPIF. One was based on linear blending, i.e., the intermediate shape was calculated to be at a height of 0.5 times the final height. In the other approach, they calculated the intermediate shape so that highly deformed regions in the final shape were subjected to lesser deformation in the intermediate shapes. Their methodologies yielded better thickness distributions than single-pass forming. They concluded that the double-pass forming method results in improved formability as well as higher mechanical strength of the formed component. Young and Jeswiet (2004) experimentally studied the effect of single-pass and double-pass forming strategies on the thickness distribution in forming a 70˚ wall angle cone. They concluded that double-pass strategy causes marked thinning at the flange near the backing plate. In addition, they concluded that the sine law will not predict the thicknesses correctly when multiple passes are used for forming angles exceeding 40˚. For better understanding of formability in terms of wall angle for different materials and process variables, a Table 2.1 is provided below.

Table 2. 1 Maximum formed wall angle for various parameters

S.No	Material	Sheet thickness t (mm)	Tool Diameter D (mm)	Incremental depth Δz (mm)	Formed angles (degrees)
1	Al 3003-O	2.1	-	-	78.1 (Jeswiet et al. 2005a)
2		1.3	-	-	72.1 (Jeswiet et al. 2005a)
3		1.21	-	-	71 (Jeswiet et al. 2005a)
4		0.93	-	-	67 (Jeswiet et al. 2005a)
5	Al 5754-O	1.02	-	-	62 (Jeswiet et al. 2005a)
6	Al 5182-O	0.93	-	-	63 (Jeswiet et al. 2005a)
7	Al 3003-O	2.1	4.76	1.3	77 (Ham and Jeswiet 2006)
8		1.3	12.7	-	75 (Szekeres et al. 2007)
9		1.2	10	0.5	73 (Ambrogio et al. 2007a)
10	AA 1050-O	1.0	18.0	0.3	70 (Ambrogio et al. 2006)
11		1	12	1	70 (Ambrogio et al. 2007a)
12	Aluminum	0.91	8.0	0.15	70 (Hussain et al. 2007a) (exponential profile)
13	Steel-DDQ	1.0	-	-	70 (Jeswiet et al. 2005a)
14	Steel-DC04	1	12	1	70 (Ambrogio et al. 2007a)
15	LY 12 M	0.91	8.0	0.15	66.0 (Hussain et al. 2007b)

2.2.2 Tool trajectory

In this logic, these solutions have been proposed in order to enhance SPIF performance at industrial level. In terms of toolpath strategy, it concerns the manufacture of products with high quality and accuracy, which are fundamental topics on which the interest of research groups are focused. According to the literature review, there are different proposals regarding the toolpath modification: real time toolpath optimization Meier *et al*. (2009); Rauch *et al*. (2009), iterative toolpath correction Fu *et al*. (2013); Hirt *et al*. (2004); Ndip-Agbor *et al*. (2015) and automatic toolpath generation methods, based on the behaviour of individual features, known as Feature-assisted Single Point Incremental Forming (FSPIF) Verbert, (2010) and their interactions (Behera *et al*., 2014).

Most of the researchers have used machining toolpaths available in commercial Computer Aided Manufacturing (CAM) packages for SPIF. Some efforts were made to specifically generate toolpaths for incremental forming from STL files. Typically, the toolpath generation is defined by a fixed or variable vertical pitch size (Δz) between consecutive separated contours (see Fig. 2.16a). This is also the most common technique used. Mainly, the disadvantages are scratches left at the transition points between each contour, giving origin to force peaks experimentally observed. Many authors have tested techniques to avoid the vertical step down at each contour and optimize the contours.

Blaga *et al*. (2011) investigated the influence of spiral and contour toolpaths on strain distribution, relative thinning and forces in SPIF. The material chosen to produce parts was DC04 steel, with 0.7 mm thicknesses. They observed homogeneous strain distribution and lower strain values with spiral toolpath than using other toolpath. Azaouzi and Lebaal (2012) optimized spiral toolpath using FEM combined with Response Surface Method (RMS) and Sequential Quadratic Programming (SQP) algorithm. Their objective was to reduce the manufacturing time and homogenize thickness distribution of an asymmetric part. The proposed strategy provided an optimal toolpath after 27 FEM calculations and the new trajectory length was reduced by 60 % in comparison to initial toolpath. The optimal solution has provided an improvement around 7 % of the sheet thickness distribution, due to the decrease of reaction forces. However, in order to find the shortest toolpath, the accuracy and the final surface quality of the component were deteriorated.

2.3 Numerical simulation developments

Currently, metal forming FEM simulation has been intensively used in Research and Development processes to better predict the structural behaviour during any component forming and its final geometry.

Numerical simulation of SPIF process can be very demanding and time consuming, mainly due to high nonlinearities: small contact area constantly changing between the tool and the sheet surface, as well as the nonlinear material behaviour combined with non-monotonic strain paths Eyckens *et al.* (2007). An accurate estimation from the numerical simulation results, specially related to the prediction of the formability during the forming process, is important as it contributes to the safe use of the hardware. Also, the formability prediction is particularly important in the case of using adapted machinery not designed for the SPIF process. For instance, the CNC milling machine adopted which does not support high axial forces. In the following, a review of numerical studies about different aspects of the simulation found is presented.

2.3.1 Integration algorithms: Explicit and Implicit

The FEM is an approximation technique which computes the solution of algebraic equation systems, based on equilibrium equations, which depend on the problem type which can be static or dynamic. The integration of these equations over time can be based on two different integration schemes: explicit or implicit. Both solution procedures are commonly available in commercial FEM codes, having been investigated for SPIF process simulation in the literature. The explicit integration is a dynamic approach which gives the equation system solution without request of an iterative procedure. The algorithm scheme uses a diagonalzed mass matrix and the final force balance is not checked. The differences between the internal and external forces are used to calculate the nodal acceleration, velocity and the displacement. This method is conditionally stable, which means that there is no check of unbalanced forces and the solution converges as long as the increment size is smaller than the critical value. The most important advantage of the dynamic explicit scheme is the fact that it is not necessary to check the unbalanced forces due to no convergence control. Consequently, the computational efficiency increases, the memory requirement and the programming complexity are lower than with the static implicit scheme. However, the disadvantages are: the explicit time integration solution converges if the mass matrix is diagonal and the simulation performance depends of the number of elements in the mesh. It is claimed that the error introduced by the diagonalzed mass matrix can be compensated by the type of integration scheme of the element. This approach can leads to an inconsistent computation of stress and springback Tekkaya, (2000).

Bambach *et al*. (2007) have carried out FEM analysis of SPIF process with ABAQUS/Explicit, for optimizing the toolpath. Those authors compared the values of sheet thickness and geometry accuracy with the experimental results, along a radial section of a conical shapes. The blank was modelled with shell finite elements and five analyses with varying friction coefficients, from 0.0 to 0.5 on the contact surface between tool and sheet. As a result, the authors have shown that no considerable influence on the prediction of geometry and thickness was found, regarding the five different values of friction coefficients chosen. Resorting to an explicit scheme combined

with mass-scaling (with a time step of 10^{-5} s), the results did not considerably deteriorate. However, the calculation time increased from 30 minutes to more than three hours.
Yamashita *et al.* (2008) have used the dynamic explicit finite element code LS-DYNA to perform a quadrangular pyramid with variations in its height. According to the results, the density of the sheet material and the travelling speed of the tool cause inertial effect on deformation. They were pre-examined and optimized to determine the computational condition to use in the simulations in LS-DYNA, to reduce the computational time. The conclusion was that numerical simulations using explicit scheme might be used for the toolpath optimization of the SPIF process.

2.3.2 Finite element types

Bambach and Hirt (2005) tested the performance of different Finite Element types available in ABAQUS software package. The finite elements used were all types of solid elements available and a shell element named S4R. The finite element S4R is a shell element with reduced integration. More details of the finite elements chosen can be found in the user manuals of ABAQUS elements library (ABAQUS 6.5). The numerical simulations were performed varying the elements types on the benchmark part, which consisted into an axisymmetric cup made of 1.5 mm DC04 steel. The toolpath consisted into five circles with a vertical step of 5 mm, which described a cone opening from the centre of the toolpath with a d=0mm at z=0 mm to d=115 mm at z=-25 mm. Fig. 2.13 exhibits schematically an alternative toolpath for a vertical wall angle cone.

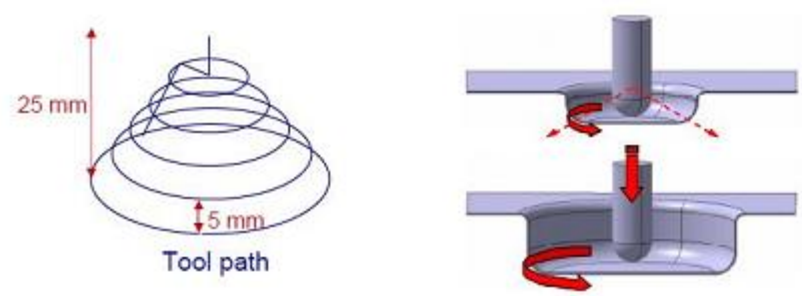

Figure 2. 13 Schematic representation of an alternative toolpath Bambach and Hirt, (2005).

The number of elements used in the in-plane mesh discretization was kept constant for all simulations performed with different element formulations. For solid elements meshes, only two layers in the sheet thickness direction were used which is a minimum for modelling the bending state present in SPIF. With such a choice it is without surprise that the results showed that the finite element with the best results in terms of shape accuracy were the simulations performed using shell element S4R (plane stress).

Sena *et al*. (2011) validated the results coming from numerical simulations of SPIF process using the reduced enhanced solid-shell (RESS) formulation Alves de Sousa *et al*. (2007), and compared it with results from solid finite elements available in ABAQUS software ABAQUS, (2005). In this preliminary work, isotropic hardening and implicit analysis were considered. The experimental results were used as reference to assess the effectiveness of several finite element formulations: the RESS formulation and a set of hexahedral finite element options, namely C3D8 (full integration), C3D8R (reduced integration) and C3D8I (full integration with incompatible deformation modes) available in ABAQUS. From the user point of view the main differences between ABAQUS solid elements and the RESS element was the possibility to vary the number of integration points through the sheet thickness, in the latter formulation. For ABAQUS solid elements, the number of layers through the thickness direction must be increased in order to have more than one (C3D8R) or two (C3D8/C3D8I) integration points per layer in this direction. Concerning the role of the finite elements adopted here, it was concluded that reduced integrated solid element has significant error when simulating the SPIF process Sena *et al*. (2011).

2.3.3 Constitutive laws

Bambach and Hirt (2005) tested two different hardening laws in simulations of a cylindrical component. The authors have used isotropic and mixed (isotropic/kinematic) hardening laws, in order to verify its results sensitivity. Results obtained with the mixed hardening law presented a more accurate prediction than using a simple isotropic hardening law. However, it depends on the material sensitivity to Bauschinger effect. Consequently, a complex law requires a large number of parameters which can be difficult to identify. The accuracy of the material parameter set has a huge influence on the numerical results.

Bouffioux *et al.* (2008 a; b; 2010) used a specific inverse method for adjusting the material parameters with the experimental measurements. The main concept consisted in FEM simulations of simple tests involving the SPIF specificities. The inverse method was coupled to an in-house code named LAGAMINE in order to fit the material data and the material used was AA3103-O. Firstly, a set of material parameters were adjusted by inverse method using classical tests, tensile, monotonic shear and cyclic shear tests. The Swift hardening law was coupled with a Hill yield locus. A new identification procedure adjusted the material data using both, tensile test and an indent test corresponding to the first step of the line test. The results of the line test simulations, using two different kinematic hardening models, showed an acceptable good correlation between the predicted and measured tool force, especially for the first two steps of the line test. From the comparison between LAGAMINE in-house code and implicit scheme of ABAQUS software, they demonstrated that the material parameters identified depended on the stiffness of the solid element.

2.3.4 Interaction between tool and sheet

Eyckens *et al.* (2008) and Eyckens (2010) used ABAQUS/Standard implicit for FEM simulation of SPIF. The authors performed Finite Element analysis of three different mesh model scales for each of the four cone shapes with different wall angles, 20º and 60º, using AA3003-O sheet. The first sheet mesh scale is referred as the global model (GL) modelling only a sheet section of 40º and using a relative coarse mesh with 3 layers of elements through thickness. The second large Sub-model (S1) considered only a small section from the central region of GL, also using 3 layers of elements. Finally, the small sub-model (S2) is located at the centre of S1 sub-model, and consisted in 5 layers of elements. All scales were modelled with a reduced integration brick element named C3D8R from ABAQUS package. The material was considered isotropic described by Swift hardening law in combination with the isotropic von Mises yield criterion. It makes an important contribution to the overall contact, even when the wall angle was large as 60°. At very low wall angles, such as 20°, it was responsible for the radial components of the forming forces to become nearly zero or even negative, which means that the tool was pushed outwards instead of in the direction of the cone centre.

2.3.5 Domain decomposition methods

Sebastiani *et al*. (2007) applied a decoupling algorithm to reduce computing time in Finite Element analysis of incremental sheet forming (ISF) processes. The decoupling algorithm consists into divide a Finite Element model discretization in an elastic and an elastoplastic deformation zones. These two separated systems are alternately solved resorting to an algorithm which results in a partial model providing boundary conditions for the other system.

Hadoush and van den Boogaard (2009; 2012) proposed a sub structuring method to reduce the computation time of SPIF simulations using implicit integration scheme. This proposal consisted into dividing the Finite Element mesh in regions with different computation treatments. The hypothesis is that plastic deformation is localized and restricted to the tool vicinity, while elastic deformation region is considered in the rest of the sheet mesh due to a low geometrical nonlinearity. The strong nonlinearity requires the use of the standard Newton method, but it was not efficient to use in large elastic deformation part.

2.3.6 Adaptive refinement strategies

Lequesne *et al.* (2008) modelled the SPIF process using LAGAMINE. In order to decrease the simulation time of SPIF simulation combined with an implicit integration scheme, a new method using adaptive remeshing procedure was developed. The sheet mesh was modelled with 4-node shell element implemented in the code, called COQJ4. The contact surface uses the node connectivity of the shell finite element combined with classical penalty method (Habraken and Cescotto, 1998). The spherical tool was modelled as a rigid body. The validation of adaptive remeshing in SPIF process for shell elements was performed using a line test simulation from the work of Bouffioux *et al.* (2008a).

Giraud-Moreau *et al*. (2013) analyzed SPIF using a remeshing method based on refinement and coarsening strategies in order to decrease the time simulation. The numerical results were calculated with the dynamic explicit solver of ABAQUS software coupled with the remeshing method. The finite element used to mesh the sheet was S4R shell element with 4 nodes and reduced integration. The validation of the numerical results has been carried out through the comparison of geometrical profile and thickness profile. The comparison was based on the experimental measurements of a 45° wall angle cone in AA1050 sheet. Only the shell elements close to the tool could be refined.

Bambach (2014) introduced an approach based on dynamic explicit Finite Element simulation analysis of ISF combining adaptive remeshing and sub-cycling methods, in order to reduce the computing time. This proposal allows the decrease of the CPU time by different ways: increasing the tool velocity or applying mass-scaling, use of parallel computation, reduction of the number of elements by adaptive remeshing and additionally, integration of the elements with different time steps through sub-cycling. The simulations were modelled with shell element with reduced integration (S4R). The sub-cycling is applied to the coarse elements integrated with a larger time step than the refined elements in the deformation region. The numerical simulations carried out with only adaptive remeshing reduced 28.8% of the time needed for a globally refined mesh. Applying adaptive remeshing combined with sub-cycling with a factor of 2 reduced the CPU time to 24.8% and to 12% for a factor of 10. This combination of adaptive remeshing with sub-cycling demonstrated tremendous reduction of CPU time.

2.4 Formability and SPIF mechanisms

It is appealed that formability on the SPIF process is higher than in conventional sheet forming process. In conventional stamping operations, the metallic sheet is considered subjected to an in-plane and bending deformation with, occurrence of necking. However, the deformation mechanisms on SPIF process are still a questionable subject among different metal forming research groups.

The boundary of sheet metal forming processes is defined as the maximum deformation level achieved before fracture. The most common procedure to determine the forming limit of sheet metal forming can be named as Forming Limit Diagram (FLD) also known as a Forming Limit Curve (FLC). It consists into plotting the major principal strain and minor principal strain showing the safe and the failure zones. These curves are experimentally established, providing the values of major and minor principal strains, for various loading patterns, such as, equibiaxial, biaxial, plane strain and uniaxial. Fig. 2.14 exhibits a schematic comparison between the FLC of conventional forming (stamping/deep drawing) and SPIF.

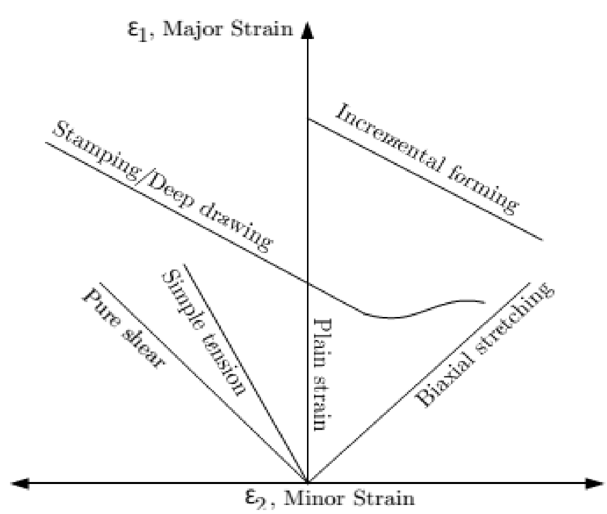

Figure 2. 14 Schematic representation of FLC in SPIF against conventional forming (Keeler and Backhofen, 1964).

The SPIF FLC is generally a straight line with a negative slope in the positive region of minor strain, whereas the conventional stamping is presented in both regions of minor strain, as shown in Fig. 2.14.

Kim and Park (2002) have summarized the effects of different parameters on the formability of AA1050 sheet. The use of freely rotating ball tool tip enhances the formability and reduces the friction at the tool/sheet interface. The formability decreases when increasing the tool diameter and vertical increment, and the best formability is obtained with a tool of 10 mm. Due to plane-anisotropy, the formability differs according to the direction of the tool motion. Formability in SPIF process can be analyzed using the maximum forming wall angle as being an indicator. It can be the first step to know the formability limits of the material. For instance, Ham and Jeswiet (2006) have analyzed several SPIF parameters and their combined influence on the maximum wall slope angle. Similarly, Malwad and Nandedkar (2014) have performed experiments to study the combined influence of wall angle, step size and tool diameter on formability. The formability analysis of AA8011 was performed using conical shapes with different wall angles, at 55º, 65º and 75º. Afterwards, a multistage test with continuous variation of wall angle from 35º to 90º was carried out to assess the maximum forming wall angle achieved in function of depth. From their experimental work, it was observed that the thickness reduction was possible at large wall angle, but uniform thickness distribution along the wall was found for angles smaller than 65º. Concerning the wall angle, when it was increased, the occurrence of stretching was more significant than shearing. For smaller wall angles the deformation mainly occurred by shearing. Using constant wall angle shapes, the cone forming achieved the target final depth without fracture occurrence. However, using multistage (variable wall angle) tests the fracture occurred earlier than using constant wall angle shapes.

Emmens and van den Boogaard (2009) presented a mechanisms that have been suggested to explain the enhanced formability in ISF processes. In their review, several mechanisms were mentioned: contact stress, bending-under-tension, stretching, shear, cyclic straining, necking stabilization and hydrostatic pressure. The mechanism explanations were based on theoretical considerations and some of them have been experimentally validated (Martins *et al.*, 2008; Silva *et al.*, 2008). They claimed that the identification of a single mechanism occurrence in ISF cannot be imposed or generalized as being the main mechanism.

2.4.1 Analytical analyses

An analytical model of SPIF based on the experimental observation of contact interaction between forming tool and sheet surface have presented by Martins *et al.* (2008) and Silva *et al*. (2008). A similar examination was performed for material failure at the transition regions between the inclined wall and the corner radius of the shape. Their analytical membrane theory model proposes the fundaments of the process and it was explained through experimental and numerical results.

A theoretical model based on membrane analysis with bi-directional in-plane contact friction focused on the deformation modes commonly found in SPIF have been presented by Martins *et al.* (2008). It was explained by experimental and numerical results available in the literature. The formability limits of the process are analyzed by combining the proposed membrane analysis with ductile damage mechanics. The analytical model approach was only focused on three modes of deformation: a) the flat surfaces under plane strain stretching conditions; b) rotational symmetric surfaces under plane stretching conditions; and c) corners under bi-axial stretching conditions. These modes were considered in order to explain the high formability of the process. The explanation of the increased formability of SPIF was compared with conventional stamping operations through the Fracture Forming Limit Diagram (FFLD) based on the onset of fracture instead of FLD based on the onset of necking. The evolution of thickness with depth along two meridional cross sections revealed that plastic deformation takes place by uniform thinning until fracture. From their experimental observations, the authors claimed that there is no evidence of necking before the failure occurrence in the component. The crack propagates under tensile meridional stresses acting under stretching modes of deformation.

A reviewed theoretical model for rotational symmetric SPIF, which was employed under membrane model analysis considering bi-directional in-plane contact friction forces have been provided by Silva *et al*. (2008). The main purpose of their analysis was the understanding of state of stress and strain in the localized deformation and the material fracture initiation during SPIF process. A schematic representation of the shell element details the acting stresses in the meridional, circumferential and in thickness directions. Fracture in SPIF was claimed as being happened by meridional tensile stress and not by in-plane shearing stress.

An analytical approach for SPIF process to describe the localized deformation mechanism have been developed by Fang *et al*. (2014). In their work, they assumed a plane strain condition in the analytical model, which is only the material deformation in the plane perpendicular to the tool motion direction. The localized deformation region was divided into sub deformation regions: the first one, the contact area between the tool and the sheet, and the second one, the wall of the formed part on the neighborhood of the first region. In each one, the state of stress and strain was analyzed through the thickness direction to include the bending effect. In addition, the stretching effects were also considered by calculating the thickness strain and, finally, the strain hardening was assessed. In order to validate the theoretical study, simulations and experiments of a cone shape were performed. The results confirmed the accuracy of the analytical model using both Finite Element simulation and experiments. The experimental validation was performed by measuring the circumferential and meridional strain variations, the growth of crack and morphological analysis of the fractured region. The measured meridional strain was larger than the circumferential strain, which confirmed the plane strain assumption used in the analytical modelling. The analytical evaluation revealed that the deformation occurred not only in the contact zone, but also in the inclined wall in the vicinity of the contact zone. The deformation in the noncontact area may affect the geometrical accuracy. Finally, the results also suggested that the fracture tends to appear at the transitional zone between the contact area and formed wall.

2.4.2 Combination of stretch, bending and shear

Emmens and van den Boogaard (2009) have mentioned in their review that simple shear is responsible for the lack of necking appearance, as no tensile force is applied in the plane of the sheet. An additional shear stress decreases the yield stress in tension. It was observed as occurring in ISF as referred in Emmens and van den Boogaard (2007). Fig. 2.18 exhibits the lateral cut section view of different deformation modes: bending, stretching and shearing in the orientation of the original vertical cross-sections (XZ plane).

Malhotra *et al*. (2012b) have established a fracture model combined with Finite Element analysis in order to predict the occurrence of fracture in SPIF using two conical shapes. Experiments were performed to validate the predictions from Finite Element analysis in terms of formability, thinning and fracture depths. It was reported that fracture in SPIF was controlled by both local bending and shear. Local stretching and bending of sheet on the tool vicinity originated higher plastic strain on the outside surface of the sheet increasing damage as compared to the inner surface. Additionally, the deformation mechanism in SPIF was compared to conventional forming process using the deformation history obtained from Finite Element analysis. The shear effect in SPIF delayed damage accumulation while high local bending of the sheet around the tool caused greater damage accumulation in SPIF than in conventional forming. These facts explain the increased formability in SPIF in comparison to conventional forming. It was claimed that both through-the-thickness shear and local bending of the sheet around the tool play a role in fracture in SPIF process.

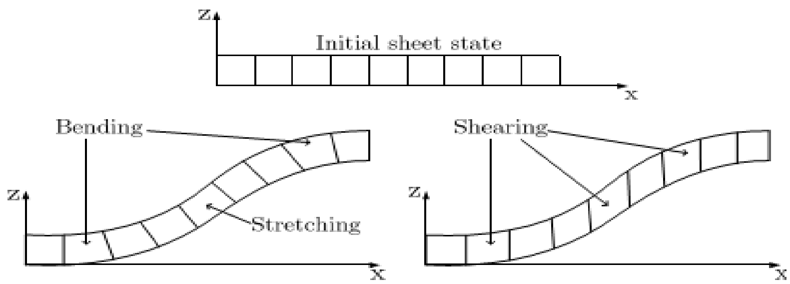

Figure 2. 15 Difference between forming by stretch (left) and forming by shear (right) Emmens and van den Boogaard, (2009).

2.4.3 Cyclic strain effect

During SPIF operation, the forming tool has a contact with a material point several times. Each path causes bending and unbending with possible strain reversal, so the material is subjected to cyclic straining. However, this cyclic effect should not be confused with the BUT. It involves repetitive bending but not necessarily cyclic and presents inhomogeneous stress distribution in the thickness direction. The stabilizing effect of cyclic loading, involves cyclic straining but not necessarily bending and the stress distribution over the thickness may be homogeneous. In a practical situation, these mechanisms will be hard to separate, but their effects are fundamentally different Emmens and van den Boogaard, (2009).

Eyckens *et al.* (2007, 2010) have showed the non-monotonic strain path of the material submitted to SPIF process, playing a role in the high formability, compared to the monotonic loading in the traditional FLC. They have analyzed the deformation history retrieved from a Finite Element simulation of a 50º wall angle cone shape formed by SPIF using AA3003-O. The finite element simulation revealed complex deformations occurring during the SPIF process. To illustrate this, three elements along the thickness direction were selected in the centre of the inclined wall mesh. The simulation showed that the final deformation at the cone wall was approximated by a plane strain deformation with elongation along the local radial direction, and this final deformation was reached incrementally by the forming tool. Along the direction of the tool motion, the sheet was repeatedly bent in one way by the moving tool, bent in the other way, and unbent. The usage of different constitutive models in this analysis showed that mixed hardening contributed to the delay of the onset of necking in SPIF process. Afterwards, the strain paths at three finite elements in thickness direction are used as input into a MK forming limit model.

CHAPTER THREE

MATERIALS and METHODOLOGY

3.1 Materials and experimental procedure:

3.1.1 Experimental materials and properties

Many industries such as automotive and aircraft industry use aluminum alloy 6061 sheets which have high strength to weight ratio for production of body parts. In this study, Formability of AA6061 with the thickness of 0.8mm, 1mm and 1.2mm are investigated using the experimental method. The AA 6061 alloy sheets were cut into 150×150 mm blanks by shearing operation. The chemical composition of aluminum alloy 6061 is shown in Table 3.1. These mechanical properties are yield stress (YS), ultimate tensile strength, work hardening exponent (n), work hardening coefficient (K) and elongation which were evaluated by standard tensile testing of ASTM-E8 specification at 2 mm/min cross-head speed (ASTM,1999). Hollomon's equation ($\sigma = K\varepsilon^n$) was used to model the plastic behavior of sheet material.

Table 3. 1 The chemical composition of AA6061 alloy

Chemical composition	Al	Mg	Si	Fe	Cu	Mn	Cr	Zn	Ti	Ca
AA6061	97.73 %	1.16 %	0.247 %	0.420 %	0.24 0%	0.033 %	0.138 %	0.014 %	0.0136 %	0.011 8%

3.1.2 Tensile Test

The test samples for the tensile test were equipped as per ASTM E8/E8M -13 Standards. They were cut by wire cut EDM and one sample is shown in Fig. 3.1. The samples were prepared by cutting the chosen sheet metal in three different directions, namely at 0° (parallel), 45° (diagonal) and 90° (perpendicular) to the rolling direction. The tensile test was executed on these specimens in 50kN Universal Testing Machine (UTM) with a strain rate of 1mm/min.

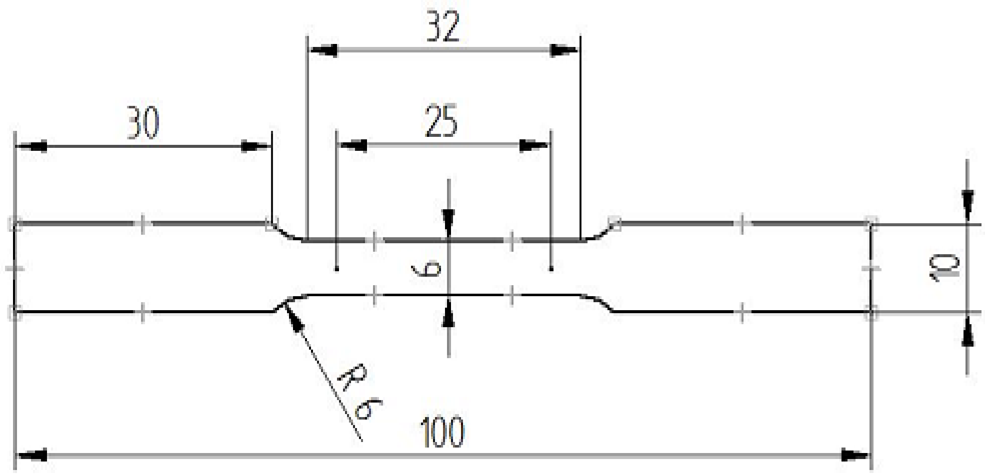

Figure 3. 1 ASTM E8/E8M–13 tensile test specimens with dimensions

Load versus extension data was attained. Using the tensile test, yield strength, ultimate tensile strength, ductility, true stress and true strain are determined along 0°, 45° and 90° to the rolling direction. Using the stress-strain curve of the tensile tests, the strength coefficient and the strain hardening exponent are determined along 0°, 45° and 90° to the rolling direction.

3.1.3 Incremental Sheet Forming Machine

The SPIF can be carried out using a CNC vertical milling machine or robots. A CNC vertical milling machine shown in Fig. 3.2 was chosen for this work. Due to the availability and the close dimensional control, this machine was chosen. The following is the specification of the machine.

Figure 3. 2 Incremental Sheet Forming Machine

General specifications of the first CNC milling machines

Table size: 810×400 mm

Travel: x-axis:510 mm, y-axis:400 mm and z-axis:400 mm

Spindle speed: 60 - 800 rpm

Feed rate: 1 - 7000 mm/min

3.1.4 Forming Tool

Three forming tools with hemispherical ends were employed in the experimental tasks. The tools are with two different diameters, 5mm, 10mm, and 15mm and with a same of length of 110 mm. Moreover, these tools were hardened and tempered with 60 HRC and made from high-speed steel (HSS) material. In order to decrease friction effect at the contact zone thereby increase the tools life and surface quality of the final product, tool tips were polished. Fig.3. 3 explains the dimensions of the tools used in the experiments.

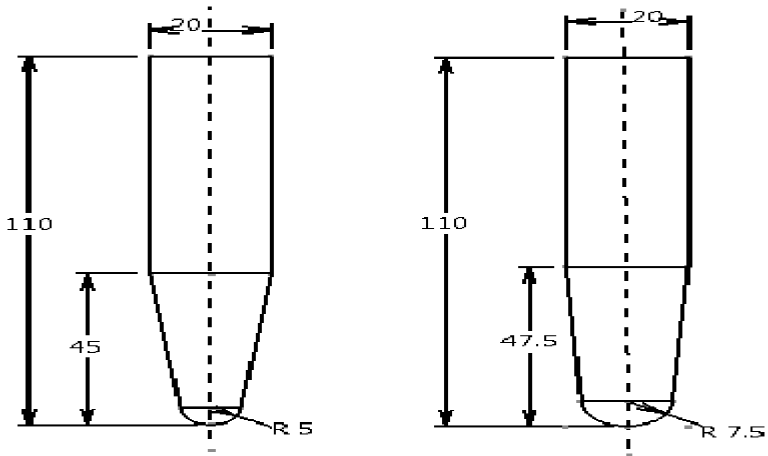

Figure 3. 3 The forming tools (all dimensions in mm)

As shown in Fig.3.4, the tool used was made from hardened High-speed steel (HSS). After hardening, it was ground in cylindrical grinding and then CNC profile grinding was done. In order to reduce friction and increase material formability, oil was applied as a lubricant. The forming tool, as well as the surface of the blank, was lubricated.

Figure 3. 4 Hemispherical forming tool with 15 diameters tip

3.1.5 Straight Groove Test

The straight groove test was conducted using the CNC vertical milling machine. To study the incremental formability of AA6061 alloy sheets straight groove test was conducted. The sheet was clamped using a fixture on the machine table. A hemispherical ended tool as shown in Fig. 3.4 was mounted on the spindle of CNC vertical milling machine.

The CNC Programme was prepared to form a straight groove in the sheet blank. The steps in making straight groove are as follows:

Step: i. SPIF tool was made to touch the surface of the sheet blank.

Step: ii. SPIF tool was made to penetrate by a programmed depth into the sheet blank.

Step: iii. SPIF tool was made to move on a straight path to make a straight groove for about 40 mm length.

Step: iv. SPIF tool was brought to the starting of groove and depth of penetration was increased by programmed quantity.

Step: v. Steps iii & iv were repeated until fracture occurs in the sheet blanks.

In this work, the different incremental depths of penetration used are 0.15 mm, 0.2 mm, 0.25 mm, 0.30 mm and 0.35mm. Straight groove was made in each blank by following one particular incremental depth of penetration until the fracture occurs. The experimental set up during the straight groove test is given in Fig. 3.5. In this test, there are two locations where the fracture occurs. One location is the end of the groove. Another location is at a point along the groove between the two ends. Due to the nature of the process, biaxial strain condition is generated at the end of the groove and plane strain condition is generated between the ends of the groove.

$$\text{True Major Strain} = \ln(\text{major axis length}/\text{original circle diameter}) \qquad \text{Eq 3. 1}$$

$$\text{True Minor Strain} = \ln(\text{minor axis length}/\text{original circle diameter}) \qquad \text{Eq 3. 2}$$

Figure 3. 5 Straight groove test set up.

Figure 3. 6 Sample formed in straight groove test

3.1.6 Varying Wall Angle Conical Frustum (VWACF) test

A varying wall angle conical frustum test (VWACF) was used to attain the tests because of its consistent geometry with the symmetrical parts. The intended model of the product was designed to get maximum diameters (outer and inner of 70 mm and 12 mm, respectively), a height of 41 mm and a radius with 60 mm of the varying slops. Figure 3.7 explains the designed dimensions of the targeted cone.

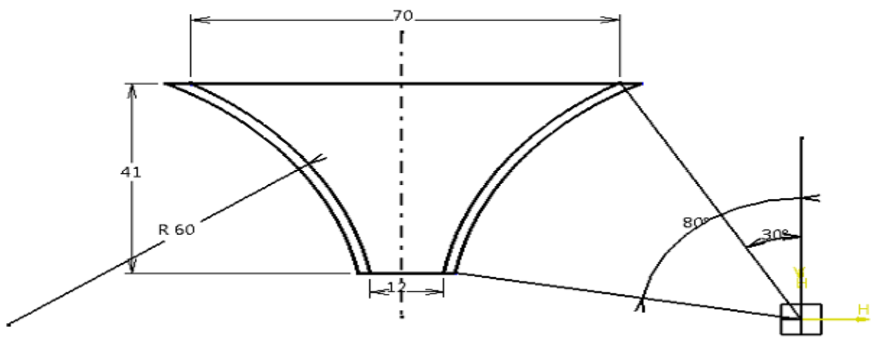

Figure 3. 7 The conical profile (dimension in mm)

A spiral trajectory of the forming tool with a definite step size was premeditated to generate the tool path. This path can be branded by a pure stretch deformation during the forming process, which helps to create a sheet thickness that uniformly distributed. Moreover, it assists to remove the peaks of the forming forces and at the same time, no stretch marks can leave on the working sheet surface. On the other hand, these openings regularly happen with counter type. The CAD/CAM was used to create the product profile and generate the spiral tool path by NC code, as displayed in Fig.3.9.

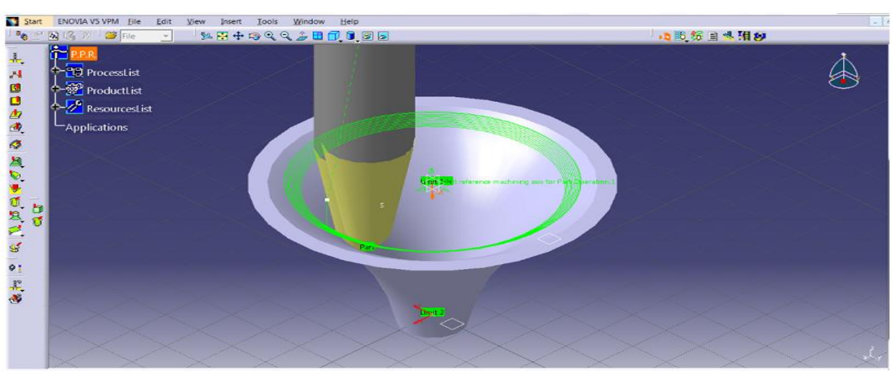

Figure 3. 8 Generating the tool path by CATIA

3.2 Part profile and CAD-CAM process

In order to investigate the ISF process, especially the formability of material by ISF, truncated conic parts was normally shaped. According to descriptions provided in preceding sections and also during the first chapter, the maximum inclination angle of successfully formable part can be regarded as a criterion for formability of material in ISF process Filice et al. (2002; Hirt et al. (2002); Hirt, et al. (2003); Jeswiet & Hagan, (2003); Jeswiet et al. (2005). However, application of specimens with constant inclination angle of sides implies many trials to be required for assessment of maximum achievable slop angle. For this reasons, Hussain and Gao (2007) and also Hussain, Gao, and Dar (2007) proposed truncated conic parts with varying wall angle along the symmetry axis, as a new benchmark for examination of material formability in ISF process. Subsequently, forming parts with circular, parabolic, exponential and elliptical curvature of profile, they explored the height (depth) along the symmetry axis of part, at which fracture occurred. Using this value along with the equation of each curvature, they rendered the relevant maximum attainable slop angle. Ultimately, they declared that the maximum wall angle for parts of curved profile depends on the characteristics of each profile (e.g. the radius of the circular curvature, or generally the rate of increase in angle). Additionally, they demonstrated that the maximum wall angle corresponding to the part of constant slop angle is lower compared to that of all parts with varying wall angle (for the curved walls of given specifications).

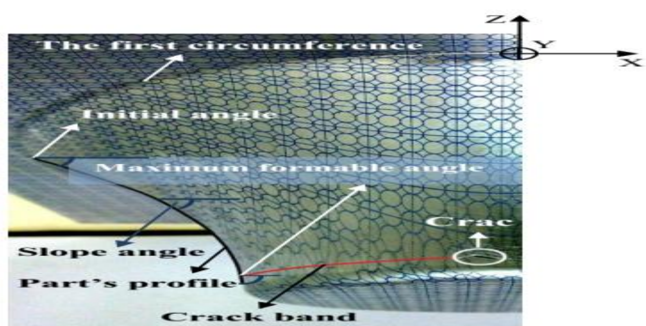

Figure 3. 9 Design of part’s profile and the coordinate system

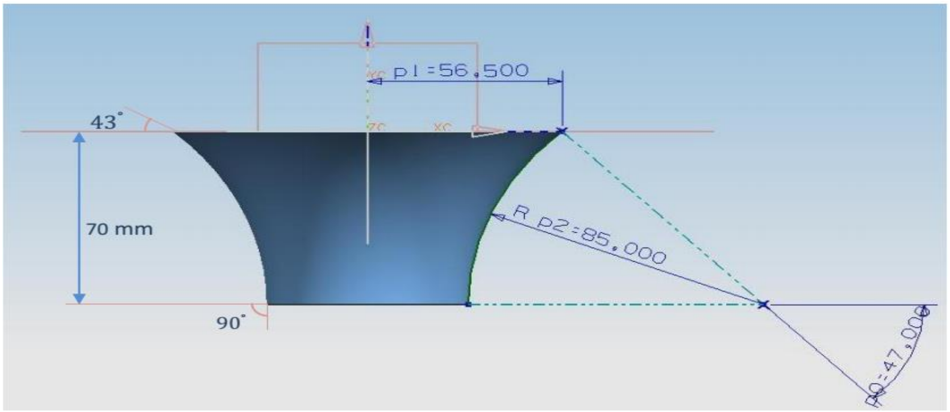

Figure 3. 10 Schematic representation of specimen modeled

3.3 Theoretical Thinning

If t_o and t_f are the initial and final thickness of the part with wall angle α with horizontal then the final thickness can be predicted by using the sine law. After the stable thinning an interrupted excessive thinning can occur and the result can deviate from the sine law.

$$t_f = t_0 * \sin(90-\alpha) \qquad \text{Eq 3. 3}$$

3.4 Numerical simulation procedures

In this thesis, ABAQUS is the software used for the finite element simulation combined with the characteristics of SPIF. ABAQUS implicit requires long computational time. Because of this, the ABAQUS explicit method has been chosen for conducting of the Numerical Simulation.

Finite Element Analysis

This is where the usage of ABAQUS - a FEM software is incorporated, the steps followed in order to simulate the process is as illustrated in the flowchart Fig. 3.11.

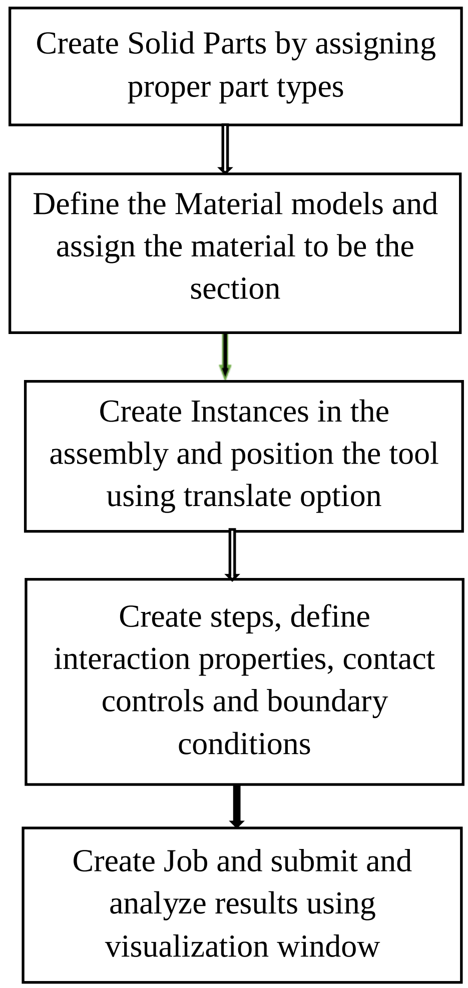

Figure 3. 11 Flow of steps to be followed while simulation the model in ABAQUS

Creating the Solid models, Mesh, Creating the Material models and Assembly

In this phase a Standard/Explicit model has been created with 2 parts, the sheet from which the shape is supposed to be formed out of and the tool that deforms the sheet. The type of the part must be chosen in accordance with its nature. Thus for Part1:Aluminium alloy Sheet, the part is chosen to be a 3 dimensional, deformable, planar shell square in shape with dimensions 200mm x 200mm x1mm. Part2: Tool will be 3D, Analytical rigid.

In order to perform any numerical simulation using finite element method meshing plays a key role in determining the accuracy of the solutions for the problem that is being solved. In order to maintain the precision of the results the mesh must be fine and refined. In this case only the sheet needs to be meshed as the tool is an analytical rigid part. The sheet will be meshed with shell elements with a certain shell thickness. Before meshing the part the edges must be seeded in order to control the cell size followed by which the mesh controls are assigned where the element type. Blank is defined as a deformable body and meshed with shell elements (S4R). It is a 4-node, quadrilateral, stress/displacement shell element with reduced integration and a large-strain formulation. The initial element size is taken as 2mm. The friction coefficient of 0.15 has used between the tool and the forming sheet.

Hemispherical forming tools of 15mm diameter have chosen and defined as analytical rigid part. Table 3.2 depicts the blank material properties, the elastic behavior specified in numerical simulations. To define the displacement, the position vs time data was introduced to ABAQUS software. The Gauss quadrature was used for the shell section integration.

Table 3. 2 Mechanical properties of aluminium alloy 6061

YS (N/mm^2)	UTS (N/mm^2)	Elongation (%)	n	K (N/mm^2)	E MPa	Y	R^2
217.5	372.56	17.5	0.1829	511.9	7000	0.33	0.984

In this section the material needs to be defined that to assign only to the Aluminum alloy sheet, i.e the Physical and mechanical properties of Aluminium – Mass density, Elasticity (isotropic) young's modulus and poisons ratio, Plasticity. Plasticity is defined according to the coordinates extrapolated from the stress strain curve that is obtained after performing the tensile and compression tests in the UTM. After the material model is created a section of the aluminum alloy sheet must be assigned with a homogeneous material of the previously defined properties.

In this particular section the instances of the tool and the sheet must be created and the reference point at the bottom center of the tool must be translated to the center of the sheet which is the origin.

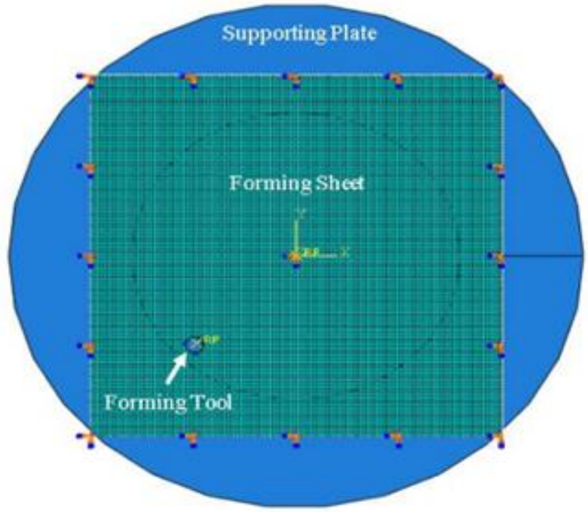

Figure 3. 12 Tool sheet assembly with tool at origin

Steps

The analysis is divided in to 3 steps namely – Initial, Goto: touch and Deform. Initial step is where the interaction between the tool and the sheet and the contact controls are defined these properties are propagated into the further steps in the simulation. Boundary conditions are defined in individual steps.

Boundary conditions:

The boundary conditions are defined within the steps and few of which are propagated and the rest are modified from step to step. In the initial step only one boundary condition is defined i.e. fixing the edges of the sheet using the encastre command which will make u1, u2, u3 which are the displacements in all the 3 directions and ur1, ur2 and ur3 which are the rotations about x, y and z axes of the cells along periphery of the sheet zero. This boundary condition (BC-1) is propagated to the rest of the steps without any modifications.

The second boundary condition is assigned in the second step i.e., Goto Touchdown where u1 and u2 values are given to be the initial x and y coordinates of the tool to the reference point of the rigid tool. This makes the tool move from the origin or center of the sheet to the starting point of the tool path.

In the third and final step the second boundary condition is modified to only u1 = 1 with an amplitude Amp vs x assigned to it. Amp vs x defined the tool path in x direction with respect to time steps. Similarly, two more boundary conditions are defined with u2 = 1 with amplitude

Amp vs y and u3 = 1 with amplitude Amp vs z. In the final boundary condition along with z motion definition and have also set ur1, ur2 and ur3 of the tool to be zero.

These boundary conditions help in defining the tool path during the simulation. Tool path can be defined for the same geometry in two different ways, one is called helical where the path is continuous with all three x, y and z coordinates changing monotonically with time. Other way to define the tool path is steps i.e. one set of coordinates in the xy plane followed by a decrement in z direction and then again another set of coordinates.

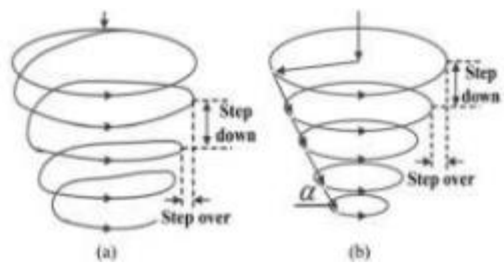

Figure 3. 13 Tool path definition (a) helical or spiral, (b) Step wise with draw angle alpha.

Interaction Properties:

Interaction between the bottom surface of the tool and the top surface of the sheet must be defined in order to simulate the behavior of the sheet under deformation caused by the rigid tool. This is defined using a Master slave system. Master is the rigid surface that deforms which in this case is the bottom surface of the tool and the surface that follows the master and deforms will be the slave surface which in this case is the top surface of the sheet. Define the general contact between these two surfaces with a certain coefficient of friction at default conditions. Also have to link this particular interaction property with a contact control.

The computation time required for the simulation of the SPIF process by an implicit method is double the time taken for simulation by using an explicit method even for small parts. However, the prediction of accurate geometry remains a problem in the simulations done by the explicit method. Time scaling and mass scaling are used to minimize the computational time. Mass scaling is done by increasing the density of material and time scaling is done by artificially increasing the velocity of the tool.

Output requests

Before submitting the job to assign the history output requests and field output requests is necessary. In the field output requests there are PE – plastic strain components, PEEQ – equivalent plastic strain, S – Stress components and invariants, STH – Section thickness, U – Translations and rotations, UR – rotations.

3.5 Estimation of formability

3.5.1 Maximum wall angle

The maximum wall angle that can be formed in single stage is used as a major parameter for the evaluation formability in ISF. This is estimated by forming the conical parts with different wall angles. However, the geometrical parameters of these parts such as top diameter, height are not yet standardized. Also, this method requires large number of experiments. To overcome this problem, varying wall angle parts with different generatrices such elliptic, parabolic, circular, exponential, hyperbolic etc. have been anticipated. The varying wall angle parts are also not standardized and different scholars adopted different geometries. It is also observed that varying wall angle parts are over predicting maximum formable wall angle over the constant wall angle parts.

3.5.2 Construction of FFLD

A more detailed analysis of formability in ISF can be obtained by constructing FFLD. Different methods have been proposed to construct FFLD in the literature. A brief review has been provided in this section.

Method one: Construction of FFLD by forming different shapes in ISF

Filice et al. (2002) formed frustum of square pyramid, cross shape consisting of two perpendicular line and cone to get the limiting strains in uni-axial stretching and bi-axial stretching. Jeswiet & Young (2005) used pyramid, cone, dome, hyperbolic and five lobe shapes to construct the forming limit diagrams of AA3003-O in incremental forming. The limit strains under different strain paths are obtained by measuring the strains near fracture through circle grid analysis.

Method two: FFLD based on material properties

Fratini et al. (2004) proposed following empirical equation as a function of mechanical properties of material to get the limit strain of material under plane strain condition (FLD_0). The slope of the FFLD is considered as -1.

$$FLD_{oincre} = 8.64-36.2n-0.00798K+0.373Rn-0.104A\%+0.0301K*n+0.607n*A\% \quad \text{Eq 3. 4}$$

3.6 Tool Path and G-code Generation

Truncated Cone with an initial opening of 120mm and depth of 70mm was the geometry chosen to verify the thickness distribution (thinning). Contour toolpath was defined by using the Mastercam environment. Surface Finish Contour tool-paths perform multiple cuts at constant Z step depths. It has adopted for the multiple forming at constant step depth in SPIF.

The G-code created was extracted to coordinate points by using the Excel approach to define the displacement (amplitude versus time) data for the numerical simulation. The parameters used for the definition of toolpath for the chosen sample parts are described in Table 3.3. Figure 3. 15 shows the sample toolpath defined for the chosen parts.

Table 3. 3 Parameters for the toolpath definition

Part	Parameters			
Truncated Cone	Step Depth (mm)	Feed Rate (mm/min)	Tool Diameter (mm)	Wall Angle
	1	1000	15	50˚

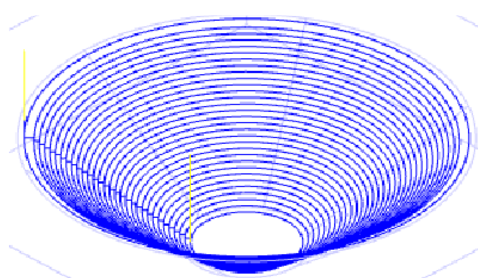

Figure 3. 14 Toolpath definition for the Truncated Cone

Two of the most common methods for the definition of tool path are the contour and the spiral. The contour tool path uses CAM packages whereas; the spiral tool path uses CAM or programming script. The profile tool path created by using a CAM package can produce complex geometry but it produces scarring on the surface of the part. The helical tool path is more suitable for Incremental Sheet Forming (ISF). It completely eliminates scarring on the surface of the formed part and produces homogeneous thinning.

3.7 Design of Experiments and Optimization Techniques

Design of Experiments (DOE) methods enables the designer to decide the optimum number of experiments to study the effect of process parameters on the output. The DOE technique has significant effect on accuracy and cost of the experiments. In the present work, Box–Behnken design was used to study the effect of feed rate, tool diameter, step depth and material thickness on formability. In this design each parameter is varied over three levels and recommends total 27 experiments with different combination of process parameters.

3.7.1 Response Surface Methodology

The Design of Experiment is used to organize the experimental run in order to get a fruitful outcome. Response surface methodology (RSM) is a widely used statistical tool to carry out systematic set of experiments. RSM is a collection of mathematical and statistical techniques useful for the modeling and analysis of problems in which a response of interest is influenced by several variables. The input parameters and their levels were defined after the pilot experimental study of each factor using one-factor-at-a-time. RSM answers the question of how to select process parameters to obtain the desirable value of the response with a reduced number of experiments. The behavior of the response with the changes in the variables can be represented by the surface not a curve, thus, a response surface methodology is needed. In this design, the process parameter combinations are at the midpoints of edges of the process space and at the center Mulay et al., (2017). The design matrix was built considering four input parameters (feed rate, step depth, tool diameter, and material thickness) at three levels. The 27 data sets were generated according to single block Box–Behnken design with four factors at three levels. Then Analysis of Variance (ANOVA) is conducted using Minitab 18.0.

The analysis is run for each response (Maximum wall angle and Thinning) separately. All terms (factors and interactions) are included in the first analysis. Then the mode is reduced by removing items which were not significant one by one. The item with the biggest P-value is removed first (unless it is a part of significant higher interaction) and the fitting process is preformed again. The significance of every item is rechecked and the refining process is repeated until a reduced model is reached with all items are significant (P value < 0.05)

3.7.2 Development of Empirical Model

The experimental results are based on planning and executing the experimental procedures accurately. In order to achieve optimum results, the experiments are planned on the basis of RSM technique used in experimental design. RSM is a collaboration of empirical and statistical techniques for modeling and optimizing the response variables which incorporates quantitative independent variables.

If all the variables are assumed to be measurable, the response surface can be expressed as

$$Y = \Omega\ (x_1, x_2, x_3, ...x_n) + \varepsilon \qquad \text{Eq 3. 5}$$

where Y is the desired response, Ω is the response function, x_1, x_2, x_3------x_n are the independent input variables and ε is the fitting error.

The second-order polynomial regression model also called a quadratic model is used for describing the behaviour of the system, which is expressed as

$$y = C_0 + \Sigma C_i x_i + \Sigma C_{ii} x_i^2 + \Sigma C_{ij} x_i x_j \pm \varepsilon \qquad \text{Eq 3. 6}$$

where y is the corresponding response, xi is the coded level of n controlling forming parameters, ε is the experimental error and Ci, Cii, Cij are the second order regression coefficients.

Using the Response Surface Methodology, a mathematical relationship was established between the Maximum Wall Angle, the wall thinning and the forming parameters.

Table 3. 4 Input process parameters and their levels

Input process parameters and their levels				
Parameter	Unit	Coded process parameters (Levels)		
		-1	0	1
Tool diameter (d)	mm	5	10	15
Sheet thickness (t)	mm	0.8	1	1.2
Feed rate (f)	mm/min	1000	1500	2000
Step depth (z)	mm	0.2	0.5	0.8

CHAPTER FOUR

RESULTS and DISCUSSION

This section has endeavored to deliver a brief summary of the numerical simulation, experimental investigation and response surface methodology and optimization results relating to the maximum wall angle and thinning within the given displacement.

4.1 Numerical simulation

An explicit dynamic approach was used to simulate the SPIF process to produce a truncated cone with 45° angle, 70mm depth, and 113 mm base diameter with a tool, modeled as a rigid body, with hemispherical head of 15 mm in diameter, feed rate of 1000 mm/min. The sheet metal was AA6061 with the elastic properties of E= 7000 MPa and υ= 0.33. The sheet is with 200mm x 200mm, and a 1.0 mm thickness. Figure 4.1 represents shots of forming a conical part with SPIF process in ABAQUS. For modeling the blank sheet, 87,773, S4R elements with dimensions of 0.7mm×0.7mm×0.5333mm (through-the-thickness) were used. All the elements at the blank boundaries were considered to be rigidly fixed to simulate the role of blank holder. The fixed mass scaling factor of 1.0E7 was applied. A coulomb friction coefficient of 0.15 was used, as commonly assumed in well lubricated sheet metal forming simulations.

It appeared that because of through-the-thickness shears, considering a 3D yield function, like Yld2004-18p, was essential. However, as predicted strain histories were almost identical for various yield functions in previous studies by the authors, von Mises yield function was used in this study due to its simplicity and less computational time (Eyckens et al., 2009b). In addition, Hollomon’s hardening law was used as it represented the material hardening behavior accurately. For this reason, the RD direction true stress-strain curve was used to calculate the parameters of the Hollomon’s type hardening law as shown here:

$$\sigma = K\varepsilon^n \qquad \text{Eq 4. 1}$$

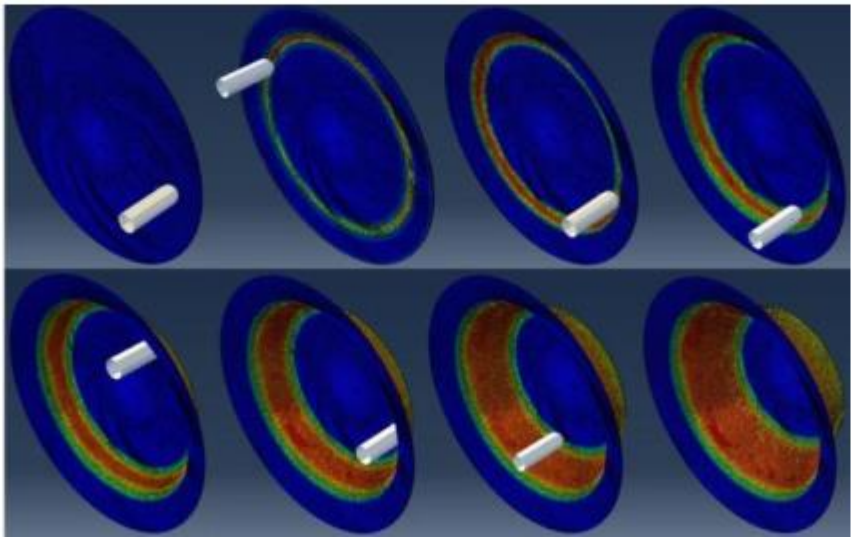

Figure 4. 1 Simulation shots

In ISF processes, designing the desirable tool paths were needed to provide optimal range of geometric accuracies in the formed part (Blaga et al., 2011). Two common types of toolpath i.e., spiral (helical) and z-level (profile) tool paths are shown in Fig. 4.2.

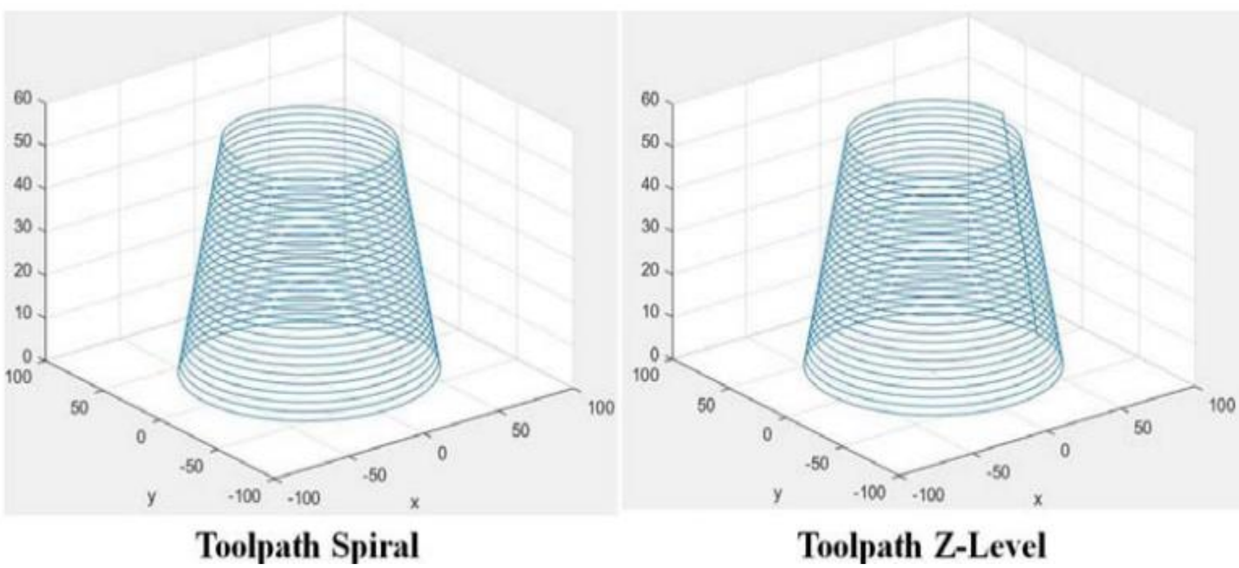

Figure 4. 2 Common tool paths in the ISF process: left) Spiral (Helical), right) Z-Level (Profile)

These two types of toolpath were used in the FE simulation of SPIF process. A MATLAB code was written to generate these toolpaths to be used in ABAQUS (See appendix B). Then, SPIF process was applied to form a conical geometry. Figure 4.7 shows effective strain distributions from the SPIF simulations of the sheet metal surface in contact with the tool for different toolpath types. As can be seen, the contour of the z-level toolpath presents a line of severe effective strain distribution which can make a scarring on the surface due to the upward transition between the following contours. As the excessive thinning of sheet metal makes failure in ISF process, the thickness was calculated as the distance from the inner to the outer sheet surface in direction of the normal to the surface, which is in contact with the tool. The determined thickness distribution for various toolpaths is presented in Fig. 4.8. More thinning can be seen in the z-level toolpath thickness distribution, which shows this toolpath has a higher failure chance. Before the deformation, the sheet thickness was 1.0 mm, while for the formed sheet, it is about 0.4 mm in some areas.

The simulation was run and the results were obtained. The tool motion in the x, y and z directions were plotted from the coordinate points against the times steps. The plots were demonstrated in Fig. 4.3, Fig. 4.4 and Fig. 4.5 below.

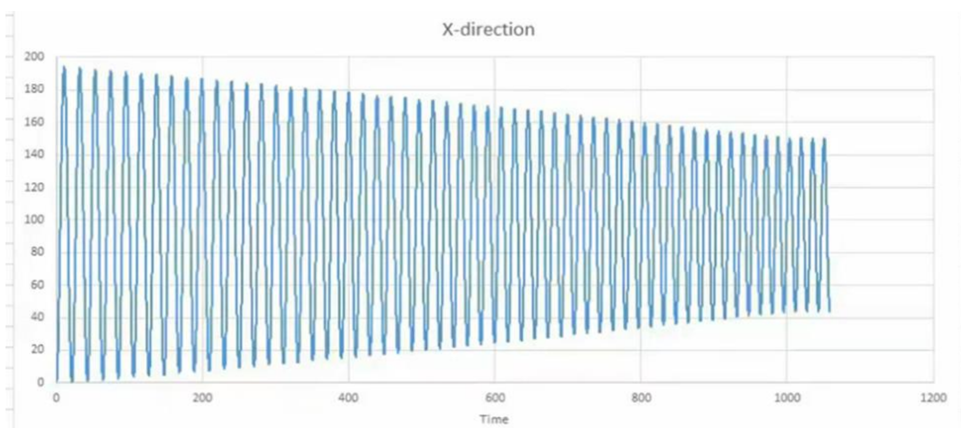

Figure 4. 3 Tool motion in X-axis

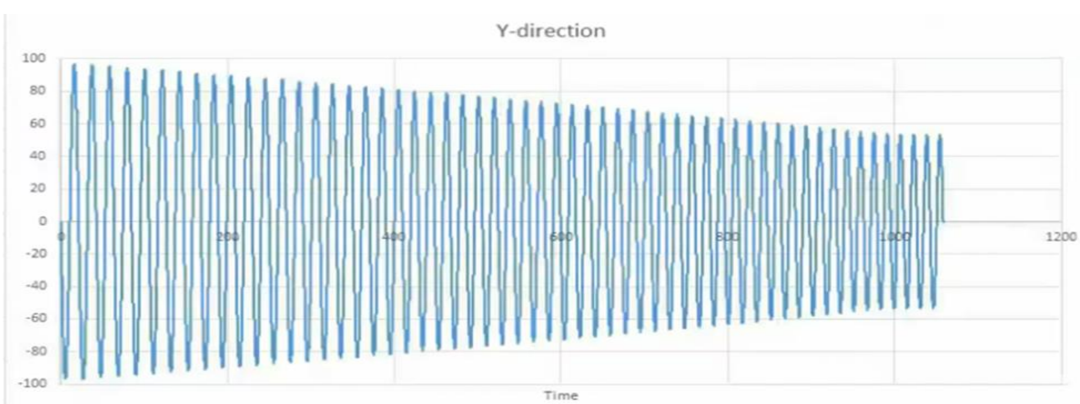

Figure 4. 4 Tool motion in Y-axis

Figure 4. 5 Tool motion in Z-axis

Post analysis plots were also obtained for the stresses and the energy over the time period of the simulation of all the elements in the sheet. The stresses in the system intuitively increase as the depth or the tool motion in the z direction increases. The Section thickness of the deformed sheet the deformed sheet and was shown in Fig 4.6. The plot depicts the Mises stresses on the sheet. Fig .4.7 depicts the final deformed sheet. This particular resultant deformed sheet was compared to the experimentally formed aluminium sheet of the same shape as simulated in ABAQUS.

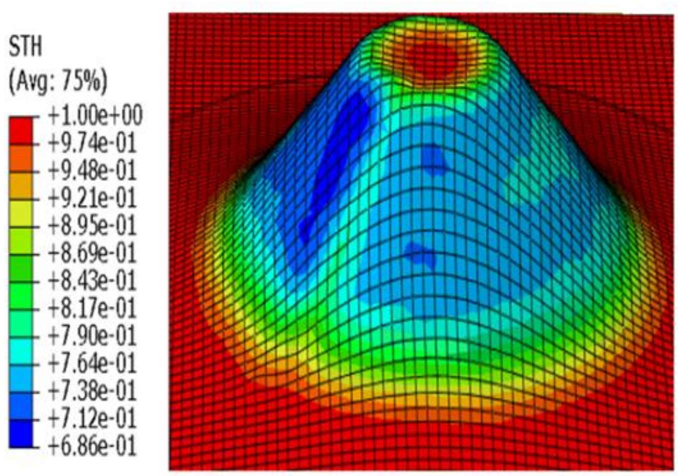

Figure 4. 6 Section thickness of the deformed sheet

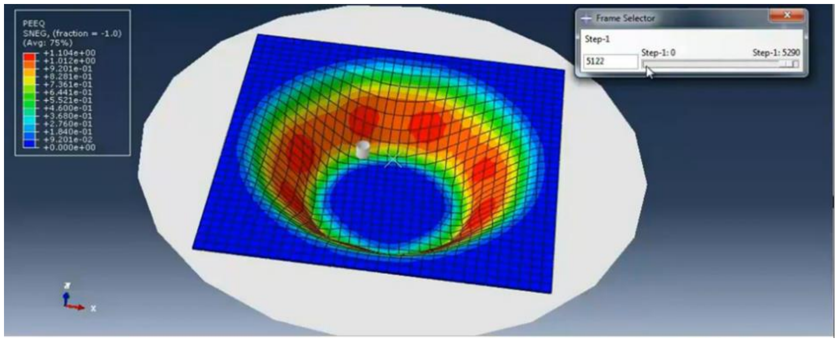

Figure 4. 7 depicts the Von Mises final deformed sheet

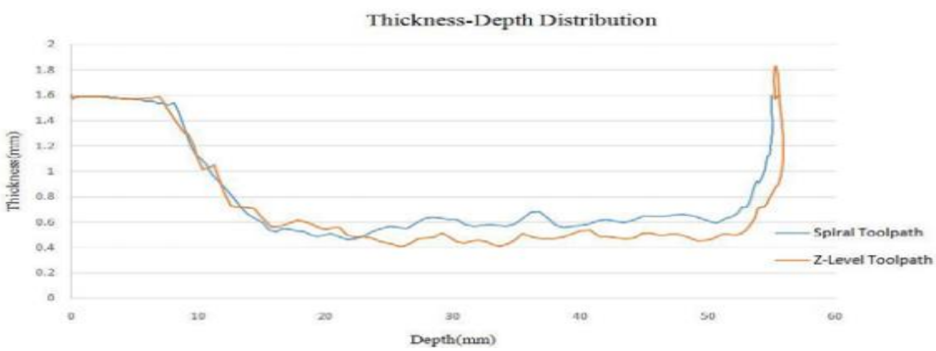

Figure 4. 8 Thickness distribution as a function of sheet depth using various toolpaths

4.1.1 Numerical simulation effects on maximum wall angle

The maximum wall angle was the principal parameter to assess the formability in ISF. To obtain the maximum wall angle, the varying wall angle conical frustums were formed on the CNC milling machine till the fracture. A part was formed for circular generatrix design to improve the accuracy of results. After the occurrence of fracture, the machine tool was stopped manually and the part was removed from the fixture. The depth of the part up to the fracture was measured using Vernier Height Gauge. The angle corresponding to this depth was called as the maximum formable angle. The maximum wall angle was calculated for all 27 simulated parts and the average value was taken as a liming wall angle for AA6061 in ISF as shown in Table 4.1

Table 4. 1 SPIF input process parameters and corresponding Numerical simulation responses

Std Order	Run Order	Step depth (mm)	Tool diameter (mm)	Feed rate (mm/min)	Material thickness (mm)	Maximum Wall angle (degrees)	Thinning (mm)
2	1	0.2	5	1000	0.8	77.5	0.487
22	2	0.2	5	1000	1	77.2	0.653
13	3	0.2	5	1000	1.2	76.82	0.737
11	4	0.2	10	1500	0.8	77.2	0.489
6	5	0.2	10	1500	1	76.82	0.614
17	6	0.2	10	1500	1.2	75.78	0.747
10	7	0.2	15	2000	0.8	75.4	0.569
14	8	0.2	15	2000	1	75.2	0.628
18	9	0.2	15	2000	1.2	74.2	0.763
15	10	0.5	5	1500	0.8	73.4	0.514
24	11	0.5	5	1500	1	72.45	0.651
16	12	0.5	5	1500	1.2	72.04	0.785
1	13	0.5	10	2000	0.8	73.1	0.516
20	14	0.5	10	2000	1	72.9	0.647
5	15	0.5	10	2000	1.2	71.86	0.787
9	16	0.5	15	1000	0.8	72.3	0.522
26	17	0.5	15	1000	1	72.04	0.654
7	18	0.5	15	1000	1.2	71.04	0.795
23	19	0.8	5	2000	0.8	70.4	0.534
19	20	0.8	5	2000	1	69.4	0.676
12	21	0.8	5	2000	1.2	68.6	0.819
8	22	0.8	10	1000	0.8	69.9	0.538
25	23	0.8	10	1000	1	68.5	0.683
4	24	0.8	10	1000	1.2	66.58	0.839
21	25	0.8	15	1500	0.8	69.6	0.539
27	26	0.8	15	1500	1	69.4	0.676
3	27	0.8	15	1500	1.2	69.2	0.813

The maximum wall angle and thinning was found to be 77.5˚ for the input parameter combinations of 0.2mm step depth, 5mm tool diameter, 1000 rpm feed rate and 0.8mm material thickness and 0.839 mm for the FEM simulation model for the fabricated part respectively. This was an indication for being a formable material. Consequently, maximum wall angle was a factor which determined formability of AA6061. The minimum wall angle and thinning was measured and its values were 66.58˚ for the input parameter combinations of 0.8mm step depth, 10mm tool diameter, 1000 rpm feed rate and 1.2mm material thickness and 0.487mm for Numerical simulation. From this maximum wall angle influenced substantially the thinning effect, hence formability enhanced when wall angle increased without causing catastrophic failure of the material. The result showed that lower step depth, lower tool diameter and lower feed rate enhanced material formability.

4.1.2 Numerical simulation effects on thinning

The Sheet thickness (STH) distribution form the numerical simulation was shown in Fig.4.6. Based on the result 0.686 mm (32%) thinning was achieved.

In order to get the thickness distribution along the depth, the parts were sectioned from the middle for ease of thickness measurement, and the cut parts were shown in Fig. 4.10. For measuring the thickness, the points were marked for every 5 mm from the top to the bottom of the part using Vernier Height Gauge. For better clarity of thickness distribution in the bending region, the points were marked for every 2.5 mm. Thickness at every point was measured using Digital Micrometer having a least count of 0.01 mm. In case of VWACF the wall angle and hence the thickness changes continuously with the depth. Hence, the wall angle and theoretical thickness corresponding to each marked point were calculated respectively.

The thinning from the numerical simulation was evaluated using the view section function. As shown in Fig. 4.9, the part is symmetrically cut along the Y–Z section; "STH" is selected to display the wall thickness.

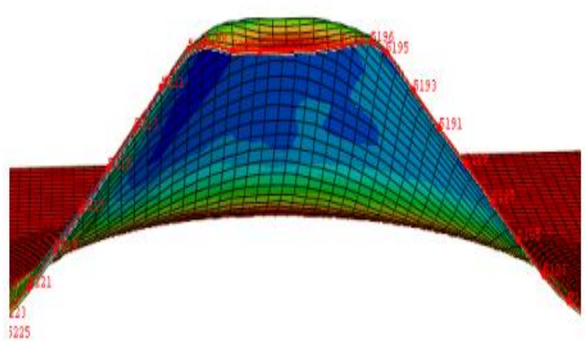

Figure 4. 9 Cut part and the nodal points in which thinning measurement was taken.

The fabricated part was cut symmetrically and the thickness values were obtained using a 0.001 precision digital micrometer. Measurement was taken at 10 equivalent positions with the numerical simulation in Fig. 4.10.

a)

b)

Figure 4. 10 a) Symmetrically cut part and b) The wall thinning measuring Method for the experimentally formed part.

4.2 Experimental Investigation

4.2.1 Effects of Chemical Composition of AA6061 on formability

The major alloying elements added in the AA 6xxx alloy are Magnesium and Si. The Mg and Si are added mostly in balanced amount for the formation of Mg2Si. Any excess amount of Si makes this alloy brittle. The congruent phase that was formed in this particular alloy, Mg2Si, has properties similar to that of the pure metal and it could dissolve in α phase upto1.85% at 595^{o}C (eutectic) and it was made to 0.2% at 200^{o}C. The chemical composition of AA6061 alloy tested for formability was provided in Table 3.1

This particular alloy, AA6061, taken for this formability study contains 1.16 % of Mg and 0.247 % Si. The major alloying element in the AA 6xxx alloys was Magnesium which was followed by Silicon. In order to increases the strength of this aluminium alloy without unduly decrease in the ductility of the sheet, magnesium was added to it. At the same time, the other properties, the corrosion resistance and weldability of these alloys were also found to be good. This particular alloy, AA6061, taken for this formability study contains 1.16 % of Mg. This magnesium addition results in solute hardening of this alloy and thus there was an increase in the strength. The presence of silicon, after magnesium, was as the highest impurity level in AA6061 alloy.

This particular alloy, AA6061, taken for this formability study contains 0.247 % of Si. Generally for silicon up to 12 %, there was a possibility for precipitation hardening of the alloys when silicon was combined with magnesium making the 6xxx series strong alloys. The addition of Magnesium and silicon form Mg2Si precipitates in the alloy. Furthermore, Si improves the corrosion resistance also. The presence of Si also improves the fluidity of the molten alloy and it reduces the susceptibility to hot cracking during solidification and heating. More than 13 % of Si presence reduces the machinability of the alloy. The Chromium additions, together with the presence of Mn, were specified for high Mg containing AA6061 alloys to reduce susceptibility to forms of inter-granular corrosion. This AA6061 alloy sheet considered for this formability study contains 0.138% Cr and 0.033% Mn. At higher content levels chromium in this alloy tends to form coarse constituents with some other impurities or addition of elements such as manganese, iron and titanium. Chromium has a slow diffusion rate and usually forms finely dispersed phases that can inhibit nucleation and grain growth in this alloy. The chromium was such an element to control grain structure, by possibly preventing the recrystallization in aluminium-magnesium-silicon and aluminium-zinc alloys during hot working or heat treatment. Manganese was a usual impurity in primary aluminium, in which the concentration of it normally varies from 5 to 50 ppm. Iron was also a most common impurity that is found in aluminium. In fact it has a high solubility in molten aluminium also and therefore it can be easily dissolved at all molten stages of production. This particular alloy sheet considered for this formability, AA6061, contains 0.42 % of Fe.

4.2.2 Effects of Tensile properties and limiting strain

The results of tensile test were conducted using UTM as per the standard ASTM E8 on the AA6061 alloy sheets of 0.8 mm, 1.0 mm and 1.2 mm thickness are shown in Table 4.2. The average strain hardening exponent (n value) indicates stretchability (see appendix D). In incremental sheet metal forming, there was no tension-compression strain condition. Therefore, in the tensile test the normal anisotropy value had not been considered in this study. Among the sheet metals considered for the study, the AA6061 with 1.2 mm thickness was showing highest average strain hardening exponent value of 0.1472 and the same sheet metal possesses the highest sum of strain values under different operating conditions viz., 0.8112, 0.6794, 0.6308, 0.8378, 0.8687, and 0.8583. Next to AA6061 with 1.2 mm thickness, AA6061 with 1.0 was showing higher average strain hardening exponent value of 0.12369 and the same sheet metal possesses the higher sum of strain values under different operating conditions viz., 0.6726, 0.6812, 0.7635, 0.927, 0.692, and 0.8084. The AA6061 with 0.8 mm thickness was showing lowest average strain hardening exponent value of 0.1122 and the same sheet metal possesses the lowest sum of strain values under different operating conditions viz., 0.7723, 0.7203, 0.4896, 0.6592, 0.748, and 0.8468. The true strain values at maximum load for the three sheets considered in this section were also in good correlation with the forming limit strains under various set of operating parameters. All other parameters obtained from the tensile test for the AA6061 with all three thicknesses were in good correlation with the forming limit strains under various operating conditions. The results of the tensile test are given in Table 4.2. Figure 4.11 shows true stress–strain curve of aluminum alloy 6061.

Table 4. 2 Tensile properties of AA6061 aluminium sheet metals

Sheet metal thickness	Orientation relative to rolling direction	UTS (MPa)	YS (MPa)	Elongation at break at non-proportional elongation	Strain hardening exponent (n-value)	Strength coefficient K (MPa)
AA6061 0.8mm	0˚	535	438.37	0.049326	0.09256	750.001
	45˚	557	442.45	0.052824	0.15433	961.29
	90˚	555	399.08	0.0599	0.04767	670.44
	Average*	551	430.59	0.0537	0.11222	835.76
AA6061 1.00mm	0˚	476	350.24	0.05606	0.12221	736.30
	45˚	452	185.79	0.05042	0.10273	654.01
	90˚	482	281.11	0.0582772	0.16709	854.29
	Average*	466	250.73	0.05379	0.12363	724.65
AA6061 1.2mm	0˚	444	282.42	0.06337	0.17065	789.82
	45˚	439	296.89	0.0721	0.1692	776.48
	90˚	246	168.84	0.0822	0.0796	335.08
	Average*	392	261.26	0.0725	0.14718	669.47

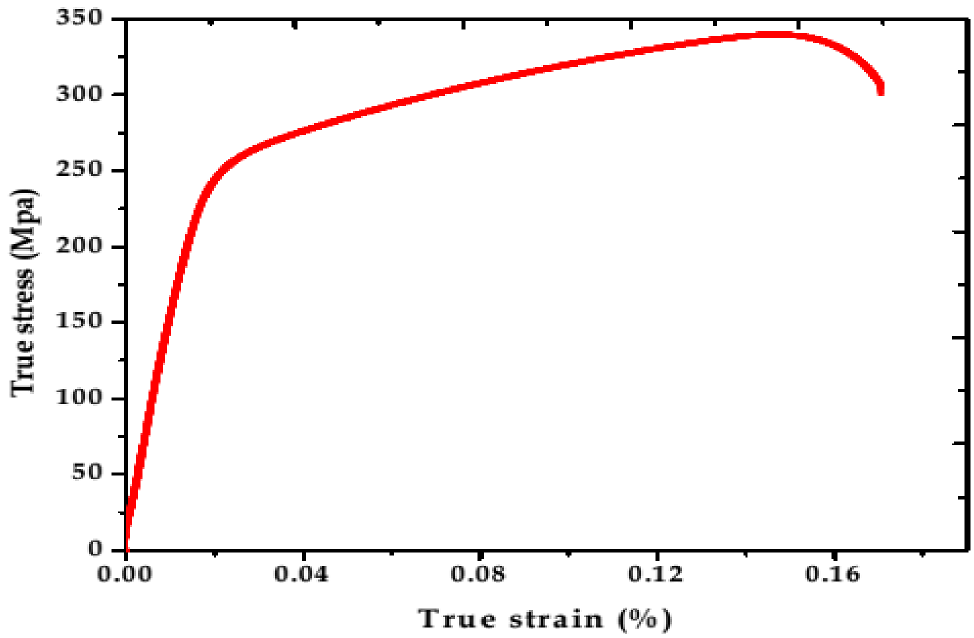

Figure 4. 11 True stress-true strain diagram of 6061 aluminum sheet.

4.2.3 Effects of Straight Groove Test of AA6061 in Formability

In incremental sheet forming, at the end of the straight grooves formed, the sheet metals experience a biaxial strain and at the remaining portions, the sheet metal experience plane strain condition. Therefore, in this work, the Forming Limit diagram for the sheets along the rolling direction have been plotted. For the case when the tool path was complex with mixed directions, the least forming limit could be taken for the consideration. The forming limit diagram, then, can be considered as a band between the lowest line and top most line. A notable thing in the incremental sheet forming was that the sum of major strain and minor strain was always constant. In incremental forming, the fracture occurs at any one region either where plane strain condition exists or where the biaxial strain condition exists. Therefore, in this work, when the fracture occurs at the plane strain condition, the limiting strain values for biaxial strain condition were corrected with the assumption that the sum of major strain and minor strain is always constant and vice versa. Since, the sum of strain is the indication of formability and the end user of the forming limit diagram can easily interpret this.

The representative forming limit diagrams for the AA6061 alloy sheets with 0.8 mm thickness, 1.0 thickness and 1.2 mm thickness formed by incremental sheet forming under various set of parameters were shown in Fig 4.12. These AA6061 alloy sheets experience plain strain condition to equi-biaxial strain. The range of limiting strain for AA6061 with 0.8 mm thickness for various operating conditions were viz., 0.772 to 0.870, 0.650 to 0.720, 0.489 to 1.175, 0.659 to 0.722, 0.748 to 1.131 & 0.796 to 0.986.

The range of limiting strain for AA6061 with 1.0 mm thickness for various operating conditions were viz., 0.672 to 0.992, 0.681 to 0.738, 0.690 to 0.729, 0.862 to 1.037, 0.558 to 0.806 & 0.781 to 0.887. The range of limiting strain for AA6061 with 1.2 mm thickness for various operating conditions are viz., 0.758 to 0.973, 0.665 to 0.701, 0.613 to 0.733, 0.761 to 0.837, 0.859 to 0.937 & 0.690 to 858. From these values, it was clear that the AA6061 alloy sheet possesses a very good formability in plane strain condition in incremental sheet forming when comparing to the conventional punch and die type forming.

In conventional punch and die type forming, the limiting strain under plane strain condition was roughly equal to the average strain hardening exponent value of the sheet. The average strain hardening exponent value for the AA6061 with 0.8 mm thickness was 0.11222 and the corresponding maximum possible limiting strain in plane strain condition under favorable operating conditions was 1.175 which was very high comparing to the conventional sheet forming. The average strain hardening exponent value for the AA6061 with 1.0 mm thickness was 0.12369 and the corresponding maximum possible limiting strain in plane strain condition under favorable operating conditions was 1.037 which was very high comparing to the conventional sheet forming.

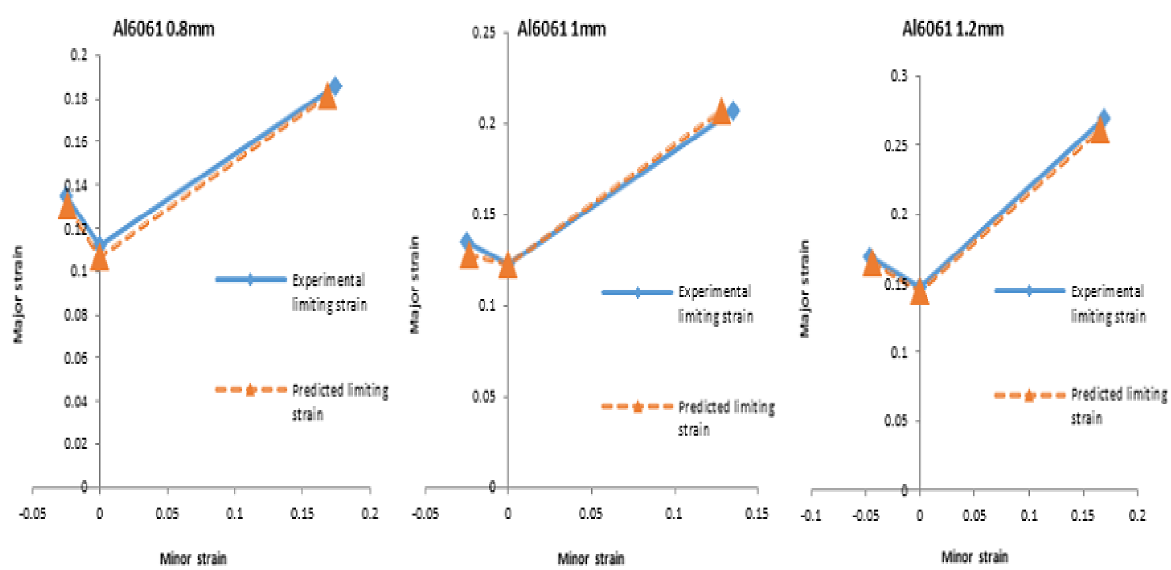

Figure 4. 12 Forming limit diagrams for the AA6061 alloy sheets with 0.8 mm, 1.0 mm and 1.2 mm thickness formed by incremental sheet forming under various set of parameters

Table 4. 3 Tensile data for AA6061

Sheet Metal Thickness		UTS	Proof Stress	%Elongation at Break at Non-proportional Elongation	True strain at maximum load	True stress at maximum load	Strain Hardening Exponent (n-Value)	Strength Coefficient (K)
		(GPa)	(MPa)	(%)	(mm/mm)	(Pa)		(MPa)
AA6061 0.8mm	Average*	0.551	430.59	5.37264	0.04318	575296059.3	0.11222	835.761345
AA6061 1.00mm	Average*	0.466	250.73	5.37978	0.04585	487582999.1	0.12369	724.652883
AA6061 1.2mm	Average*	0.392	261.26	7.25043	0.047615	412044010.8	0.14718	669.465638

The average strain hardening exponent value for the AA6061 with 1.2 mm thickness was 0.14718 and the corresponding maximum possible limiting strain in plane strain condition under favorable operating conditions was 0.973 which was very high comparing to the conventional sheet forming. Therefore, it could be concluded that the limiting strain in incremental forming under plane strain condition was roughly 7 to 10 times greater than the average strain hardening exponent of the sheet metal. The reason for the high limiting strain was the forming of sheet in a very small increment. When forming in small increments, the severity strain hardening was less, initiation of void was postponed and void coalescence and growth would be at slow rate. These were the reasons for high forming limit in incremental sheet forming.

Under biaxial tension conditions the AA6061 alloy sheet with 0.8 mm thickness possesses limiting major true strain values of 0.38 to 0.49, 0.38 to 0.54, 0.2 to 0.55, 0.32 to 0.48, 0.48 to 0.66 & 0.36 to 0.57. Under biaxial tension conditions the AA6061 alloy sheet with 1.0 mm thickness possesses limiting major true strain values of 0.38 to 0.46, 0.236 to 0.45, 0.08 to 0.48, 0.44 to 0.54, 0.29 to 0.64 & 0.28, 0.52.

Under biaxial tension conditions the AA6061 alloy sheet with 1.2 mm thickness possesses limiting major true strain values of 0.42 to 0.54, 0.25 to 0.34, 0.44 to 0.5, 0.4 to 0.48, 0.45 to 0.58 and 0.48 to 0.56. From these values, it was clear that the Aluminum 6061 alloy sheet possesses a very good formability in tension-tension condition in incremental sheet forming when comparing to the conventional punch and die type forming. In conventional punch and die type forming, the limiting true major strain under tension-tension condition was roughly equal to 1.5 times the average strain hardening exponent value of the sheet. The average strain hardening exponent value for the AA6061 with 0.8 mm thickness was 0.11222 and the corresponding maximum possible limiting major true strain in tension-tension condition under favorable operating conditions was 0.66 which was 5.9 times higher than that of conventional sheet forming. The average strain hardening exponent value for the AA6061 with 1.0 mm thickness was 0.12369 and the corresponding limiting major true strain in tension-tension condition under favorable operating conditions is 0.64 which was 5.17 times higher than that of the conventional sheet forming. The average strain hardening exponent value for the AA6061 with 1.2 mm thickness was 0.14718 and the corresponding limiting major true strain in tension-tension condition under favorable operating conditions is 0.58 which is 4 times higher than that of the conventional sheet forming.

Therefore for various conditions, the limiting major true strain for AA6061 alloy sheets varies from 4 to 6 times of that in conventional die and punch forming. The limiting strain values were higher for rolling direction in many sheets. However there are few graphs possessing higher limiting strain values in transverse direction and angular direction. The reason was the average strain hardening exponent and the grain orientation. Since the formability was read as a band between the line corresponding to highest strains and the line corresponding to the lowest strains, it was out of scope to analyze the direction which was favorable.

4.2.4 Limiting Wall Angle of AA6061 Alloy Sheets

Incremental forming does not favor the formation of vertical walls in the formed product. There was a limit for the maximum wall angle that can be formed by 45 the incremental forming process in a particular quality of the sheet metal. The maximum angle formed in AA6061 alloy sheet with various thicknesses using the optimized process parameters are presented in Table 4.4. It was a notable point that the maximum wall angle that could be formed was decreased with the increased thickness of the sheet. The thinning effect of formed for the AA6061 with various thickness are also presented in the Table 4.4. The thinning, maximum wall angle and the limiting strains were in good correlation with the tensile parameters.

Table 4. 4 Maximum wall angle, thinning for AA6061

Material	Feed rate (mm/min)	Step Depth (mm)	Diameter of tool (mm)	Spindle Speed (RPM)	Maximum Wall angle	Thinning
AA6061 0.8mm thick	1500	0.2	10	1000	77.2	0.489
AA6061 1.0mm thick	1500	0.2	10	1000	76.82	0.614
AA6061 1.2mm thick	1500	0.2	10	1000	75.78	0.747

4.2.5 Maximum wall angle and thinning

Table 4. 5 SPIF input process parameters and corresponding experimental responses

Std Order	Run Order	Step depth (mm)	Tool diameter (mm)	Feed rate (mm/min)	Material thickness (mm)	Maximum Wall angle (degrees)	Thinning (mm)
2	1	0.2	5	1000	0.8	77.1	0.486
22	2	0.2	5	1000	1	77.0	0.650
13	3	0.2	5	1000	1.2	76.30	0.730
11	4	0.2	10	1500	0.8	76.9	0.482
6	5	0.2	10	1500	1	76.32	0.610
17	6	0.2	10	1500	1.2	75.0	0.727
10	7	0.2	15	2000	0.8	74.4	0.529
14	8	0.2	15	2000	1	75.0	0.620
18	9	0.2	15	2000	1.2	74.0	0.760
15	10	0.5	5	1500	0.8	73.0	0.510
24	11	0.5	5	1500	1	72.30	0.646
16	12	0.5	5	1500	1.2	71.50	0.780
1	13	0.5	10	2000	0.8	72.90	0.510
20	14	0.5	10	2000	1	72.10	0.640
5	15	0.5	10	2000	1.2	71.20	0.782
9	16	0.5	15	1000	0.8	72.0	0.518
26	17	0.5	15	1000	1	72.0	0.650
7	18	0.5	15	1000	1.2	71.1	0.790
23	19	0.8	5	2000	0.8	70.10	0.531
19	20	0.8	5	2000	1	69.0	0.670
12	21	0.8	5	2000	1.2	68.6	0.810

8	22	0.8	10	1000	0.8	69.6	0.530
25	23	0.8	10	1000	1	68.0	0.680
4	24	0.8	10	1000	1.2	66.50	0.830
21	25	0.8	15	1500	0.8	69.20	0.530
27	26	0.8	15	1500	1	69.10	0.672
3	27	0.8	15	1500	1.2	69.12	0.810

The maximum wall angle and thinning was found to be 77.1˚ for the input parameter combinations of 0.2mm step depth, 5mm tool diameter, 1000 rpm feed rate and 0.8mm material thickness and 0.830 mm for the experimental investigation of the fabricated part respectively. This was an indication for being a formable material. Consequently, maximum wall angle was a factor which determined formability of AA6061. The minimum wall angle and thinning was measured and its values were 66.50˚ for the input parameter combinations of 0.8mm step depth, 10mm tool diameter, 1000 rpm feed rate and 1.2mm material thickness and 0.486mm for experimental investigation. From this maximum wall angle influenced substantially the thinning effect, hence formability enhanced when wall angle increased without causing catastrophic failure of the material. The result showed that lower step depth, lower tool diameter and lower feed rate enhanced material formability.

From this maximum wall angle influenced substantially the thinning effect, hence formability enhanced when wall angle increased without causing catastrophic failure of the material.

From this Numerical simulation and experimental investigation were found in good agreement, thus predicted formability of AA6061.

From the obtained maximum wall angle for numerical simulation and experimental investigation we could able to determine for theoretical sine law, it was found 0.216mm final thickness. Thus, numerical simulation and experimental investigation was found to predict formability more accurate than theoretical sine law.

4.3 Response Surface Methodology and Optimization of effects of process parameters on formability

4.3.1 Effects of process parameters on maximum wall angle

Formability was a main spectacle that made the component dependable with dimensional specifications. The storage of elastic energy is predictable in all kind of forming processes however; the springback could be abated by selecting appropriate forming parameters.

Deviation in wall angle was because of the elastic energy stored in the formed component which has a direct relation with the forming parameters (Behera et al. 2016)(Otsu et al. 2014). Thereby the wall angle was considered as one of the output responses for studying the influence of process parameters in formability. The analysis of variance for wall angle was shown in Table 4.6, from which it could be seen that step depth affect the wall angle significantly followed by material thickness. Furthermore, the feed rate had no effect on wall angle of the formed components.

From the plots shown in Fig. 4.13, it was evident that the maximum wall angle attained was very less when formed with maximum step depth. The increased step depth in the deformed region has high elastic energy stored with it and also the energy dissipates over time, thereby decreasing the formability. The decreased step depth caused higher localized deformation, which means that proportionally it has less elastic energy stored with it causing extended formability.

From the Fig.4.13 and Fig. 4.14, the step depth, as an individual factor, affects the wall angle to a greater extent, thus considered a predominant factor in influencing the maximum wall angle of the formed component Belchior et al. (2014).

The second order response surface representing the maximum wall angle is modelled by the following relation

$$\text{Maximum Wall angle} = 80.77-21.76(z)-0.047(d)+0.00054(f)+3.98(t)+3.36*(z^2) -0.01111*(d^2)-0.000001*(f^2)-4.03*(t^2)+0.296(z)*(d)+0.00438(z)*(f)-3.08(z)*(t) + 0.082(d)*(t)+0.00085(f)*(t) \quad \text{Eq 4. 2}$$

Table 4.6 shows ANOVA final results for formability analysis in the maximum wall angle after model reduction and refinement (**See appendix F for detail**). If the P value in ANOVA table was less than 0.05 indicated statistical significance for the source on the corresponding response. Model adequacy was evaluated using the coefficient of determination (R-squared, adjusted R-squared and predicted R-squared) given in Table 4.6. Their values showed levels very close to 1 which proves the appropriateness of the model. Considering the adjusted R-squared, the model explains 99.04% of the variation in the data. The 94.53% value of the predicted R-squared shows that the model is not over fit and has a good predictability.

Scrutinizing the adjusted sum of squares (Adj SS), it was evident that factor step depth had the greatest effect (1212.07) on the maximum wall angle, followed by material thickness (46.79) which agrees with the results of [Bhattacharya et al. (2011); Fiorentino et al. (2011); G. Hussain, Gao & Zhang (2007); Ham & Jeswiet (2007) and Fan et al. (2009)]. From the interaction effects step depth and feed rate (10.16), followed by step depth and tool diameter (4.66) were significant. The established model was more acceptable for the prediction of the wall angle, as could be seen from the model F value of 102.17 implying that the model was significant. As a result, it was to be said that selecting a machine for SPIF process was dictated mostly by these three factors: step depth, sheet thickness and tool diameter.

Table 4. 6 Revised ANOVA values for Maximum wall angle

Source	DF	Adj SS	Adj MS	F-Value	P-Value
Model	13	253.589	19.507	102.17	0.000
z	1	231.412	231.412	1212.07	0.000
d	1	0.344	0.344	1.80	0.202
f	1	0.281	0.281	1.47	0.247
t	1	8.932	8.932	46.79	0.000
z*t	1	0.889	0.889	4.66	0.050
z*f	1	1.940	1.940	10.16	0.007
Error	13	2.482	0.191		
Total	26	256.071			
Model Summary R-Sq = 99.03%; R-Sq (pre)= 94.53%; R-Sq (adj) = 98.06%					

The appropriateness of the regression model was known by the determination coefficient R^2. The value of this coefficient refers to the close fitting of the regression equation. The values of the R^2, adjusted R^2, and predicted R^2 were 99.03%, 98.06%, and 94.53%, respectively. Therefore, regarding the values of these coefficients, the established regression equation fits well and describes the maximum wall angle response. Lastly, normal distribution plot, Fig. 4.13, clarified that the residuals track the normal distribution. It can be noted that the regression equation has a good fit to their experimental data and are reliable to use.

In the present study, linear regression analysis in Minitab 18.0 software tool has been used to develop the predictive mathematical models for the dependent variables of maximum wall angle ($Ø_{max}$) and thinning (Δt) as a function of step depth, tool diameter, feed rate, and material thickness.

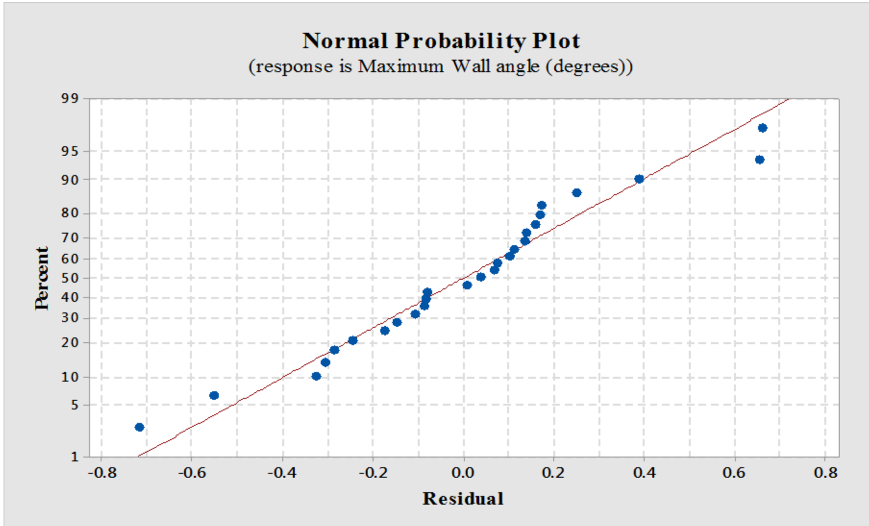

Figure 4. 13 Normal distribution of the maximum wall angle

Contour Plots of maximum wall angle

Contour plot and 3D response surface plots for maximum wall angle, were developed from response surface method and illustrated with the help of Fig.4. 14 and Fig. 4.15. From the results, it could be analyzed that with a decrease in step depth, wall angle increases and resulted in higher formability. Increase in material thickness increases local strains that were imposed on sheets, leading to a decrease in the formability. It could be observed from ANOVA and F test (confidence interval of 95%), given in Table 4.6, which the most significant factor in maximum wall angle study was step depth with the significance of 1212.07, and followed by material thickness 46.79. The other interaction effects, step depth and feed rate (10.16), followed by step depth and tool diameter (4.66) are significant. A linear model is fitted to the data and regression equation for maximum wall angle in un-coded units, is given in (Eq 4.2).

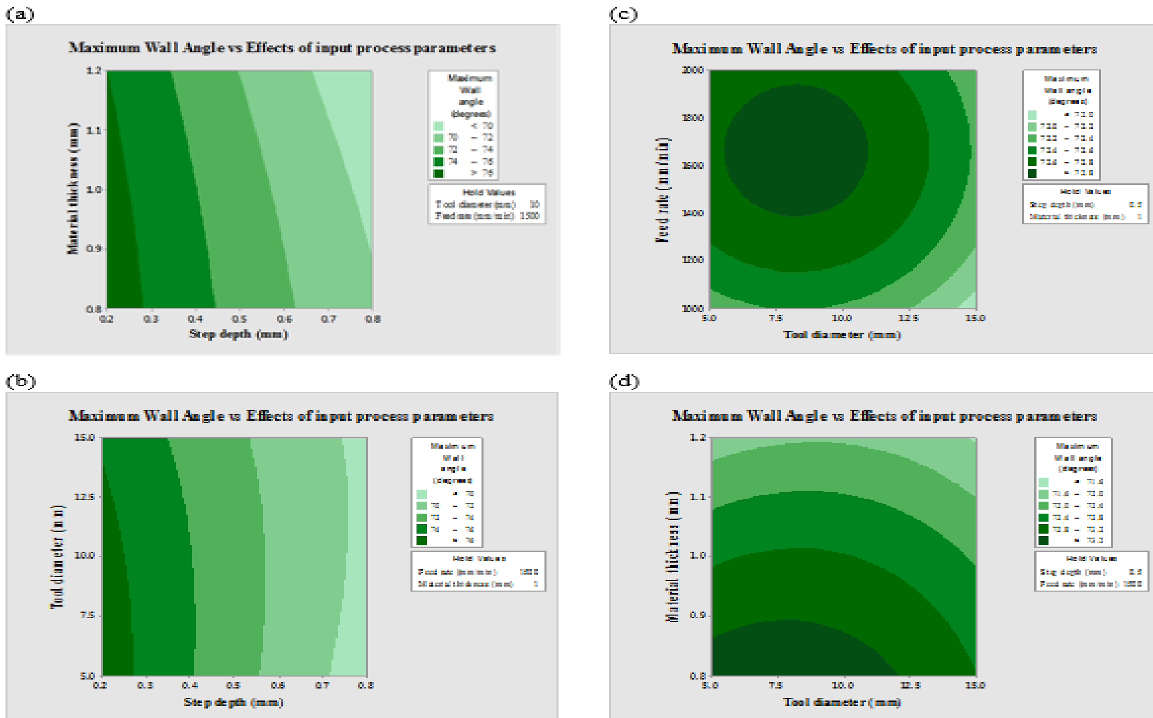

Figure 4. 14 Contour plots for maximum wall angle and effects of input parameters

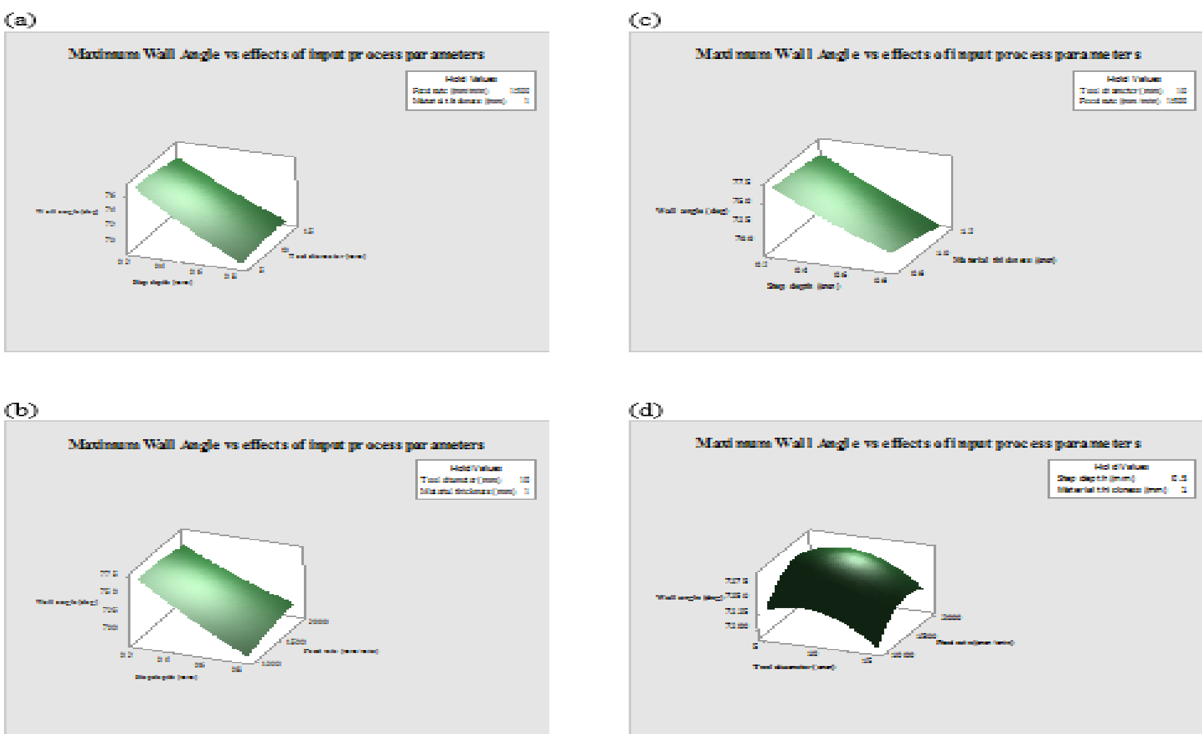

Figure 4. 15 3D Surface Plots for Maximum Wall Angle and effects of input process parameters

4.3.2 Effects of process parameters on thinning

During the incremental forming process, there was a reduction in thickness of the sheet, which is called thinning. In most practical applications, thinning of the material below permissible limit is considered a failure and therefore minimum wall thickness observed in the formed region of the truncated pyramid is used for wall thickness analysis. Even though thinning is inevitable, it could be reduced within the permissible level by optimizing the process parameters (Ambrogio et al. 2005). From the ANOVA shown in Table 4.7, it was seen that material thickness and step depth predominantly affect the thinning of the formed component.

The plots shown in Fig.4.17 indicate that the material thinning was maximum when working with high step depth and thicker materials. Higher step depths lead to increased stretching in the deformation zone leading to reduced wall thickness. Thicker materials do not allow the component to strain harden by reducing the time between successive tool paths, thereby leading to reduction in wall thickness. Also, under high step depth, stretching was less rapid, causing prolonged shear in the vicinity of the tool, resulting in wall thickness reduction (Jackson and Allwood 2009). From Fig.4.17, it was evident that decreasing the step depth increases the wall thickness, irrespective of feed rate; the material thickness has same effect on thinning of the component.

The plots shown in Fig.4.17 and Fig. 4.18 indicate that material thickness followed by step depth has a very high impact on thinning of the component. When working with higher step depth 0.8 mm sheet gets thinned upto 0.839 mm thickness. Therefore, with minimum step depth premature failure of the component could be avoided which also increases the formability of the material. It was also clear that the combined effect of step depth and material thickness with value of (9.49), followed by step depth and feed rate influencing material thinning.

The second order response surface representing the thinning is modelled by the relation:

$$\text{Thinning} = 0.026-0.048(z)-0.00451(d)-0.000021(f)+0.617(t)+0.0383*(z^2) + 0.000478*(d^2)+0.040*(t^2)+0.00037(z)*(d)-0.000089(z)*(f)+0.2194(z)*(t) - 0.00542(d)*(t)- 0.000062(f)*(t) \quad \text{Eq 4.3}$$

The developed model was validated, using the analysis of variance (ANOVA) for the thinning and the results are tabulated in Table 4.7. From the analysis, it was liable that the model obtained was adequate for the prediction of average thickness as seen from the Model F-value of 115.71 implying that the model was significant. Among the model terms, the F-value of material thickness was (1432.33) followed by step depth (46.87), thus indicating its higher influence on thinning, when compared to other factors. From the interaction effects step depth and material thickness with value of (9.49), followed by step depth and feed rate (3.65) were significant. **See appendix G**

Table 4. 7 Revised ANOVA values for thinning

Source	DF	Adj SS	Adj MS	F-Value	P-Value
Model	13	0.329653	0.025358	115.71	0.000
z	1	0.010272	0.010272	46.87	0.000
d	1	0.000008	0.000008	0.04	0.851
f	1	0.000036	0.000036	0.16	0.692
t	1	0.313896	0.313896	1432.33	0.000
z*f	1	0.000800	0.000800	3.65	0.078
z*t	1	0.002080	0.002080	9.49	0.009
Error	13	0.002849	0.000219		
Total	26	0.332502			
Model Summary	R-Sq = 99.14%	R-Sq (adj) =98.29%	R-Sq (pre) = 95.73%		

The suitability of the regression model is given by the determination coefficient R^2. The value of this coefficient refers to the close fitting of the regression equation. The values of the R^2, adjusted R^2, and predicted R^2 are 99.14%, 98.29%, and 95.73%, respectively. Therefore, regarding the values of these coefficients, the established regression equation fits well and describes the thinning response. Lastly, normal distribution plot, Fig. 4.16, clarified that the residuals track the normal distribution. It can be noted that the regression equation has a good fit to their experimental data and are reliable to use.

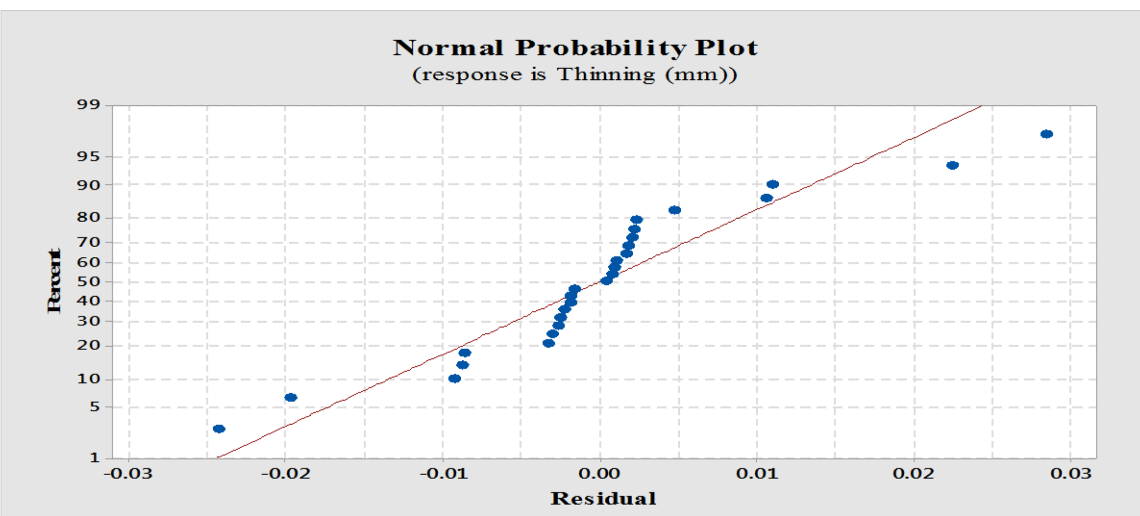

Figure 4. 16 Normal distribution of the thinning

Contour plots explaining the relation between the process parameters and thinning was shown in Fig.4.16. From Fig.4.16 (a-c), it was noticed that low thinning was obtained at high level of material thickness, step depth and tool diameter respectively. By comparing all the formability analysis, low thinning was found in thicker materials as shown in Fig. 4.10 (d-f)

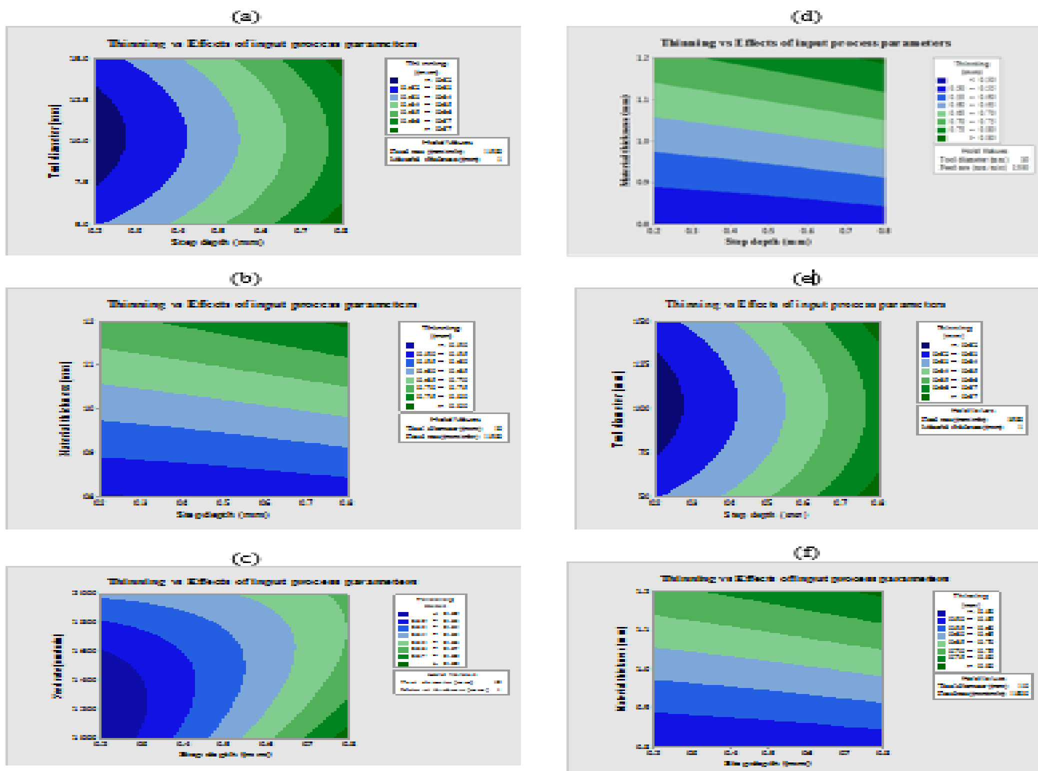

Figure 4. 17 Contour plots for Thinning and effects of input parameters

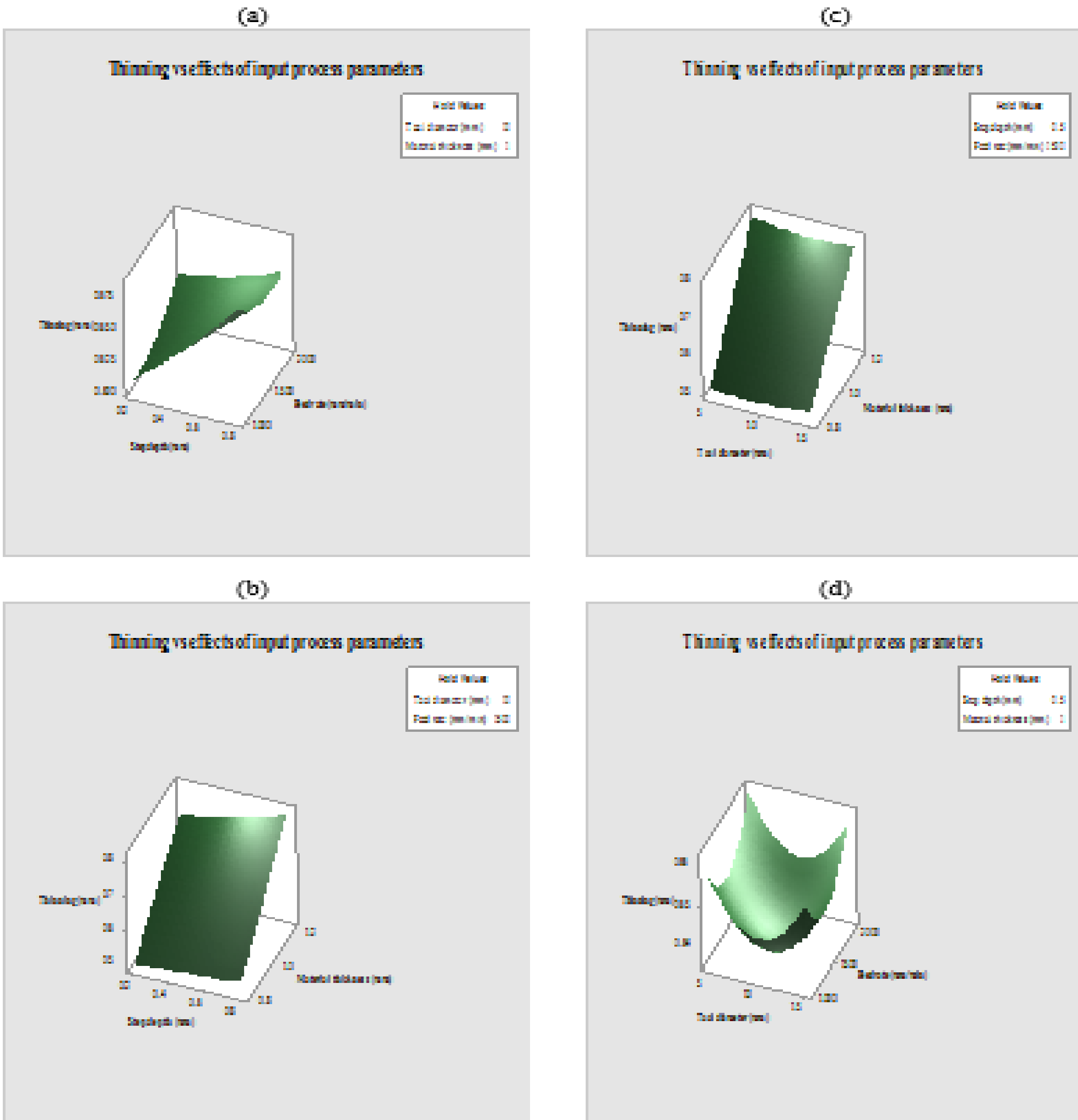

Figure 4. 18 3D surface plots for Thinning and effects of input process parameters

4.3.3 Selection of Optimum Formability Parameters for Maximum Wall Angle and Thinning

Optimization of Maximum Wall angle

Optimization is minimizing or maximizing a function with limitations on its variables. Numerical optimization was a multi-level optimization technique in which the regression equations obtained was used to predict the appropriate factor combination that gives the desired output responses. Maximum Wall angle was output response that needs to be maximized and therefore larger the better was selected as an optimization constraint. Wall angle was a direct formability determinant that was always affected by materials thinning. Because of the thinning, the wall angle was always less than the desired angle and therefore optimum parameters were predicted for achieving larger wall angle. The wall thickness might be maximum to prevent the component's failure and therefore maximum wall thickness was considered as constraint in numerical optimization technique.

Given the limitations of two output responses, the best combination of output values achieved could be 77.81°, with a 5mm tool diameter, feed rate of 1000 mm/min, step depth of 0.2 mm and a material thickness of 0.8mm, shown in Fig.4.19. Three sets of experiments with optimized process parameters values were performed and the results were found to be 99.04% accurate in predicting output responses.

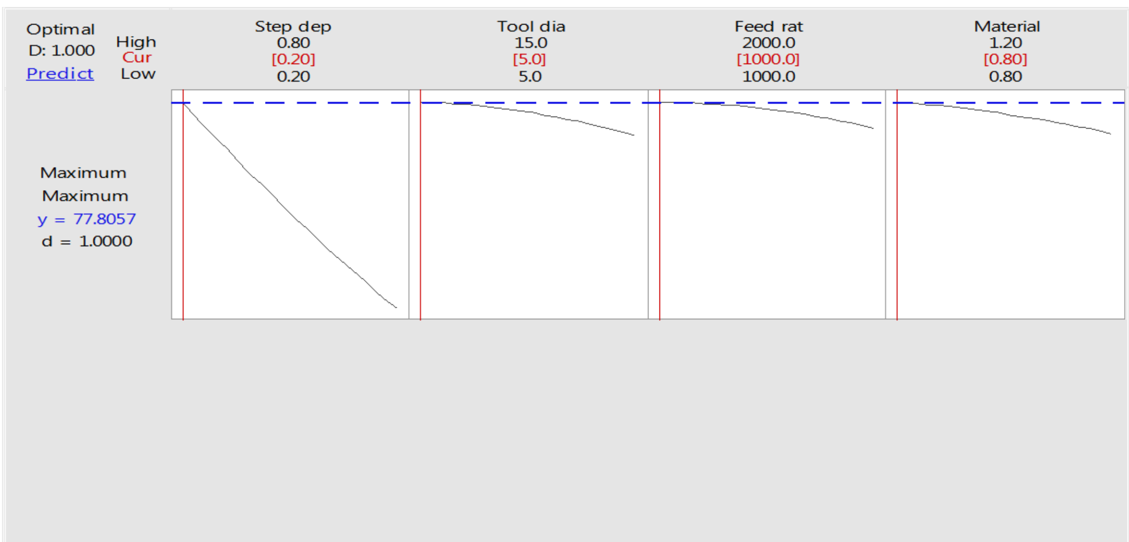

Figure 4. 19 Optimized Response and corresponding process parameters

Optimization of Thinning

Optimization was minimizing or maximizing a function with limitations on its variables. Numerical optimization was a multi-level optimization technique in which the regression equations obtained was used to predict the appropriate factor combination that gives the desired output responses. Thinning was output response that needs to be maximized and therefore larger the better was selected as an optimization constraint. Thinning was a direct formability determinant that was always affected by maximum wall angle. Because of the maximum wall angle, thinning was always less than the desired thickness and therefore optimum parameters were predicted for achieving optimum thinning. The wall thickness might be maximum to prevent the component's failure and therefore maximum wall thickness was considered as constraint in numerical optimization technique.

Given the limitations of two output responses, the best combination of output values achieved could be .8563mm, with a 5mm tool diameter, feed rate of 1000 mm/min, step depth of 0.8 mm and a material thickness of 1.2mm, shown in Fig.20. Three sets of experiments with optimized process parameters values were performed and the results were found to be 99.14% accurate in predicting output responses.

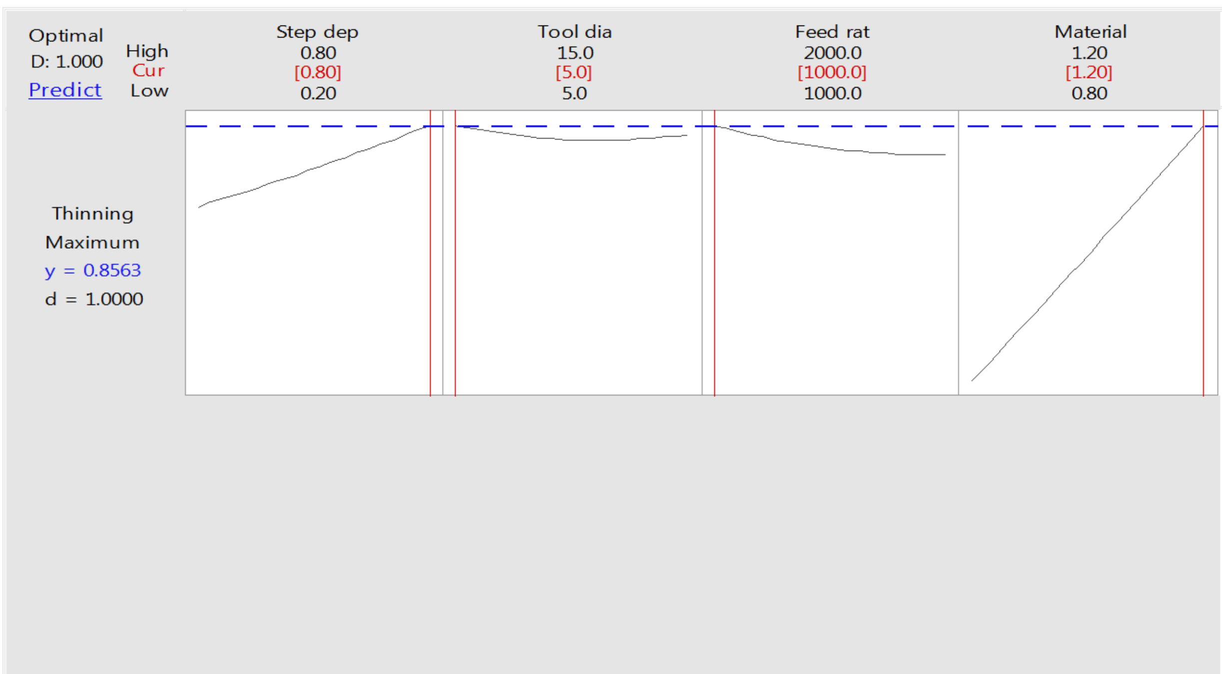

Figure 4. 20 Optimized response and its corresponding parameters

CHAPTER FIVE

CONCLUSIONS and RECOMMENDATIONS

Conclusions

The maximum wall angle and thinning during the incremental forming of Aluminium AA6061alloy have been analyzed and conclusions have been drawn as follows: The significance of step depth was the most predominant with F-value of 1212.07 for the response of maximum wall angle, followed by the material thickness having the value of 46.79. From the interaction effects step depth and feed rate (10.16), followed by step depth and tool diameter (4.66) are significant. The smaller diameter tool increased the formability. In increasing the tool diameter maximum wall angle was increased to from 5mm tool diameter to 10mm and decreased the wall angle and hence formability. The step depth was found to influence the maximum wall angle more significantly than the other process parameters, thus indicating the importance of step depth control during the forming process. Among the model terms, the F-value of material thickness was (1432.33) followed by step depth (46.87), thus indicating its higher influence on thinning, when compared to other factors. From the interaction effects step depth and material thickness with value of (9.49), followed by step depth and feed rate (3.65) are significant. The results of ANOVA confirm that the developed empirical models for the output responses shows an excellent fit, and provide the predicted values of these response factors that are close to the experimental values , at 95% confidence level. The optimized forming condition predicted for maximum wall angle, and thinning were 77.81^0 and 0.856mm for a tool diameter of 5 mm, 0.2 mm step depth, 1000 mm/min feed rate and spindle speed of 1000 rpm and tool diameter of 5mm, 0.8mm step depth, 1000mm/min feed rate and spindle speed of 1000rpm, respectively. The value of the determination coefficient R^2 of the established regression equation of the maximum wall angle and thinning were 99.03 % and 99.14%, respectively. This high value refer to the close fitting of the suggested equation to describe the expected experimental data; it also means the response values highly adhere to the normal distribution. Combination of higher tool diameter and higher step size resulted in the fracture of components at the lower depth which was an indicator of the loss of formability. Increase in step depth and sheet thickness increased the formability significantly to some extent then tends to decrease based on size of forming tool and capacity of SPIF machine. The nature of increasing formability with the increase in sheet thickness was also related to the material's mechanical properties. More stretching of the sheet can be possible since the minimum thinning achieved in both FEM simulation and experiment results was higher than the minimum value of thinning predicted by the sine law (0.230mm). The obtained result from the numerical simulation was in good agreement with the measured value. From this, we could conclude that FEM simulation successfully predict thinning. Results showed that due to the gradual transition between following contours, helical (spiral) tool path generates homogeneous thinning, and removes the surface scarring which was seen in z-level (profile) toolpath. It could be concluded that helical (spiral) tool path was a decent choice for ISF processes.

Recommendations and Future work

More work will need to be done to get a more uniform distribution of thinning and to determine the formability limit of AA6061.

Future work would focus on the analysis of thickness distribution and forming forces of the formed components which finds importance and suitability in setting the guidelines for industrial application.

Extend single point incremental forming to Polymers and composite materials and study forming limit diagram and formability.

References

ASTM, A., (1999). Metals test methods and analytical procedures. *American Society for Testing & Materials (ASTM), Washington*, pp. 78– 98, 501– 508.

ABAQUS , ABAQUS, Theory Manual,. (2008). Version 6.8,: Simulia, Providence, RI.

Allwood JM, Bramley AN, Ridgman TW, Mileham AR., (2006). A novel method for the rapid production of inexpensive dies and moulds with surfaces made by incremental sheet forming. *Proc Inst Mech Eng Part B J Eng Manuf 220*, pp. 323–327.

Allwood JM, Shouler DR, Tekkaya AE., (2007). The increased forming limits of incremental sheet forming processes. *Key Eng Mater 344*, pp. 621–628.

Allwood, J.M., Houghton, N.E. and Jackson, K.P., (2005). The design of an incremental forming machine. *Proceedings of the 11th Conference on Sheet Metal*, pp. 471-478.

Alves de Sousa, R.J., Cardoso, R.P.R., Fontes Valente, R. a., Yoon, J.-W., Grácio,J.J and Natal Jorge, R.M., (2006). A new one-point quadrature enhanced assumed strain (EAS)solid-shell element with multiple integration along thickness part II: non-linear applications. *International Journal for Numerical Methods in Engineering, Vol. 67 No. 2*, pp. 160-188.

Alves de Sousa, R.J., Ferreira, J.A.F., Sá de Farias, J.B., Torrão, J.N.D., Afonso, D.G. and Martins, M.A.B.E., (2014). SPIF-A: on the development of a new concept of incremental forming machine. *Structural Engineering and Mechanics, Vol. 49 No. 5*, pp. 645-660.

Alves de Sousa, R.J., Natal Jorge, R.M., Fontes Valente, R.A. and César de Sá, J.M.A., (2003). A new volumetric and shear locking-free EAS element. *Engineering Computations, Vol. 20*, pp. 896-925.

Alves de Sousa, R.J., Yoon, J., Cardoso, R., Fontes Valente, R. and Gracio, J., (2007). On the use of a reduced enhanced solid-shell (RESS) element for sheet forming simulations. *International Journal of Plasticity, Vol. 23 No. 3*, pp. 490–515.

Ambrogio G, Cozza V, Filice L, Micari F., (2007b). An analytical model for improving precision in single point incremental forming. *J Mater Process Technol 191*, pp. 92–95.

Ambrogio G, De Napoli L, Filice L, Gagliardi F, Muzzupappa M., (2005c). Application of incremental forming process for high customized medical product manufacturing. *J Mater Process Technol 162–163*, pp. 156–162.

Ambrogio G, Filice L, Gagliardi F, Micari F., (2005a). Sheet thinning prediction in single point incremental forming. *Adv Mater Res 6–8*, pp. 479–486.

Ambrogio, G., Filice, L. and Manco, G.L., (2010b). Improving process performance in incremental sheet forming (ISF). *AIP Conference Proceedings, Vol. 1315*, pp. 613–618.

Ambrogio, G., Filice, L., Gagliardi, F. and Micari, F., (2005). Three-dimensional FE simulation of single point incremental forming: experimental evidences and process design improving. *VIII International Conference on Computational Plasticity COMPLAS VI.*

Amino, H., Lu, Y., Maki, T., Osawa, S., Fukuda, K. and Maki, T., (2002). Dieless NC Forming, prototype of automotive service parts. *Proceedings of the 2nd International Conference on Rapid Prototyping and Manufacturing (ICRPM).* Beijing.

Araghi, B.T., Manco, G.L., Bambach, M. and Hirt, G., (2009). Investigation into a new hybrid forming process: Incremental sheet forming combined with stretch forming. *CIRP Annals - Manufacturing Technology, Vol. 58 No. 1*, pp. 225–228.

Arfa, H., Bahloul, R. and Bel Hadj Salah, H., (2012). Finite element modelling and experimental investigation of single point incremental forming process of aluminum sheets: influence of process parameters on punch force monitoring and on mechanical and geometrical quality of parts. *International Journal of Material Forming, vol.6 No.4*, pp. 483-510.

Attanasio, A., Ceretti, E. and Giardini, C., (2006). Optimization of tool path in two points incremental forming. *Journal of Materials Processing Technology, Vol. 177 No. 1-3*, pp. 409–412.

Attanasio, a., Ceretti, E., Giardini, C. and Mazzoni, L., (2008). Asymmetric two points incremental forming: Improving surface quality and geometric accuracy by tool path optimization. *Journal of Materials Processing Technology, Vol. 197 No. 1-3*, pp. 59–67.

Azaouzi, M. and Lebaal, N., (2012). Tool path optimization for single point incremental sheet forming using response surface method. *Simulation Modelling Practice and Theory, Vol. 24,*, pp. 49–58.

Azevedo, N.G., Farias, J.S., Bastos, R.P., Teixeira, P., Davim, J.P., Jose, R. and Sousa, A. De., (2015). Lubrication Aspects during Single Point Incremental Forming for Steel and Aluminum Materials. *International Journal of precision engineering and manufacturing, vol.16 No.3*, pp. 1-7.

Bambach, M., (2014). Fast simulation of asymmetric incremental sheet metal forming by adaptive remeshing and subcycling. *International Journal of Material Forming, Vol. 847*, pp. 844–847.

Bambach, M. and Hirt, G., (2005). Performance assessment of element formulations and constitutive laws for the simulation of incremental sheet forming (ISF). *COMPLAS. CIMNE, Barcelona*, pp. 1–4.

Bambach, M. Cannamela, M., Azaouzi, M., Hirt, G. and Batoz, J.L., (2007). Computer-Aided Tool Path Optimization for Single Point Incremental Sheet Forming", Advanced Methods in Material Forming. *Springer Berlin Heidelberg* , pp. 233–250.

Behera AK, Verbert J, Lauwers B, Duflou JR., (2013). Tool path compensation strategies for single point incremental sheet forming using multivariate adaptive regression splines. *ComputAided Des 45*, pp. 575–590.

Behera, A.K., Lauwers, B. and Duflou, J.R., (2014). Tool path generation framework for accurate manufacture of complex 3D sheet metal parts using single point incremental forming. *Computers in Industry, Vol. 65 No. 4*, pp. 563–584.

Ben Ayed, L., Robert, C., Delamézière, A., Nouari, M. and Batoz, J.L., (2014). Simplified numerical approach for incremental sheet metal forming process. *Engineering Structures, Vol. 62-63*, pp. 75–86.

Bhattacharya, A., Maneesh, K., Venkata Reddy, N. and Cao, J., (2011). Formability and Surface Finish Studies in Single Point Incremental Forming. *Journal of Manufacturing Science and Engineering, ASME, Vol. 133 No. 6.* , pp. 166-179.

Blaga, A., Bologa, O., Oleksik, V. and Breaz, R., (2011). Influence of tool path on main strains, thickness reduction and forces in single point incremental forming process. *Proceedings in Manufacturing Systems, Vol. 6 No. 4*, pp. 2–7.

Bouffioux, C., Eyckens, P., Henrard, C., Aerens, R., Bael, A. Van, Sol, H., Duflou, J.R. and Habraken, A.M., (2008a). Identification of material parameters to predict Single Point Incremental Forming forces. *International Journal of Material Forming*, pp. 1147-1150.

Bouffioux, C., Henrard, C., Eyckens, P., Aerens, R., Bael, A. Van, Sol, H., Duflou, J.R., et al. ., (2008b). Comparison of the tests chosen for material parameter identification to predict single point incremental forming forces. *International Deep Drawing Research Group-IDDRG 2008 International Conference.* Sweden: olofstrom.

Bouffioux, C., Pouteau, P., Duchêne, L., Vanhove, H., Duflou, J.R. and Habraken, a. M., (2010). Material data identification to model the single point incremental forming process. *International Journal of Material Forming, Vol. 3 No. S1*, pp. 979–982.

Ceretti, E., Giardini, C. and Attanasio, A., (2004). Experimental and simulative results in sheet incremental forming on CNC machines. *Journal Material Proceeding Technology, Vol. 152*, pp. 176-184.

Cerro, I., E. Maidagan, et al., (2006). Theoretical and experimental analysis of the dieless incremental sheet forming process. *Journal of Materials Processing Technology, Vol. 177(1-3)*, pp. 404-408.

Cescotto, S. and Grober, H., (1985). Calibration and application of an elastic viscoplastic constitutive equation for steels in hot-rolling conditions. *Engineering Computations, Emerald, Vol. 2 No. 2*, pp. 101–106.

Cui, Z., Cedric Xia, Z., Ren, F., Kiridena, V. and Gao, L., (2013). Modeling and validation of deformation process for incremental sheet forming . *Journal of Manufacturing Processes, Vol. 15 No. 2*, pp. 236–241.

Dejardin, S., Thibaud, S., Gelin, J.C. and Michel, G., (2010). Experimental investigations and numerical analysis for improving knowledge of incremental sheet forming process for sheet metal parts. *Journal of Materials Processing Technology, Vol. 210 No.2*, pp. 363-369.

Delamézière, A., Yu, Y., Robert, C., Ben Ayed, L. and Nouari, M., (2011). Numerical Simulation of Incremental Sheet Forming by Simplified Approach. *AIP Conference Proceedings, AMPT2010*, pp. 619–624.

Duflou JR, Verbert J, Belkassem B, Gu J, Sol H, Henrard C, Habraken AM., (2008b). Process window enhancement for single point incremental forming through multi-step toolpaths. *CIRP Ann 57*, pp. 253–256.

Durante, M., Formisano, a., Langella, a. and Capece Minutolo, F.M., (2009). The influence of tool rotation on an incremental forming process. *Journal of Materials Processing Technology, Vol. 209 No. 9*, pp. 4621–4626.

Echrif, S.B.M. and Hrairi, M., (2011). Research and Progress in Incremental Sheet Forming Processes. *Materials and Manufacturing Processes, Vol. 26 No. 11*, pp. 1404–1414.

Emmens WC, Seba stiani G, Googaard AH., (2010). The technology of incremental sheet forming-a brief review of the history. *J Mater Process Technol 210*, 981–997.

Emmens, W.C. and Boogaard, A.H. Van Den., (2007). Strain in Shear , and Material Behaviour in Incremental Forming . *Key Engineering Materials, Vol. 344,*, pp. 519–526.

Emmens, W.C. and Boogaard, A.H. Van Den., (2008). Tensile tests with bending: a mechanism for incremental forming. *11th ESAFORM Conference*, pp. 23–25.

Emmens, W.C. and van den Boogaard, a. H., (2009). An overview of stabilizing deformation mechanisms in incremental sheet forming. *Journal of Materials Processing Technology, Vol. 209 No. 8*, pp. 3688–3695.

Emmens, W.C., Sebastiani, G. and Boogaard, A.H. Van Den., (2010). The technology of Incremental Sheet Forming-A brief review of the history . *Journal of Materials Processing Tech., Elsevier B.V., Vol. 210 No. 8*, pp. 981–997.

Essa, K. and Hartley, P., (2010). An assessment of various process strategies for improving precision in single point incremental forming. *International Journal of Material Forming, Vol. 4 No. 4*, pp. 401–412.

Eyckens, P., (2010). *Formability in incremental sheet forming: Generalization of the Marciniak-Kuczynski model.* Belgium: Katholieke Universiteit Leuven.

Eyckens, P., Bael, A. Van, Aerens, R., Duflou, J. and Houtte, P. Van., (2008). Small-scale Finite Element Modelling of the Plastic Deformation Zone in the Incremental Forming Process. *International Journal of Material Forming*, pp. 1159–1162.

Eyckens, P., Belkassem, B., Henrard, C., Gu, J., Sol, H., Habraken, A.M., Duflou, J.R., Bael, A. and Houtte, P., (2010). Strain evolution in the single point incremental forming process: digital image correlation measurement and finite element prediction. *International Journal of Material Forming, Vol.4 No. 1*, pp. 55-71.

Eyckens, P., Del-lero Moreau, J., Duflou, J.R., Bael, A. and Houtte, P., (2009b). MK modelling of sheet formability in the incremental sheet forming process, taking into account through-thickness shear. *International Journal of Material Forming, Vol. 2 No.S1*, pp. 379-382.

Eyckens, P., He, S., Van Bael, a., Van Houtte, P. and Duflou, J., (2007). Forming Limit Predictions for the Serrated Strain Paths in Single Point Incremental Sheet Forming. *AIP Conference Proceedings, Vol. 908 No. 2007*, pp. 141–146.

Eyckens, P., Van Bael, A. and Van Houtte, P., (2009a). Marciniak–Kuczynski type modelling of the effect of Through-Thickness Shear on the forming limits of sheet metal. *International Journal of Plasticity, Vol. 25 No. 12*, pp. 2249–2268.

Eyckens, P., Van Bael, A. and Van Houtte, P., (2011). An extended Marciniak–Kuczynski model for anisotropic sheet subjected to monotonic strain paths with through-thickness shear. *International Journal of Plasticity, Vol. 27 No. 10*, pp. 1577–1597.

Fang, Y., Lu, B., Chen, J., Xu, D.K. and Ou, H., (2014). Analytical and experimental investigations on deformation mechanism and fracture behavior in single point incremental forming. *Journal of Materials Processing Technology, Vol. 214 No. 8*, pp. 1503–1515.

Filice, L., Fratini, L., Micari, F., (2002). Analysis of material formability in incremental forming. *Annals of CIRP, 51*, pp. 199-202.

Fratini, L., Ambrogio, G., Di Lorenzo, R., Filice, L. and Micari, F., (2004). Influence of mechanical properties of the sheet material on formability in single point incremental forming. *CIRP Annals - Manufacturing Technology, Vol. 53 No. 1*, pp. 207–210.

Giraud-Moreau, L., Cherouat, A., Zhang, J., Borouchaki, H., (2013). Comparison between an advanced numerical simulations of sheet incremental forming using adaptive remeshing and experimental results. *Key Enginneering Materials, Vol. 554–557*, pp. 1375–1381.

Guzmán, C.F., Gu, J., Duflou, J., Vanhove, H., Flores, P. and Habraken, A.M., (2012). Study of the geometrical inaccuracy on a SPIF two-slope pyramid by finite element Simulations. *International Journal of Solids and Structures, Vol. 49 No. 25*, pp. 3594–3604.

Hadoush, a. and Boogaard, a. H., (2009). Substructuring in the implicit simulation of single point incremental sheet forming. *International Journal of Material Forming, Vol. 2 No. 3*, pp. 181–189.

Hadoush, A. and Boogaard, A.H. Van Den., (2012). Efficient implicit simulation of incremental sheet forming. *International Journal for Numerical Methods in Engineering*.

Hadoush, A. and Boogaard, A.H. Van Den., (2008). Time reduction in implicit single point incremental sheet forming simulation by Refinement /Derefinement. *International Journal of Material Forming*, pp. 1167–1170.

Hadoush, A.M.H., (2010). *Efficient simulation and process mechanics of incremental sheet forming.* Netherland.: University of Twente.

Ham, M. and Jeswiet, J., (2006). Single Point Incremental Forming and the Forming Criteria for AA3003 . *CIRP Annals - Manufacturing Technology, Vol. 55 No. 1*, pp. 241–244.

Hamilton, K. and Jeswiet, J., (2010). Single point incremental forming at high feed rates and rotational speeds: Surface and structural consequences. *CIRP Annals - Manufacturing Technology, CIRP, Vol. 59 No. 1*,, pp. 311–314.

He, S., Bael, A. Van, Houtte, P. Van, Tunckol, Y., Duflou, J., Henrard, C., Bouffioux, C. and Habraken, A.M., (2005). Effect of FEM choices in the modelling of incremental forming of aluminium sheets. *8th ESAFORM conference* (pp. pp. 1–4). Romania: Cluj-Napoca.

Henrard, C., (2008). *Numerical Simulations of the Single Point Incremental Forming Process.* Belgium: University of Liège.

Hibbitt, Karlsson & Sorensen., (2005). *ABAQUS, Theory Manual, Version 6.5.* USA.: Hibbitt, Karlsson & Sorensen Inc.

Hirt G, Ames J, Bambach M, Kopp R., (2004). Forming strategies and Process Modelling for CNC Incremental Sheet Forming. *CIRP Ann 53(1),* pp. 203–206.

Hirt G., Ames J., Bambach M., (2006). Basic Investigation into the Characteristics of dies and suppot tools used in CNC-Incremental Sheet Forming. *Proceedings of the International Deep Drawing Research Group Conference, IDDRG 2006,* (pp. 341-348). Porto, Portugal.

Hussain G, Dar NU, Gao L, Chen MH., (2007b). A comparative study on the forming limits of an aluminum sheet-metal in negative incremental forming. *J Mater Process Technol 187*, pp. 94–98.

Hussain G, Gao L., (2007). A novel method to test the thinning limits of sheet- metals in negative incremental forming. *Int J Mach Tool Manuf 47*, pp. 419–435.

Hussain G, Gao L, Dar NU., (2007a). An experimental study on some formability evaluation methods in negative incremental forming. *J Mater Process Technol 186*, pp. 45–53.

Iseki H, Kumon H., (1994). Forming limit of incremental sheet metal stretch forming using spherical rollers . *J JSTP 35*, pp. 1336–1341.

Jackson KP, Allwood JM, Landert M., (2007). Incremental forming of sandwich panels. *Key Eng Mater 344*, pp. 591–598.

Jackson, K. and Allwood, J., (2009). The mechanics of incremental sheet forming. *Journal of Materials Processing Technology, Vol. 209 No. 3*, pp. 1158–1174.

Jeswiet J, Micari F, Hirt G, Bramley A, Duflou A, Allwood J., (2005a). Asymmetric single point incremental forming of sheet metal. *CIRP Ann 54(2)*, pp. 623–649.

Jeswiet, J., Hagan, E. and Szekeres, A., (2002). Forming parameters for incremental forming of aluminium alloy sheet metal. *Proceedings of the IMechE 216, Part B, No. 10*, pp. 1367-1371.

Jeswiet, J., Micari, F., Hirt, G., Bramley, A., Duflou, J. and Allwood, J., (2005). Asymmetric Single Point Incremental Forming of Sheet Metal. *CIRP Annals - Manufacturing Technology, Vol. 54 No. 2*, pp. 88–114.

Kim TJ, Yang DY., (2000). Improvement of formability for the incremental sheet metal forming process. *Int J Mech Sci 42(7)*, pp. 1271–1286.

Kim, Y.. and Park, J., (2002). Effect of process parameters on formability in incremental forming of sheet metal. *Journal of Materials Processing Technology, Vol. 130-131*, pp. 42–46.

Kopac, J. and Kampus, Z., (2005). Incremental sheet metal forming on CNC milling machine-tool. *Journal of Materials Processing Technology, Vol. 162- 163*, pp. 622–628.

Lequesne, C., Henrard, C., Bouffioux, C., Duflou, J.R. and Habraken, A.M., (2008). Adaptive remeshing for incremental forming simulation. *Numisheet 2008, Interlaken, Switzerland, Vol. 32*, pp. 4–8.

Leszak, E., (1967). *Apparatus and Process for Incremental Dieless Forming.* USA: Patent US3342051A1.

Malhotra, R., Cao, J., Beltran, M., Xu, D., Magargee, J., Kiridena, V. and Xia, Z.C., (2012a). Accumulative-DSIF strategy for enhancing process capabilities in incremental forming. *CIRP Annals - Manufacturing Technology, Vol. 61 No. 1*, pp. 251–254.

Malhotra, R., Xue, L., Belytschko, T. and Cao, J., (2012b). Mechanics of fracture in single point incremental forming. *Journal of Materials Processing Technology, Vol. 212 No. 7*, pp. 1573–1590.

Malkus, D.S. and Hughes, T.J.R., (1978). Mixed finite element method-reduced and selective integration techniques: a unification of concepts. *Computer Methods in Applied Mechanics and Engineering, Vol. 15*, pp. 63-81. .

Malwad, D.S. and Nandedkar, V.M., (2014). Deformation Mechanism Analysis of Single Point Incremental Sheet Metal Forming. *Procedia Materials Science, Vol. 6*, pp. 1505–1510.

Martins, P. a. F., Bay, N., Skjoedt, M. and Silva, M.B., (2008). Theory of single point incremental forming. *CIRP Annals - Manufacturing Technology, Vol. 57 No. 1*, pp. 247–252.

Matsubara.S., (2001). A computer numerically controlled dieless incremental forming of a sheet metal. *Proc Inst Mech Eng 215*, pp. 959–966.

Meier, H., Buff, B., Laurischkat, R. and Smukala, V., (2009). Increasing the part accuracy in dieless robot-based incremental sheet metal forming. *CIRP Annals - Manufacturing Technology, Vol. 58 No. 1*, pp. 233–238.

Mirnia, M.J., Mollaei Dariani, B., Vanhove, H. and Duflou, J.R., (2014). An investigation into thickness distribution in single point incremental forming using sequential limit analysis. *International Journal of Advanced Manufacturing Technology, Vol. 70 No. 9-12*, pp. 2029-2041.

Nimbalkar, D.H. and Nandedkar, V.M., (2013). Review of Incremental Forming of Sheet Metal Components. *International Journal of Engineering Research and Applications, Vol. 3 No. 5*, pp. 39–51. .

Park, J.-J. and Kim, Y.-H., (2003). Fundamental studies on the incremental sheet metal forming technique. *Journal of Materials Processing Technology, Vol. 140 No. 1-3*, pp. 447–453.

Petek, A., Jurisevic, B., Kuzman, K. and Junkar, M., (2009a). Comparison of alternative approaches of single point incremental forming processes. *Journal of Materials Processing Technology, Vol. 209 No. 4*, pp. 1810–1815.

Reddy, N.V. and Cao, J., (2014). *Incremental Sheet Metal Forming: A Review : Research Report.*

Riadh, B., Henia, A. and Hedi, B., (2013). Application of Response Surface Analysis and Genetic Algorithm for the Optimization of Single Point Incremental Forming Process. *Vol. 557*, pp. 1265–1272.

Robert, C., Delamézière, A., Dal Santo, P. and Batoz, J.L., (2012). Comparison between incremental deformation theory and flow rule to simulate sheet-metal forming processes. *Journal of Materials Processing Technology, Vol. 212 No. 5*, pp. 1123–1131.

Sebastiani, G., Brosius, a., Tekkaya, a. E., Homberg, W. and Kleiner, M., (2007). Decoupled simulation method for incremental sheet metal forming. *AIP Conference Proceedings, Vol. 908*, pp. 1501–1506.

Sena JIV, Guzmán CF, Duchêne L, Habraken AM, Valente RAF, Alves de Sousa RJ., (2013). Numerical simulation of a conical shape made by single point incremental. *AIP Conference Proceedings, NUMISHEET 2014*, pp. 852-855.

Sena, J.I.V., Sousa, R.J.A. De and Valente, R.A.F., (2011). On the use of EAS solid-shell formulations in the numerical simulation of incremental forming processes. *Engineering Computations, Vol. 28 No. 3*, pp. 287–313.

Shim, M.S. and Park, J.J., (2001). The formability of aluminum sheet in incremental forming. *Journal of Materials Processing Technology*, *Vol. 113 No. 1-3*, pp. 654–658.

Silva, M.B., Skjoedt, M., Bay, N. and Martins, P.A.F., (2009). Formability in multistage single point incremental forming. *7th EUROMECH Solid Mechanics Conference.*

Silva, M.B., Skjoedt, M., Martins, P.A.F. and Bay, N., (2008). Revisiting the fundamentals of single point incremental forming by means of membrane analysis. *International Journal of Machine Tools and Manufacture, Vol. 48 No. 1*, pp. 73–83. .

Skjoedt M, Hancock MH, Bay N., (2007). Creating helical tool paths for single point incremental forming. *Key Eng Mater 344*, pp. 583–590.

Skjoedt M, Silva MB, Martins PAF, Bay N., (2010). Strategies and limits in multi-stage single-point incremental forming. *J Strain Anal Eng Des 45*, pp. 33–44.

Suresh, K. and Regalla, S.P., (2014). Effect of Mesh Parameters in Finite Element Simulation of Single Point Incremental Sheet Forming Process. *Procedia Materials Science, Vol. 6*, pp. 376–382.

Tekkaya, A.E., (2000). State-of-the-art of simulation of sheet metal forming. *Journal of Materials Processing Technology, Vol. 103 No. 1,* pp. 14–22.

Wang, J., (2004). A New Hexahedral Solid Element for 3D FEM Simulation of Sheet Metal Forming. *AIP Conference Proceedings, Vol. 712*, pp. 2181–2186.

Wong, C.., Dean, T.. and Lin, J., (2003). A review of spinning, shear forming and flow forming processes. *International Journal of Machine Tools and Manufacture, Vol. 43 No. 14*, pp. 1419–1435.

Yamashita, M., Gotoh, M. and Atsumi, S.-Y., (2008). Numerical simulation of incremental forming of sheet metal. *Journal of Materials Processing Technology, Vol. 199 No. 1-3*, pp. 163–172. “Triangular gimbal”, Patents US6240799.

Young D, Jeswiet J., (2004). Wall thickness variations in single-point incremental forming. *J Eng Manuf 218*, pp. 1453–1459.

Zeradam Y., Krishnaiah A., (2020). Numerical Simulation and Experimental Validation of Thickness Distribution in Single Point Incremental Forming for Drawing Quality Steel. *International Journal of Applied Engineering Research ISSN 0973 -4562, 15*, pp.101 - 107.

Appendices

A. Basic parameters required to formulate the truncated cone

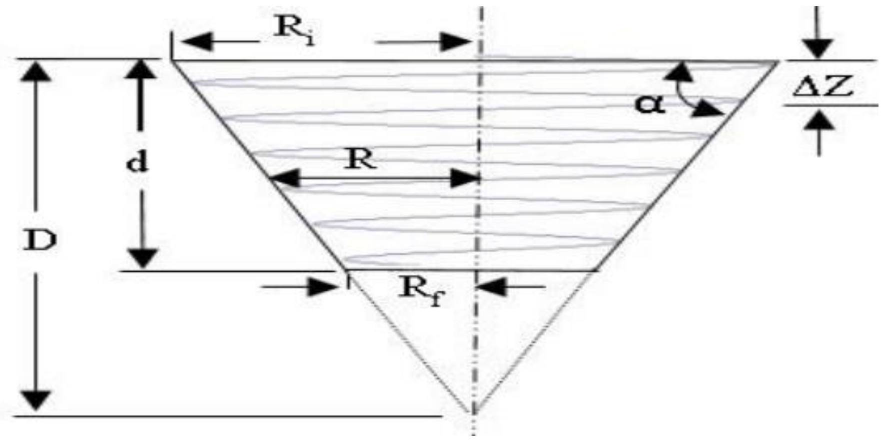

$$\Delta r = \frac{\Delta Z}{\tan(\alpha)} \quad (1)$$

$$N = \frac{d}{\Delta Z} \quad (2)$$

$$X = R\cos(\theta) \quad (3)$$

$$Y = R\sin(\theta) \quad (4)$$

$$Z = -\left(\left(\frac{\Delta Z}{360}\right)\theta\right) \quad (5)$$

B. Matlab Programme for extracting coordinate axis and toolpath generation

```
>> time=linspace(0,800,8501);
>> time=linspace(0,800,4001);
>> xlswrite('time.xlsx',time)
>> m=113/70;
```

```
>>  dh=1; % Step depth
>>  a=45; % angle of inclination of cone
>>  h=70; %Depth of cone
>>  R1=56.5; %largest radius of the cone (top part)
>>  D=R1*tand(a);
>>  N=h/dh; % Number of loops or contour
>>  m=1; for n=0:1:360*N % dividing loop into 360 angles
>>  Z(m)=0-((dh/360)*n);
>>  R=R1-(((dh/360)*n)/tand(a)); % radius at any depth
>>  X(m)=Rcosd(n);
>>  Y(m)=R*sind(n);
>>  X(m)=R*cosd(n);
>>  m=m+1;
end
>>Plot3(Y,X,Z,'b') % 3D visualization of helix
```

C. G-code and tool path simulation based

Part	G-Code	G-code Simulation
Truncated Cone	% N110 G21 N112 G0 G17 G40 G49 G80 G90 N114 T493 M6 N116 G0 G90 G54 X35 Y0 A0. S0 N120 G1 X35 Y0 Z0.1 F1000. N122 X35Y0Z0 N124 X34.992Y0.611Z-0.002 N126 X34.974Y1.221Z-0.004 N128 X34.945Y1.831Z-0.007	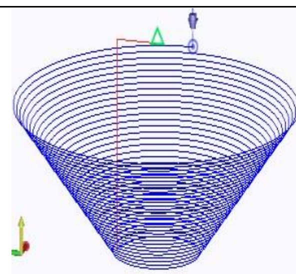

D. Tensile properties and limiting strain for AA6061

Sheet Metal Thickness	Orientation relative to rolling direction	UTS	Young's Modulus	Proof Stress	%Elongation at Break at Non-proportional Elongation	True strain at maximum load	True stress at maximum load	Strain Hardening Exponent (n-Value)	Strength Coefficient (K)
		(GPa)	(MPa)	(Mpa)	(%)	(mm/mm)	(Pa)		(MPa)
AA6061 0.8mm	0˚	0.535	38998.919	438.37	4.93261	0.0416	557490337	0.09256	750.01916
	45˚	0.557	33192.547	442.45	5.28248	0.04346	582024251.1	0.15433	961.29455
	90˚	0.555	37247.037	399.08	5.99299	0.0442	579645397.8	0.04767	670.43712
	Average*	0.551	35657.763	430.59	5.37264	0.04318	575296059.3	0.11222	835.761345
AA6061 1.00mm	0˚	0.476	33167.863	350.24	5.60607	0.04563	498445628.1	0.12221	736.29631
	45˚	0.452	28426.154	185.79	5.04266	0.04283	472192959.6	0.10273	654.01461
	90˚	0.482	31346.105	281.11	5.82772	0.05211	507500449.1	0.16709	854.286
	Average*	0.466	30341.569	250.73	5.37978	0.04585	487582999.1	0.12369	724.652883
AA6061 1.2mm	0˚	0.444	29451.897	282.42	6.33766	0.05445	469033596.2	0.17065	789.82227
	45˚	0.439	27580.07	296.89	7.21893	0.0555	463559741.7	0.1692	776.48011
	90˚	0.246	42594.854	168.84	8.22619	0.02501	252022963.6	0.07966	335.08006
	Average*	0.392	31801.723	261.26	7.25043	0.047615	412044010.8	0.14718	669.465638

E. G-code generation and simulation

Part	G-Code	G-code Simulation
Truncated Cone	% N110 G21 N112 G0 G17 G40 G49 G80 G90 N114 T493 M6 N116 G0 G90 G54 X35 Y0 A0. S0 N120 G1 X35 Y0 Z0.1 F1000. N122 X35Y0Z0 N124 X34.992Y0.611Z-0.002 N126 X34.974Y1.221Z-0.004 N128 X34.945Y1.831Z-0.007	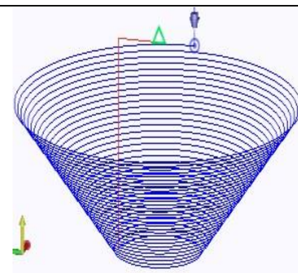

```
Start %
N100G21
N106G0G90G54X-
N108G43H1Z24.8
N112G01Z-0.2F1000
N114X-33.113Y-35.79
......
.......
......
N1258M5
N1260G91G28G0
N1262G28X0Y0
N1264M30
%
```

F. ANOVA table for maximum wall angle

Source	DF	Adj SS	Adj MS	F-Value	P-Value
Model	13	253.589	19.507	102.17	0.000
Step depth (mm)	1	231.412	231.412	1212.07	0.000
Tool diameter (mm)	1	0.344	0.344	1.80	0.202
Feed rate (mm/min)	1	0.281	0.281	1.47	0.247
Material thickness (mm)	1	8.932	8.932	46.79	0.000
Step depth (mm)*Step depth (mm)	1	0.548	0.548	2.87	0.114
Tool diameter (mm)*Tool diameter (mm)	1	0.347	0.347	1.82	0.200
Feed rate (mm/min)*Feed rate (mm/min)	1	0.325	0.325	1.70	0.214
Material thickness (mm)*Material thickness (mm)	1	0.156	0.156	0.82	0.383
Step depth (mm)*Tool diameter (mm)	1	0.889	0.889	4.66	0.050
Step depth (mm)*Feed rate (mm/min)	1	1.940	1.940	10.16	0.007
Step depth (mm)*Material thickness (mm)	1	0.411	0.411	2.15	0.166
Tool diameter (mm)*Material thickness (mm)	1	0.080	0.080	0.42	0.529
Feed rate (mm/min)*Material thickness (mm)	1	0.087	0.087	0.45	0.512
Error	13	2.482	0.191		
Total	26	256.071			

G. ANOVA table for thinning

Source	DF	Adj SS	Adj MS	F-Value	P-Value
Model	13	0.329653	0.025358	115.71	0.000
Step depth (mm)	1	0.010272	0.010272	46.87	0.000
Tool diameter (mm)	1	0.000008	0.000008	0.04	0.851
Feed rate (mm/min)	1	0.000036	0.000036	0.16	0.692
Material thickness (mm)	1	0.313896	0.313896	1432.33	0.000
Step depth (mm)*Step depth (mm)	1	0.000071	0.000071	0.32	0.578
Tool diameter (mm)*Tool diameter (mm)	1	0.000642	0.000642	2.93	0.111
Feed rate (mm/min)*Feed rate (mm/min)	1	0.000534	0.000534	2.43	0.143
Material thickness (mm)*Material thickness (mm)	1	0.000016	0.000016	0.07	0.794
Step depth (mm)*Tool diameter (mm)	1	0.000001	0.000001	0.01	0.938
Step depth (mm)*Feed rate (mm/min)	1	0.000800	0.000800	3.65	0.078
Step depth (mm)*Material thickness (mm)	1	0.002080	0.002080	9.49	0.009
Tool diameter (mm)*Material thickness (mm)	1	0.000352	0.000352	1.61	0.227
Feed rate (mm/min)*Material thickness (mm)	1	0.000456	0.000456	2.08	0.173
Error	13	0.002849	0.000219		
Total	26	0.332502			